In presenting the dissertation as a partial fulfillment of the requirements for an advanced degree from the Georgia Institute of Technology, I agree that the Library of the Institute shall make it available for inspection and circulation in accordance with its regulations governing materials of this type. I agree that permission to copy from, or to publish from, this dissertation may be granted by the professor under whose direction it was written, or, in his absence, by the Dean of the Graduate Division when such copying or publication is solely for scholarly purposes and does not involve potential financial gain. It is understood that any copying from, or publication of, this dissertation which involves potential financial gain will not be allowed without written permission.

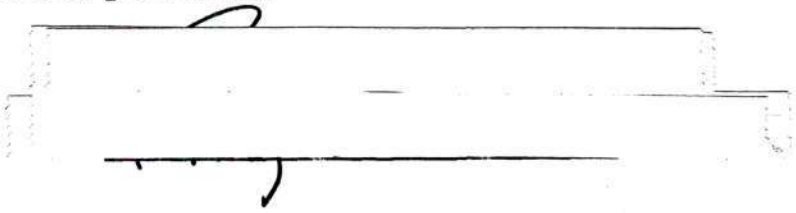

3/17/65
b

MECHANISM AND KINETICS OF IRON DETERIORATION IN CARBON MONOXIDE

A THESIS

Presented to

The Faculty of the Graduate Division

by

Richard Vernon Westerman

In Partial Fulfillment

of the Requirements for the Degree

Doctor of Philosophy

in the School of Chemical Engineering

Georgia Institute of Technology

December, 1967

MECHANISM AND KINETICS OF IRON

DETERIORATION IN CARBON MONOXIDE

Approved:

Chairman

Date approved by Chairman: 3/4/68

ACKNOWLEDGMENTS

The author wishes to express his appreciation to his thesis advisor, Dr. Robert F. Hochman, for suggesting the problem and for his interest and assistance during the study. The author is indebted to Dr. Homer V. Grubb, Director of the School of Chemical Engineering, for serving on the reading committee and for the support which the School gave to this investigation. Appreciation is also extended to Dr. Robert A. Pierotti for his conscientious service as a member of the reading committee.

The award to the author of National Science Foundation Traineeships for 1964-67 made this work a reality. The author also thanks the National Association of Corrosion Engineers for their partial support through Project A-753 of the Georgia Tech Experimental Station. Many people contributed to the work presented here. Included among these are the entire staff of the School of Chemical Engineering. Also included is my colleague, J. Titus Ratliff, whose assistance was of great help.

Numerous deserving people have not been individually acknowledged here; it is my hope that they will feel the appreciation that is due them.

Most of all, the author wishes to thank his wife. Without her encouragement and help this work could never have been accomplished.

TABLE OF CONTENTS

APPENDIX Page

LIST OF TABLES

LIST OF ILLUSTRATIONS

SUMMARY

The reaction of carbonaceous environments with iron substances and the subsequent deposition of carbon or degradation of the metal have been recognized for almost a century. Recently, with the use of more intricate process equipment, demanding greater performances and long lifetimes, carbonaceous attack has often been a severely limiting factor.

For the first quarter of the twentieth century, considerable effort was exerted in the study of the iron-carbon monoxide and related reactions. The information obtained was confusing and conflicting. The difficulty of measuring the reaction as it occurs, the variance of substances and their purities, the presence of an allotropic transformation in iron at 723°C, and the complexity of the mechanism add to the tumult.

The more recent work has usually dealt with isolated and specific problems: diversified reactants and short temperature spans. Also, most of this work has used solely initial-terminal weight differences as a measure of the reaction; samples were observed only after cooling and isolation from the reaction system. Because of the above factors, the general reaction mechanism has not been explained.

For this investigation, ultra-high purity iron wires were reacted in pure carbon monoxide over the temperature range of significant reaction, 500°C to 1000°C. The wires were exposed to the carbon monoxide in a microbalance for 20 hours at constant temperatures. Weight change measurements were made continuously during the reaction to define the

kinetics. After cooling, the wire samples were subjected to x-ray and metallographic analysis to determine the reaction products and structure of the iron. The reaction mechanism was then defined. Auxiliary experiments were undertaken to verify and support the thermogravimetric conclusions. Iron wires were subjected to carbon monoxide for extended periods. The actual reaction of carbon monoxide with iron powder was followed by x-ray observation, using a special high-temperature x-ray camera.

The results showed that the reaction effectively begins at about 475°C. Weight gain increases rapidly to a maximum at 570°C. The reaction decreases to a minimum at 710°C, where there is virtually no reaction. An increase is then observed from 710°C to 1000°C. Below 723°C, in the region of alpha-iron, carbon is essentially insoluble in the ferrite and almost the entire weight gain is due to a surface carbon deposit. Carbon is soluble up to 2.0 weight per cent in gamma-iron. In high-temperature experiments where austenite (gamma) exists, the lattice is saturated with carbon and the deposits, after cooling to room temperature, are a gray-silvery powder composed of graphite, cementite (Fe_3C), and ferrite. An incubation period was encountered at reaction temperatures below 800°C.

Metallographic and x-ray examination of the samples indicated that in the ferrite domain (below 723°C) a surface layer of cementite (Fe_3C) gradually becomes thicker as the reaction temperature is increased. When austenite is formed, carbon is dissolved in preference to forming cementite; the matrix iron becomes saturated with the carbon and further weight gains are due to surface deposits.

At 550°C two types of carbon reaction deposits were observed: a small filamentary growth, and a bulk or flake structure. Other research has shown the filamentary growth to be selective.

This research experienced a variation in reactivity between different wire shipments with identical specifications, at the lower temperatures. The divergence in reactivities is due to an excessive amount of cold work, and the greater amounts of dislocations and imperfections in the samples. The rise in reaction rate is due to additional activated centers. After annealing in the austenite region, wires reacted at 550°C exhibited normal reaction rates.

The high-temperature x-ray examinations during the reaction of carbon monoxide with iron powder verified the observations made at lower temperatures.

From the experimental results, a mechanism is postulated for the alpha region: (1) adsorption of carbon monoxide on the ferrite surface, (2) Boudouard reaction ($2CO \rightarrow CO_2 + C$) releasing the carbon, (3) formation of cementite, and (4) decomposition of cementite crystals to iron and graphite. The amount of carbon deposits from 475°C to about 570°C is controlled by the formation rate of cementite nuclei, which then decompose to ferrite and graphite ($Fe_3C \rightarrow Fe + C$). The ferrite surface supports the reaction while the cementite is passive. At about 570°C the rate of formation of cementite surpasses the decomposition rate and a maximum weight gain occurs at this temperature. As the temperature approaches 710°C, the cementite becomes more stable and covers the surface. The activation energy of nucleation was calculated to be 19.0 kcal/mole, and the activation energy for the 500°C to 570°C

portion of the reaction was 20.0 kcal/mole.

In austenite, the initial stage of the reaction is diffusion controlled. Further increases in weight are due to the formation of graphite on the iron surface. An activation energy for diffusion of carbon was calculated to be 35.4 kcal/mole, agreeing with previous diffusion data.

The data and results of this study yield a fundamental basis for the complex phenomena experienced in industrial "metal dusting" of ferrous alloys. Several phenomena are now more clearly understood as a result of this experimental work.

CHAPTER I

PREVIOUS WORK CONCERNING IRON AND CARBON MONOXIDE

Historical

Historically, the study of iron-carbon monoxide reactions has been inextricably related to the iron and steel industry. The art of iron ore smelting was known to the ancients, and their production techniques of small batch operations persisted until 1860. Even Britain's expanded use of cast iron during the first half of the nineteenth century resulted in little technical advancement of blast furnace technology. Bessemer's innovation of an inexpensive method for producing steel in 1859 initiated a hundredfold increase of iron production during the following century (1). The ensuing search for higher quality products and more economical operations has created many works alluding, if not directed, to the iron-carbon monoxide interaction and problems resulting from it.

The initial major published work concerning the iron-carbon interaction is an 1869 report to the London Chemical Society by Bell (2), in which he describes blast furnace chemistry and elaborates on related modifications yielding more economical operations.

Analysis of a maintenance problem resulted in the first recorded recognition that iron catalyzes the deposition of carbon from carbon monoxide gas. In 1876, Pattinson (3) postulated that small quantities of iron in the furnace brick caused carbon deposits, and, subsequently,

the disintegration of the fire brick.

Boudouard (4) conducted the first recognized scientific experiments on the $2CO \rightleftarrows CO_2 + C$ equilibrium (reaction) in 1901. Although he studied the above equilibrium in the presence of graphite, the work was mainly concerned with the CO reduction of iron oxides and the subsequent deposition of carbon. The oxides were concluded as catalyzing the carbon deposition. Subsequently, the $2CO \rightarrow CO_2 + C$ reaction has been commonly referred to as the Boudouard reaction.

Blast furnace conditions and practical considerations were emphasized by the investigations during the next 20 years, with a gradual evolution toward scientific and fundamental analyses of the intrinsic reactions. Charpy first looked at the carbon monoxide-iron-iron oxide reactions, but later extended research to other metals and their oxides (5,6). Also, Charpy was one of the first to realize that elementary carbon, as such, will not react with the iron (7). The Boudouard reaction was studied in equilibrium with the carbon (8) over a range of temperatures and pressures in 1911.

Schenck and Zimmerman (9) investigated the $2CO \rightleftarrows CO_2 + C$ equilibrium concluding that the metal itself catalyzed the decomposition of the CO. Later, Hilpert and Dieckmann (10) studied the reaction, attempting to resolve the differences between the conclusions of Boudouard and Schenck. This work appears to be more refined: they postulated that neither the oxide nor base metal acted as a catalyst, but an iron carbide formed during the reaction, and a carbide mechanism was postulated. Falcke (11) noted that sample history played a major role in determining reactivity, and commented on the complexity of the

reaction. Falcke, along with Stoffel (12) was an initial investigator of iron carbonyl.

The first basic and comprehensive scientific study using highly purified iron and carbon monoxide was performed by Carpenter and Smith (13) in 1918. Great difficulty in analyses was encountered; they suggested that the reaction was very complex in nature and that definitive understanding of its nature was impossible.

The decades of the 1920's and 1930's are characterized by a gradual trend away from research dictated by immediate production problems. Also, this era was dominated by several scientists; namely, Schenck, Hofmann, Falcke and Baukloh, who devoted major efforts to this field.

Matsubara (16) in 1922 investigated the iron-iron oxide equilibria concomitant to the Boudouard equilibrium and the pressure effect. Their theory was applied to casting practice and blast furnace reactions. A similar study was conducted by Johansson and Von Seth (17); steels of varying carbon content were reacted in carbon monoxide-carbon dioxide mixtures between 700°C and 1100°C. Carburizing ability of the gases and practical applications are deduced from the results. Falcke and Fischer (18) determined equations for the Boudouard reaction. Tropsch and Philippovich (19) explored the catalyzing ability of numerous metals and oxides on carbon monoxide decomposition at 400°C. Schenck and his coworkers (20,21,22) conducted an extensive series of studies on the equilibrium between iron, oxygen, and carbon, using carbon monoxide-carbon dioxide and hydrogen-methane mixtures. Some of his results are explained by percarbides (Fe_xC) and sub-oxides. Many of Schenck's results were

later disputed, owing to analyses, impurity complications, and failure to reach equilibrium. In 1928, Hofmann (23), and Hofmann and Groll (24) studied the decomposition of carbon monoxide at 400 to 700°C, observing the formation of an x-carbide, richer in carbon than cementite. Tutiya (26,27,28) alleged that Hofmann's carbide was spurious, attributing x-ray lines to oxides and free carbon and stating that cementite catalyzed the decomposition of carbon monoxide. He later rescinded this conclusion and corroborated the presence of another carbide. Bramley and Lord (29), in 1932, published a lengthy paper on the equilibria of steels with $CO-CO_2$ mixtures at 750°C to 1150°C.

There are several unresolved contentions among these authors: (1) the actual catalyzing agent, iron, iron oxide or iron carbide, (2) the presence of higher carbon carbides, and (3) the ability of carbon monoxide to oxidize. These issues prompted a more basic type of research to establish more fundamental data; however, others, such as Wüst (25), continued to study the practical aspects.

It should be noted that the experiments cover a multitude of parameters, many difficult or impossible to categorize. For example, to catalyze the reaction, researchers have used iron sheet, pulverized iron, carbonyl iron, iron wires, iron oxides, cementite, hydrogen reduced iron oxide, specialized iron base catalysts, carbon steels, alloy steels, and iron-carbon mixtures. The reacting gases have ranged from pure carbon monoxide and prepared mixtures, to undefined industrial gases. Reaction temperatures range from 300°C to 1150°C and include two phase changes. The system is further complicated by the difficulty of observing and analyzing at the reaction temperature. A number of

techniques were used, none of which were conspicuously successful. Some of the major methods were: (1) terminal weight gain (most common); (2) pressure measurements; (3) CO - CO_2 analysis; (4) magnetic susceptibility measurements and (5) analysis of room temperature products and structure.

These many parameters preclude an accurate comparative analysis and explain the conflict of results and disparity of conclusions encountered in the literature. Contemporary researchers have performed work in depth, dealing with specialized areas. These works will be cited later where appropriate. Numerous industrial studies remain inaccessible in company files. Industrial work will be given separately because of its isolated nature.

Literature Review

In the literature relating to carbon monoxide reacting with iron substances, two questions persistently recur: (1) What substance functions as the catalyst? and (2) What are the reaction products? That the compounds formed can be easily resolved by modern techniques is specious reasoning. Impeding accurate analyses are: the presence of an eutectoid allotropic transformation in the region of study (see Figure 1), the difficulty of examination under experimental conditions, the metastability of many suspected reaction intermediaries, and the similarity of these products when analyzed by the various identification techniques.

Further complicating the studies is the large number of possible products. In a reaction system consisting of only three elements, the

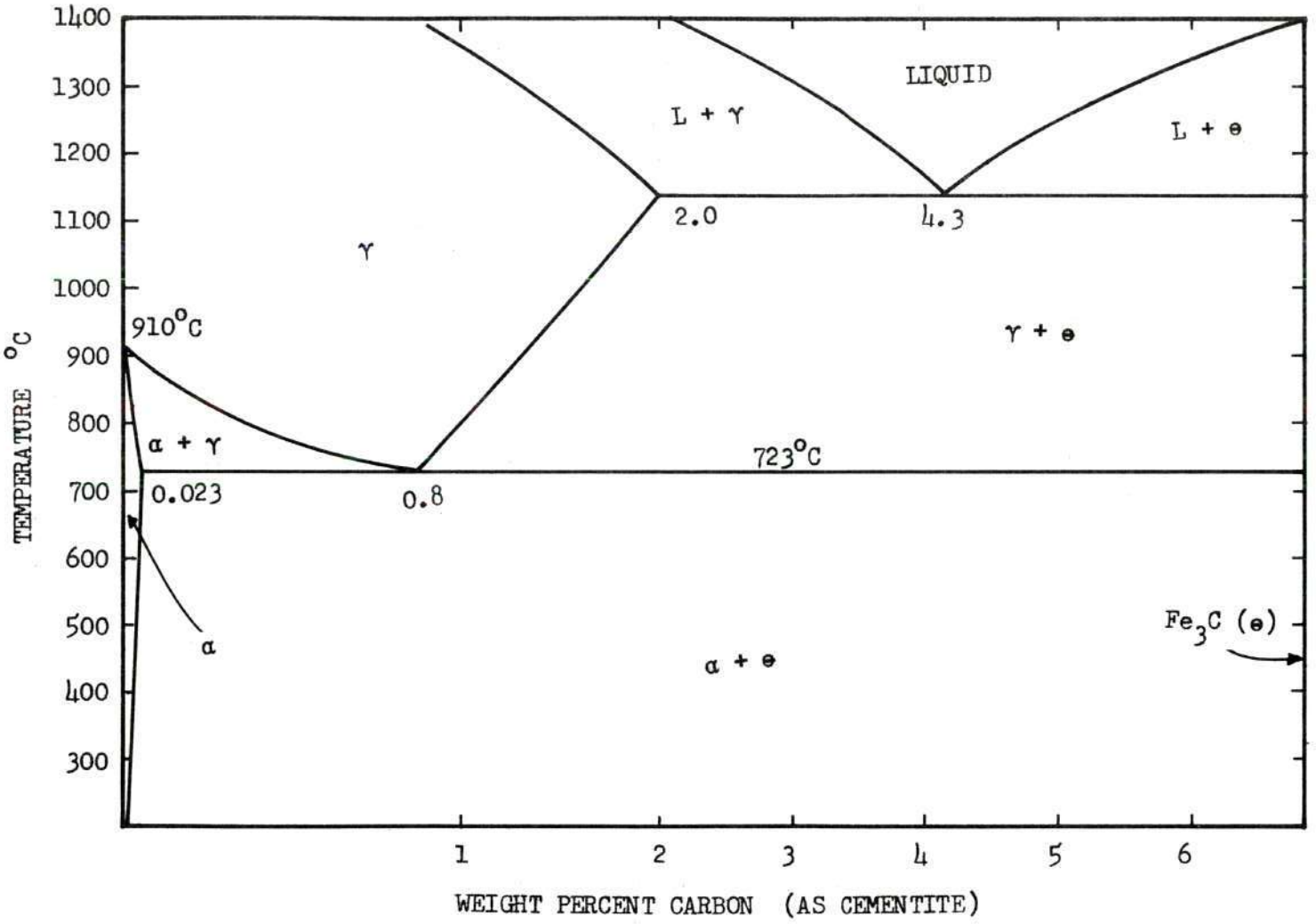

Figure 1. Iron-Cementite Equilibrium Phase Diagram

iron-carbon-oxygen system has a myriad of probable products as a result of solutions, complexes and oxidation states. Possible products include: (1) deposited carbon, (2) iron-carbon solid solutions (α-iron, γ-iron), (3) iron carbides, (4) iron oxides: wüstite (FeO), magnetite (Fe_3O_4), and hematite (Fe_2O_3), (5) mixtures or complex solid solutions of the above phases, and (6) complexes of carbon monoxide, such as iron pentacarbonyl ($Fe(CO)_5$).

The Iron-Carbon Systems

The iron-carbon system is characterized by either the iron-graphite or the iron-cementite equilibrium diagram. In a relatively pure iron-carbon system the iron-iron carbide diagram is the most congruent. The major features of the iron-iron carbide phase diagram, Figure 1, have been well established (87,38,39,88). However, it is important to realize the limitations of an equilibrium diagram, in that the rate of attainment of equilibrium and the kinetics of phase transformation must be considered in any practical situation. Furthermore, the "equilibrium" phase, cementite (Fe_3C), on the right end of the diagram, is in reality metastable and decomposes to iron and graphite under certain conditions (89). At temperatures below the eutectoid, the iron is a body-centered cubic phase known as ferrite (α). Above the eutectoid transformation temperature of 723°C, the face-centered cubic iron structure, austenite (γ) can be formed. Both phases dissolve carbon interstitially. Between 723°C and 910°C and at appropriate carbon concentrations, a two-phase mixture of austenite and ferrite exists. The most salient feature of the austenite compared to the ferrite is its

ability to dissolve carbon; the maximum dissolved carbon in ferrite is 0.0023 at 723°C while austenite has a capacity for 0.8 to 2.0 weight per cent carbon depending on the temperature.

Cementite, although less stable than graphite, is formed in preference to graphite in a pure system because of kinetic factors. The presence of impurities in the iron (silicon and sulfur) will promote graphite formation. With slight modifications, the iron-graphite equilibrium diagram is the same as the iron-cementite system exhibited as Figure 1. Figure 2 (15) compares the equilibrium factors of cementite and graphite in a pure system for the region of interest. Note the near coincidence of the graphite and cementite solubility lines: the exact location has yet to be resolved. Below temperatures of approximately 900°C graphite is the equilibrium phase, but cementite has been observed to form and last indefinitely.

The phases and compounds observed at room temperature are not necessarily those which existed at experimental conditions and identification of the high temperature phases must be established through its relation to the room temperature phases.

When a sample is exposed to a carburizing atmosphere in the temperature range of 723°C to 910°C, the carbon diffuses into the ferrite lattice forming austenite with higher carbon solubility. When the austenite is cooled, ferrite and graphite or cementite will precipitate maintaining the average concentration of dissolved carbon at the saturation level of the austenite (40). Under certain kinetic conditions, the cementite may decompose into iron and graphite (89).

▽ - (32) ○ - (34)

□ - (32) ◇ - (38)

△ - (31) ● - (34)

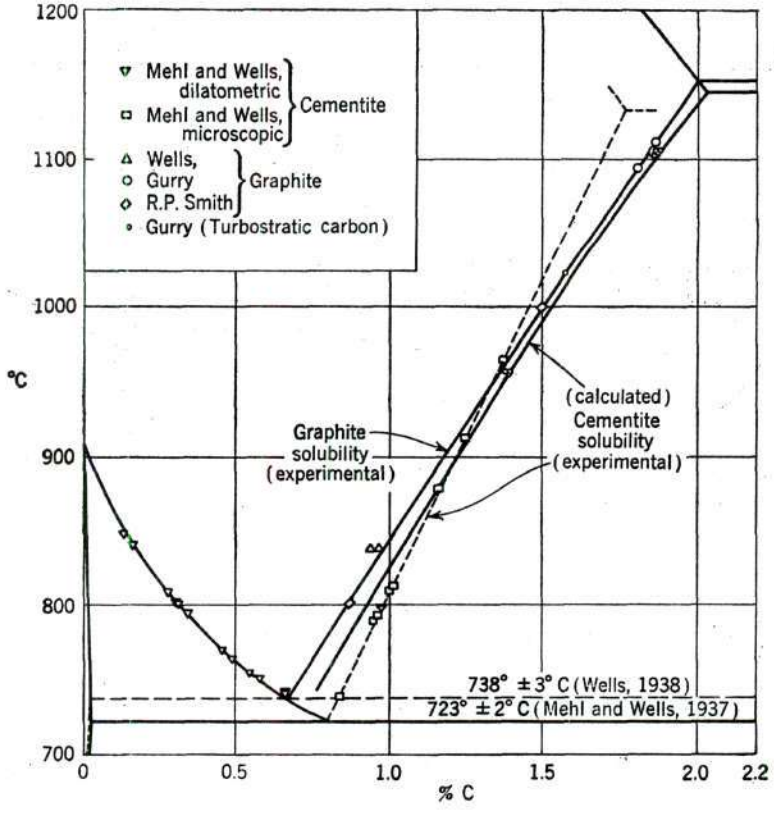

Figure 2. Cementite and Graphite Solubility in Gamma-Iron (15,65)

Figure 3 is an equilibrium diagram depicting the per cent carbon monoxide in a $CO-CO_2$ mixture for an equilibrium system as a function of temperature. Two systems are illustrated in this figure: first is the Boubouard equilibrium (S-shaped curve) for the reaction $2CO \rightleftarrows C + CO_2$ over graphite, the second (Y-shaped curve) shows carbon monoxide in equilibrium with magnetite, wüstite and iron. For example, a system at 800°C with 50 per cent CO is oxidizing with respect to iron, reducing with respect to magnetite will react with carbon to form additional carbon monoxide. It is axiomatic that any system with 100 per cent carbon monoxide is reducing, although the lower the temperature the greater the potential.

Carbides

Of the possible compounds which could be formed in the iron-carbon monoxide system, those which are the most intractable, and about which much has been written, are the carbides. The carbides are one of the more probable reaction products. Complications arise in the identification of these compounds because of their metastability, the relative large number of feasible structures in which they exist, and the similarity of physical properties. These factors tend to enhance the disparity between experimental conclusions.

The three major accepted carbides are: (1) cementite (Fe_3C), θ-carbide, with an orthorhombic structure; (2) Hägg, percarbide, or χ-carbide, (Fe_5C_2) (formerly Fe_2C and $Fe_{20}C_9$), has recently been classified with a monoclinic structure; and (3) ε-carbide (Fe_7C_3) with a hexagonal (hcp) structure. The relative stability at a temperature of approximately 400°C can be generally written as:

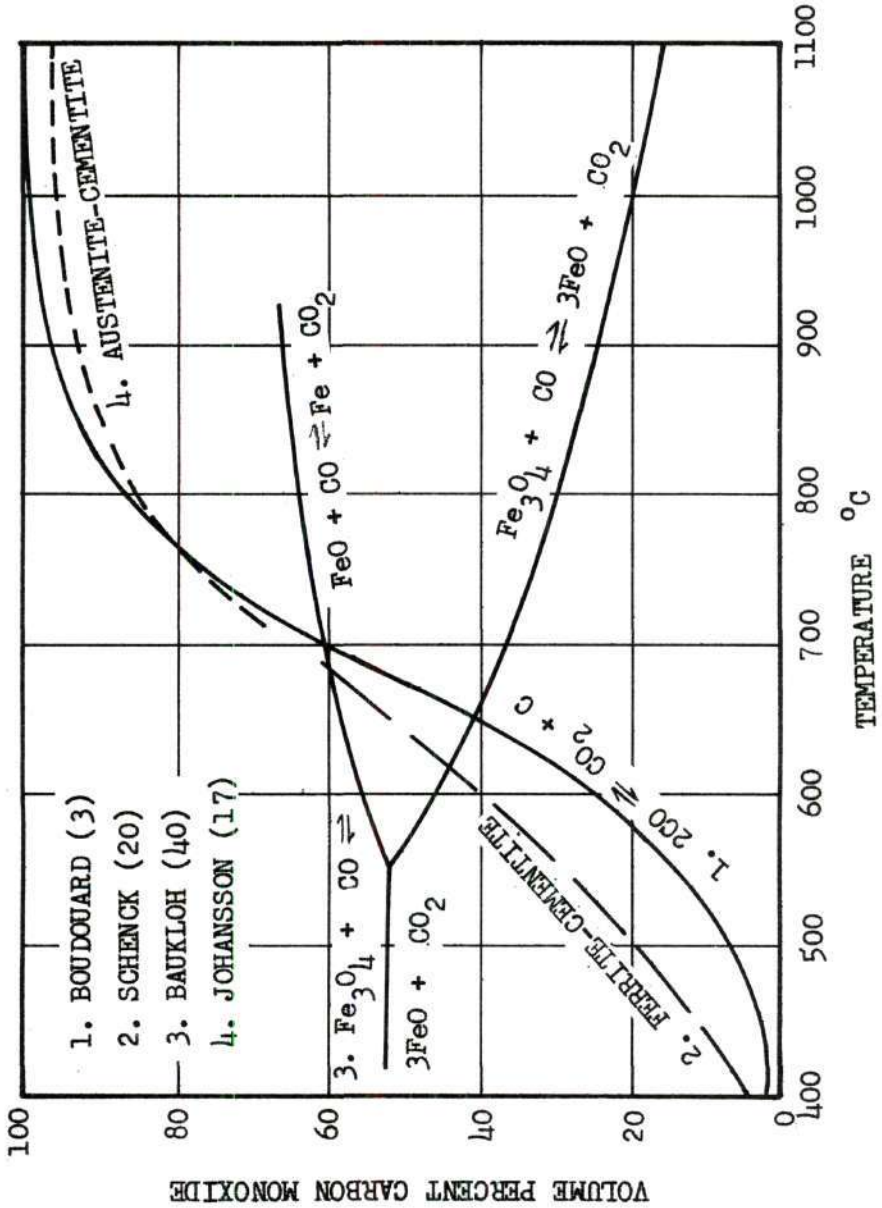

Figure 3. Equilibrium Curves for the Iron-Oxygen-Carbon System at One Atmosphere

$$Fe_7C_3(\varepsilon) \rightarrow C_{(gr)} + Fe_5C_2(\chi) \rightarrow C_{(gr)} + Fe_3C(\theta) \rightarrow C_{(gr)} + Fe(\alpha) \ . \quad (1)$$

A bureau of Mines Bulletin by Hofer (72), published in 1966, thoroughly summarizes the physical data and knowledge of the carbides through 1963. Unfortunately, this paper incorrectly identifies the formulae of ε and χ-carbides. More recently, these formulae have been revised simultaneously by Duggin and Hoffer (68), and Jack and Wild (69).

Hofer (72) states that ε-carbide is decomposed to χ-carbide in several hours at about 300°C. Further experiments indicated that ε-carbide is decomposed completely to χ-carbide in approximately eight hours at 525°C. The ε-carbide in these experiments was initially formed by the action of CO on iron. The above transformation sequence has also been reported at 400°C in another work (90), while carburizing α-iron with carbon monoxide. Schenck, Nacken and Potthast (77) have seen these changes in a carbide on single crystals of iron, formed at 400°C on a NaCl substrate, reacted in CO, and heat treated between 180°C and 240°C. Epsilon iron carbide was discovered in 1949 by Hofer, Cohn and Peebles (61) and has since assumed a central place in the carburization mechanism. It has a hexagonal (hcp) structure and was formerly listed as Fe_2C. The crystallographic properties of this carbide are established, but other properties elude definitization due to its transitory nature at higher temperatures.

At 250°C, and under restricted exposure, ε-carbide was the only product when finely divided α-iron was exposed to carbon monoxide (72). More complete carbiding at the same temperature yielded only χ-carbide;

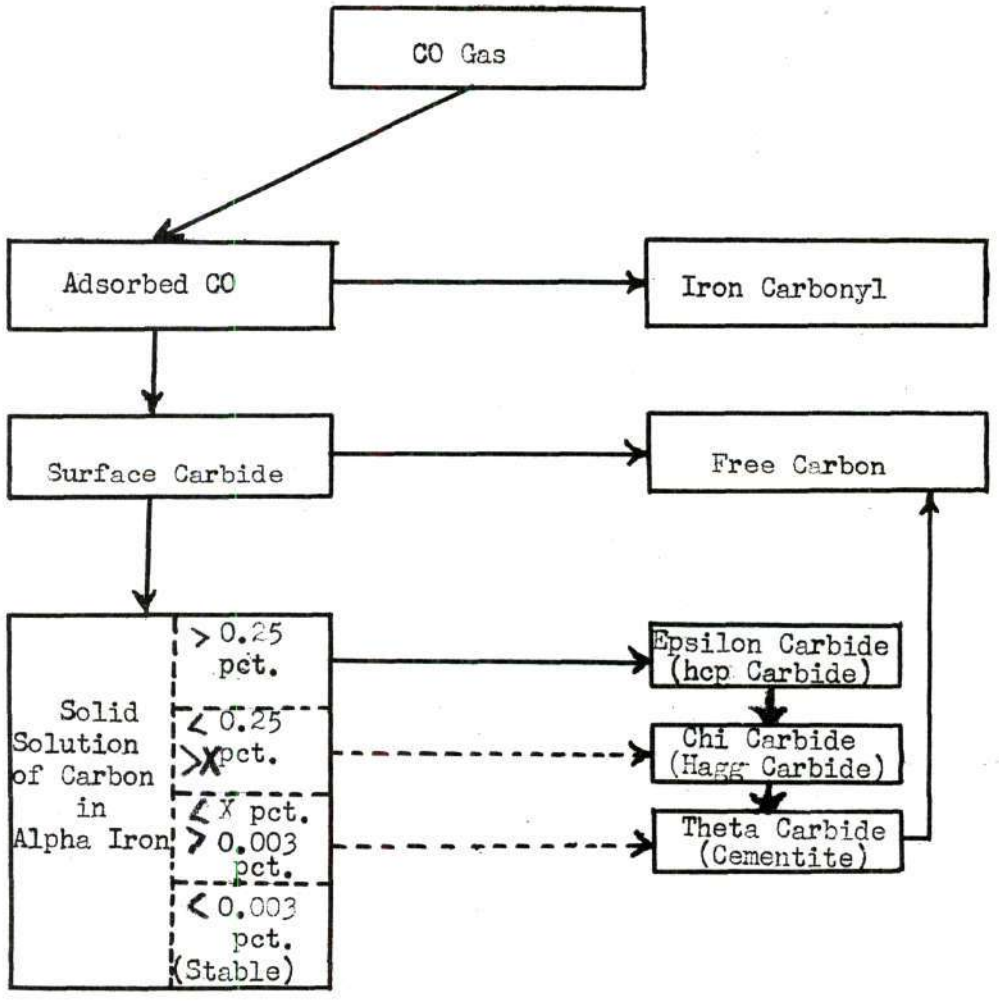

Figure 4. Hofer's (72) Sequence in the Direct Carburization of Alpha-Iron

thus, Hofer concludes that epsilon is the precursor of chi in the carburization process. However, it is interesting to note that the presence of ε-carbide in small amounts is noted at 315°C (the highest experimental temperature).

Hägg or chi iron carbide was discovered in 1934 and was hypothesized as an intermediate in the steel tempering process (91). Physical properties of this carbide now are fairly well established. Originally it was indexed using an orthohombic lattice and assigned a formula of Fe_2C and later $Fe_{20}C_9$. Finally, Jack and Wild (69) have established a Fe_5C_2 monoclinic structure.

Cementite, theta-iron carbide, is the best known of the three carbides and its physical and chemical properties are well established (87,40). It occurs in carbon steels as a component of pearlite and is considered the carbon containing phase in the iron-carbon diagram. Cementite is recognized as a metastable phase and under certain conditions will decompose to iron and carbon. Large particles of pure Fe_3C tend to decompose, but it is stabilized by portions of ferrite finely mixed in integral solution (this is white cast iron and pearlite). Cementite is also known to be stabilized by alloy addition. At temperatures from 630°C to 1100°C, it was observed not to form in carburizing atmospheres (40). Schenck and co-workers (77) noted that theta decomposed at 750°C.

Several other carbides have been observed under unusual conditions, the latest being a metastable hexagonal (hcp) form similar to epsilon. It is obtained by drastic quenching and lasts about a month at room temperature (74).

Although much work has been done on carburizing iron substances in carbon monoxide atmospheres, much of it does not evince the type of carbides present due to the mutable knowledge about them. This is particularly true in industrial carburizing studies. Little work has been done in this area in the past ten years.

As early as 1915, Hilbert and Dieckmann (10) proposed a carbide equilibrium for the decomposition of carbon monoxide on iron. In 1918, Carpenter and Smith (13) observed a substance thought to be a carbide at 650°C. In 1928 Hofmann (23) reacted CO over iron at 400°C to 700°C and observed an "x-carbide" which subsequently decomposed. X-ray attempts to characterize it as cementite were inconclusive. Tutiya, who earlier had discounted Hofmann's above "x-carbide" as wüstite (26,27), later alleged that a carbide Fe_xC is formed which decomposed to cementite and carbon. Körber, Wiemer and Fischer (42) observed that graphite-iron-cementite in carbon monoxide are entirely converted to cementite at 500°C. In 1950, Hofer and Cohn (60) formed cementite from Hägg carbide; magnetic measurements show that the reaction is always complete below 500°C and sometimes as low as 260°C. Trillot and Oketani (51) formed Fe_3C in one hour at 540°C; however, at temperatures below 500°C or above 820°C, no evidence of cementite is seen. X-ray analysis of carbon deposits from blast furnace brick reported by Davis, Slawson and Rigby (48) in 1953, contained Fe_3C and percarbide ($Fe_{20}C_9$) as well as amorphous carbon. Berry, Ames and Snow (33) synthesized Hägg carbide at 480°C and 540°C and a modified cementite at 630°C and 680°C, while no carbides were observed at 700°C. In 1962, Hui and Boulle (55) noted Fe_2C at 250°C to 300°C, and cementite at 550°C. The Dragon Project (92)

purports the formation of active centers of Fe_7C_3 at 550°C with greater stability than the Hägg carbide coupled with an intergranular precipitation of cementite in the matrix.

The findings above are summarized in Table 1.

Carbon Deposits

In the decomposition of carbon monoxide, carbon, obviously, will be one of the major products, present either internally in the metal matrix, or deposited on the surface. Samples reacted above 700°C tend to possess the internal form, while the lower temperature reactions result in more of a sooty surface product. Both amorphous and graphite have been observed as surface carbon. The physical form was both soot and filamentary.

Many of the early researchers did not attempt to ascertain carbon morphology of the reaction product. Hofmann (23) reported that carbon deposited from pure carbon monoxide at 400-700°C was distinctly crystalline, implicating carbide decomposition. Hofmann and Groll (24), in a later work, identified graphite by x-ray analysis as a product from 450° to 650°C. Akamatsu and Sato (50) studied the initial stages of the carbon monoxide reaction on iron at 500°C. After the iron lost its metallic luster, but before carbon formed, only cementite was identified by the x-rays. After surface blackening appeared, a pattern for principally amorphous carbon, with traces of cementite, was obtained and a prolonged reaction resulted in graphite. Chatterjee and Das (47) report a predominantly graphite spectrum from reaction products of iron and carbon monoxide at 500°C.

Table 1. Summary of Reaction Products

Temperature °C	Reaction Product	Initial Iron Form	Atmosphere	Year	Reference
540	Fe_3C	Fe	CO	1950	51
< 500	No Fe_3C	Fe	CO	1950	51
> 540	Graphite	Fe	CO	1950	51
> 820	No Fe_3C	Fe	CO	1950	51
100	$Fe(CO)_5$	Fe_2O_3 reduced H_2	CO	1962	55
250-300	Fe_2C	Fe_2O_3 reduced H_2	CO	1962	55
550	Fe_3C	Fe_2O_3 reduced H_2	CO	1962	55
< 550	Fe_3C (complete)	Hägg carbide	CO	1950	60
650	Carbide	Electro Fe	CO	1918	13
400-700	Carbon, carbide	Fe	CO	1928	23
700	"x-carbide"	Fe	C_6H_6	1928	23
≤ 450	Graphite, Fe_3O_4	Carbonyl Fe	CO	1930	24
450-600	Graphite FeO	Carbonyl Fe	CO	1930	24
> 655	Fe, C, Fe_3C	Carbonyl Fe	CO	1930	24
450	Fe_3C, C(am), $Fe_{20}C_9$	Blast furnace brick	CO	1953	48

Table 1. Summary of Reaction Products
(Continued)

Temperature °C	Reaction Product	Initial Iron Form	Atmosphere	Year	Reference
500	Only Fe_3C	Fe - C	CO	1943	42
400-700	Carbon	Fe_2O_3	CO	1950	41
550	Carbide	Fe_2O_3	CO	1950	41
480-540	Carbide, Fe_3O_4	Fe_3O_4	CO	1956	33
630-680	Cementite, Fe_3O_4	Fe_3O_4	CO	1956	33
> 700	No carbide	Fe_3O_4	CO	1956	33
950	C	Fe_2O_3	CO	1915	10
< 800	C, carbide	Fe_2O_3	CO	1915	10
750	Fe_3C decomposes	Fe (film)	CO	1966	77
180	ε-Carbide	Fe (film)	CO	1966	77
300	Fe_xC	Fe	CO	1931	28
300	FeO	Fe	CO	1929	27
600-700	Fe_3O_4,FeO,Fe,Fe_3C	Fe - Fe_3C	CO-CO_2eq	1927	22
450-630	Carbon, Fe_3C	Fe catalysts	CO	1959	36
550	Fe_3C interior; Fe_7C_3 surface	Fe films	CO	1965	92
500-700	Carbonyl-cementite	Fe	CO	1953	47

Threadlike carbon deposits on an iron catalyst reacted in CO at 600°C are reported by Radushkevich and Luk'yanovich (52). The authors state that the worm-like particles apparently consisted of iron carbides and graphite. Hofer, Sterling and McCartney (64) observed filamentary growth at 390°C from iron reacting with carbon monoxide. Walker, Rukszawski and Imperial (36) studied carbon filaments formed from the decomposition of CO over iron in carbon monoxide-hydrogen mixtures. At the center of growth, a particle of iron or iron carbide was located, presumably the catalyst for that particular filament. The crystalline character of the carbon increased to a maximum at about 550°C and then declined. Hofer (72) reacted carbon monoxide with an iron catalyst at 390°C. He observed filaments approximately 0.1 micron in diameter which contained an elliptical opaque spot near the midpoint. X-ray analysis revealed carbon as the major constituent. Ruston and co-workers (92) reacted carbon monoxide on iron films at 550°C observing whiskers and lamellar graphite flakes. The thin lamellar flakes were located in the immediate vicinity of the metal and were postulated to result from the rendering of protruding surface cementite crystals to graphite and ferrite. The whiskers were alleged to be growing from small crystals of ε-carbide (Fe_7C_3) on the metal surface. A small crystal of Fe_7C_3 was also found on the extremity of each filament. Hochman (93) also has noted a filamentary growth from iron reacted in CO; furthermore, similar products were found when nickel, cobalt and stainless steels were reacted in carbon monoxide. In the case of iron, x-ray diffraction established the presence of graphite and distorted lattices of Fe_2C and Fe_3C. Electron diffraction patterns indicated the presence of more than one

nucleus in each filament.

Oxides

Oxide formation in a pure carbon monoxide-iron system is nearly precluded; Figure 3 illustrates the relevant equilibrium data. However, the presence of additional substances, even in minute quantities either solid or gaseous, can alter the curves of Figure 3. Hence, the verity of published information can be challenged if the impurity level of the constituents is unknown.

Experiments using oxide as the initial material reveal that carbon deposition will occur before the oxide has been completely reduced to base metal (3,4). Taylor (56), reacting iron oxide in carbon monoxide, theorizes that the Fe - Fe_3O_4 interface serves as an active site for the reaction. Hofmann and Groll (24) exposed pure iron with carbon monoxide and report Fe_3O_4 as a product at 450°C and FeO formed at temperatures up to 650°C. Baukloh and Henke (76) noted that the form of oxide or iron did not affect the temperature of maximum CO decomposition.

Carbonyls

The presence of iron pentacarbonyl ($Fe(CO)_5$) is not uncommon at room temperature and it has been suggested that such a compound could be metastable and a feasible activated reaction intermediate; however, this is difficult to rationalize because of adverse thermodynamic conditions at elevated temperatures. Stoffel (12) states that $Fe(CO)_5$ decomposition begins at 60°C and is complete at 100°C. From Carlton and Oxley's (63) equilibrium calculations, the iron pentacarbonyl should be 99 per cent decomposed at 60°C. Ross, Haynie and Hochman (66) have compiled free energy data on this compound and report an equilibrium constant of

10^{-17} at 423°C.

Mechanism

The catalytic mechanism has eluded definition because of the variety of possible catalytic phases and the inability to completely observe the reaction as it occurs. Furthermore, as mentioned earlier, the variety of experimental conditions and parameters available to investigators impedes accurate comparison of the data.

The mechanism of carbon monoxide decomposing over iron can be divided into two general cases: (1) that of the surface build up of carbon on ferrite at lower temperatures, and (2) the carbon dissolution in the matrix of austenite at the higher temperatures. A high-temperature (above 723°C) mechanism has been proposed by Taylor (56): (1) adsorption of CO at active centers, (2) decomposition, (3) CO_2 desorption, and (4) migration of carbon into the lattice. The high free energy of atomic carbon avowedly permits this phase to be super-saturated, relative to both cementite and graphite. The mechanism for carbon surface deposition is more complex. Formation of a carbon rich carbide and a stepwise decomposition ending with cementite has recently been proposed (72,77). The exact composition and structure of carbides observed by researchers is ambiguous as noted earlier. Hofer (72) proposes the mechanism for low temperature as shown in Figure 4. A carbide equilibrium (decomposition) was proposed as early as 1915 (10). Also Tutiya (28) postulated that Fe_xC decomposed to cementite and carbon. Davis Slawson and Rigby (48) have suggested a similar mechanism. Baukloh and Henke (76) stated that the mechanism was a decomposition in the adsorption layer. Olmer (45) was presented a physical modification,

where particles agglomerate suddenly causing the capacity for adsorption to decrease. The possibility of a transient carbonyl mechanism has also been expressed (17).

The "catalysts" used by experimenters have varied greatly, consisting of iron powders, single crystals, oxides, wires, plates and "iron catalysts." The actual reaction catalyzing agent has been declared a carbide (10,26,27,42), an oxide (58), or the metallic iron (9,30,41,43,46,49,53,76). Other authors have made negative conclusions: cementite is not the catalyst (33,53) and metal is not the catalyst (33).

The preponderance of opinion is that metallic iron is the catalyst, and this is the trend of the more recent works, although there is no direct or convincing evidence to support such a conclusion.

Baukloh and Henke (76) started from all three oxides and metallic iron, observed the same temperature for maximum decomposition for each, and concluded iron was the catalyst. Previously, Baukloh (30) had studied decomposition of carbon monoxide over a large number of metal oxides and concluded that the metals catalyzed the reaction. Baukloh and others (41,43,53) attributed a rate decrease with time (1 hour) due to formation of a carbide at 550°C. Heating in a hydrogen atmosphere after reaction slightly regenerated the catalyst. Hydrogen supposedly reduces the carbide to iron and thus metal is deemed the catalyst.

Körbner, Wiemer, and Fischer (42) experimented with addition of graphite and cementite to iron systems and observed maxima at about 550°C and 900°C. Carbon was found to be neutral, while cementite caused a pronounced maximum at 550°C, the magnitude dependent on the cementite

Table 2. Summary of Catalytic Agents

Temperature °C	Catalyst	Initial Iron Form	Atmosphere	Year	Reference
500-700	Oxide	Fe_2O_3	N_2	1949	58
400-700	Metal	Fe_2O_3	CO	1953	46
400-700	Metal	Fe_2O_3	CO	1950	41
550, 900	Metal	Fe_2O_3	CO	1952	43
550	Metal	Fe,FeO,Fe_2O_3	CO	1940	76
450-750	Metal	Metal oxides	CO	1936	30
310-508	Metal	Fe_2O_3	CO	1903	9
500-700	Not Metal, Fe_3C or Fe_3O_4	Fe_3O_4	CO	1956	33
700-950	Carbide	Fe oxide	CO	1915	10
465	Carbide	Fe	CO	1929	26,27
500-600	Cementite	Fe-Fe_3C-C	CO	1943	42
450	Iron-carbide equi	Furnace Brick	CO	1953	48
550-700	Fe/Fe_3O_4 interface	Fe powder	CO	1956	56
700-1100	Carbonyl formation	Fe	CO	1926	17
550	Fe_7C_3	Fe film	CO	1965	92
300-800	Not carbide	Fe	CO	1942	45
500-900	Not Fe_3O_4 or Fe_2O_3	Iron-graphite	CO_2	1963	35
400-800	Oxide	Iron-iron oxide	CO	1901	4
450-900	Metal	Fe,Fe_2O_3	CO	1947	49

concentration. At 500°C magnetic measurements showed almost entire transformation to cementite. Korber's (42) technique has been heavily criticized by Baukloh for type of analysis (Örsat) and method of cementite preparation. Berry, Ames, and Snow (33) using magnetic susceptibility analysis and Fe_3O_4 powder reacted in CO found a 220°C to 240°C Curie point for samples treated at 480°C and 540°C. They concluded that Hägg carbide is the active catalyst.

At 630°C to 680°C cementite and magnetite were observed. Above 700°C deposition ceased, metallic iron was obtained, and no carbides were detected. From this they concluded that metal was not the catalyst.

Kinetics

There is a dearth of kinetic data on the carbon monoxide decomposition or carburization of iron. The existing data are restive because of the heretofore mentioned variety of parameters. Both linear and "S-shaped" rate curves have been reported. Apparently, a maximum amount of carbon can be deposited or absorbed at any given conditions, resulting in the "S-shaped" curve; while under less stringent conditions, linear rates would be possible.

Walker, Rakszawski, and Imperial (36) reacted pure iron in CO-H_2 mixtures at temperatures of 470°C to 630°C, and observed linear rates. Pettit, Yinger, and Wagner (67) oxidized iron in carbon dioxide and encountered "S-shaped" curves for complete oxidation. Baukloh, Chaterjee, and Das (41) observed a rate increase at 550°C for about an hour and then the rate decreased. This phenomenon was attributed to the formation of a carbide. Taylor (58) also reported a bell-shaped rate

curve with a maximum of one hour, but an iron oxide was used and the observations could be attributed to a reduction reaction. Hochman (93) has parabolic reaction curves for a number of austenitic stainless steels reacted in carbon monoxide.

When considering reaction rates or amount of carbon deposition as a function of temperature, most authors concur that a maximum occurs at approximately 550°C. Isolated citings of other maxima are seen, but there is little support or confirmation for them. Baukloh, Chaterjee, and Das (41), Baukloh and Edwin (78), Fleureau (47), Körber, Weimer, and Fischer (42), Olmer (45), and Hochman (93) are among those reporting a rate maximum for the decomposition of carbon monoxide over iron at approximately 550°C. Olmer (45) has also reported a much smaller maximum at 775°C. Körber, Wiemer and Fischer have reported a maximum at 900°C.

The rate-determining step is hard to define without a definite mechanism; it is most often attributed to diffusion. W. Baukloh, Chaterjee, and Das (41), state that it is dependent on the formation of a carbide which is unreactive. R. Baukloh, Knacke and Löscher (59) consider diffusion the rate-determining step. Das and Chaterjee (43) also note diffusion resistance. Pettit, Yinger and Wagner (67), studying the oxidation of iron by CO_2 deduced the dissociation of the CO_2 as the controlling step. Hochman's (93) rate data for certain stainless steels is a linear function versus square root of time, also characteristic of diffusion.

Incubation, before initial reaction begins, has been noted by Rhead Wheeler (8). Also, Akamatsu and Sato (50) state that it requires

5 to 10 hours for the reaction to begin at 500°C, and then reaction proceeds slowly but homogeneously.

Henry (37) has presented a mathematical model for high CO concentrations and assuming adsorption at active sites. Agreement with physical kinetic data is good.

Industrial Experience

Problems related to the Boudouard or Bell reaction abound in industry, especially in cases where the reaction is catalyzed by iron, nickel, cobalt, and their alloys. As noted in the historical review, many of the original studies were prompted by practical problems; later, more scientific work is complicated by the fact that the results are inadequate or too limited to be satisfactory.

Some of the areas dealing with the CO - CO_2 equilibrium in one fashion or another are: blast furnace and steel producing processes, ferrous casting techniques, carburizing treatments, systems dealing with industrial combustion gases, reactor technology, and the petroleum industry. In some fields the problems are tractable and present no special hardships by their presence; other cases are disguised by simultaneous and/or competing reactions and are either unrecognized or ignored; in still further instances, the problem is accepted either because of a lack of severity, or because of economic considerations. It is from this last classification which problems continue to emanate, especially in the chemical and petroleum industry as equipment life is extended and operating parameters become less tolerant.

It is difficult to separate the array of industrial literature and determine which area is more applicable or pertinent to this

dissertation. However, recent petroleum processing experiences are cited because they express the incongruous nature of the industrial problems; furthermore, studies in this area were a precursor to this work. Some representative cases of recent vintage have been selected to acquaint the reader with a brief history and scope of the problem.

Metal Dusting

The continuing demand for efficient and economical operation of petroleum equipment has resulted in an increase in operation life, which has led to a catastrophic corrosion of the equipment. This has been recognized in the last decade and termed "metal dusting." References to this phenomenon are found in the literature, and certainly many unpublished cases also exist. The varied nature of "metal dusting" is exemplified by the fact that there is no precise concurrence on the definition of the reaction.

At the 1963 Annual Conference of the National Association of Corrosion Engineers, "metal dusting" was defined as follows:

1. *Environment*--gas phase; potentially carburizing and reducing, with or without oxygen.

2. *Temperature*--usually 450°C to 800°C.

3. *Form*--localized or general pitting and/or general overall surface wastage; surface usually carburized.

4. *Product*--dust or powder composed of graphite mixed with metal, metal carbides and metal oxides.

At a regional N.A.C.E. meeting at Georgia Tech in 1967, it was still impossible to obtain a more concise description of "metal dusting."

Crude petroleum processing equipment has always been severely attacked. Sulfur content of the crude has been recognized as the major factor in controlling catastrophic corrosion; but as early as 1937, it was realized that sulfur content was not a direct measure of the corrosion tendencies.

Camp, Phillips, and Gross (94) document one of the first cases of catastrophic "metal dusting" corrosion. Their investigation concerned the failure of 304 stainless steel cracking tubes in one butadiene plant, contrasted with a similar plant where corresponding pipes had an excellent record of corrosion resistance.

Inspection of the tubes showed they were severely carburized; both heavy pitting and uniform surface attack were noted. Their studies indicated that a small amount of sulfur (present as mercaptans, carbon disulfide, or free sulfur), in concentrations up to 0.5 per cent, will act as an excellent inhibitor for the above corrosion.

Another well documented report, by Burns (82), appeared in 1950, and related heavy corrosion with low sulfur charges. One curious aspect is that the case presented occurred in new equipment, while an exact duplicate process had performed acceptably for several years previous. The carbon steel equipment operated for less than a year with several major shutdowns. Many replacements were required due to severe pitting. Burns states that temperature is the most significant variable. Although the operating temperature was only 300°C, "hot spots" of 750°C were probable. Major blame is placed on the iron sulfide found, but mention is made of sooty carbon deposits in and around the corroded area and it is quite likely this is a case of metal dusting.

In 1946, Hubbell (83) noted a problem of aircraft exhaust manifolds subject to carbon and carbon monoxide attack at high temperatures.

In 1959, Hoyt and Caughey (80) cited a case of "metal dusting" corrosion which was the first in a series of articles on this subject appearing during the next four years. Reported was deterioration of 310 stainless steel surfaces in a process producing gasoline from coal. Attack was first observed after 125 days at temperatures of 650°C to 700°C, but various types of corrosion were noticed at different times and in various places. Intergranular attack, as well as severe pitting and general metal loss, were found. Attack was inconsistent in the same tube. He concluded that optimum conditions vary from gas to gas. He theorized that the metal is corroded away by threads of carbon which are attached to metal particles which are easily lifted from the surface.

Prange (85) investigated stainless steels in corroding gas atmospheres and commented on the complex nature of the problem. He concluded that oxidation was not the significant cause, since copper, which possesses poor oxidation resistance, is not attacked. Corrosion was found to be localized; small changes in alloy composition resulted in large differences in resistance. Prange postulated an unstable vapor phase explanation.

Eberle and Wylie (86) exposed AISI types 310 and 347 stainless steel to the combustion products of methane at various temperatures. At 900°C to 1000°C, intergranular oxidation was blamed for the corrosion. With decreasing temperature, heavy carburization was accompanied with occasional oxide formation. The severest attack was at approximately 600°C. Cyclic carburization, oxidation and reduction were deemed the

probable cause of the wastage. Since materials most resistant to carburizing displayed the best performances, carburization was considered a major factor.

A case of heavy pitting in chromium-nickel alloy steel is mentioned by Merrick (84) in 1960. The pits were reddish-brown, and were formed in a temperature range of 750°C to 1100°C. In contrast with the experience of Burns' (82) work with carbon steel, the presence of sulfur did not seem to affect the corrosion rate. The CO_2/CO ratio is concluded to be a determining factor, any value above two was stated as safe, but variances were noted, and experience in their pilot plant showed that a ratio of 0.2 was highly corrosive.

Hopkinson and Copson (81) reacted iron-nickel-chromium alloys in simulated industrial atmospheres consisting of varying amounts of CO, CO_2, H_2, and H_2O. Three different types of attack were observed: (1) pitting under carbon deposits, (2) internal oxidation without free carbon, and (3) heavy carbon deposits with exfoliation--characteristic of "metal dusting." Although specific conclusions are presented, the part played by carbon and carburization in the mechanism of attack could not be clearly defined.

Lefrancois and Hoyt (79) presented an article on the subject of metal dusting and thermodynamic analysis. Three distinct cases of metal dusting in stainless steels were examined to determine the compounds comprising the deposits, and to deduce their morphology. In two of the cases $M_{23}C_6$ and/or M_7C_3 were discovered; carbon soot and metal oxides were found in the pits of the third sample, and a protective silicate oxide was found on the unblemished surface. All three cases

exhibited severe pitting. After a thermodynamic analysis, the authors concluded that carbon monoxide reduces the oxide and "cracks" the protective coating exposing fresh metal to the carburizing atmosphere. From the results only a negative analysis was possible; iron and its oxides were deemed not principals, cementite, nickel carbide and the carbonyls were eliminated on the grounds of thermodynamic instability. The carbides, $M_{23}C_6$ and M_7C_3 by their presence, were associated with the mechanism of metal disintegration.

Hochman and Burson (14) have published the most recent work about metal dusting in which the major forms of metal dusting are discussed. Also, the reactivities of iron, nickel, cobalt, and their alloys are presented for a wide range of temperatures.

Pressure

The only apparent effect of moderate pressures in the decomposition of CO over iron is one of increased concentration. Baukloh and Edwin (78) have studied the deposition of carbon monoxide at pressures up to ten atmospheres and have noted only the effect of concentration change. Tenenbaum and Joseph (44) have applied Langmuir's mathematical analysis to blast furnace conditions and have computed a concentration factor for low pressures, so that the reaction rate $\left(\frac{dc}{dt}\right)$ at low pressures is a linear function of pressure.

Impurities

Impurities are known to have a decided affect on the deleterious attack and the rate of CO decomposition. The complexity and variety is immense and defies categorization. Numerous industrial experiences are known whereby very slight additions can strongly affect the severity

Several experimenters have studied slight additions in controlled environments. Walker, Rakszawski, and Imperial (36) have comprehensively studied the reaction of CO-H_2 mixtures over an iron catalyst. From 470°C to 570°C H_2 concentration effect is small, but from 570°C to 630°C, it is more pronounced. In an isolated case, pure CO was reacted and found to be substantially less reactive than the mixtures. Baukloh and Henke (76) stated that water retarded the decomposition of CO over iron. Akamatsu and Sato (50) noted that traces of O_2 and CO at 500°C retarded reaction with a plate but not with iron powder.

Many of the earlier experimenters were unable to eliminate sample history as a major parameter in reactivity measurements; however, contemporary scientists with more assiduous and controlled preparations have been able to reduce this factor as a variable (23,51,76).

CHAPTER II

EXPERIMENTAL APPARATUS

Three major pieces of apparatus were used for the experimental work: (1) a horizontal tube furnace using initial-terminal measurements, (2) a small reaction furnace allowing x-ray analysis of iron powders at the reaction temperature and (3) a microbalance system.

The major portion of the experimental work involved continuously recording weight changes of a wire specimen over a period of time with a microbalance. A reconditioned thermobalance, TH-59 and A.D.A.M.E.L. in Paris, France, was the nucleus around which the system was built. Figure 5 is a picture of this entire system, while Figure 6 is a schematic diagram of the setup.

The reacting gas, carbon monoxide, is supplied from a standard A-1 cylinder and was purchased from the Matheson Company. Three cylinders from one batch of gas were purchased, and quantitative analysis was made to establish the exact composition in each cylinder. The overall concentration of CO was determined to be 99.82 per cent (for detailed analysis see Table 6 in Appendix A).

A supply of helium was used when it was necessary to vent the system so that an excessive amount of atmospheric water vapor would not contaminate the system and poisonous carbon monoxide would not be drawn out of exit lines.

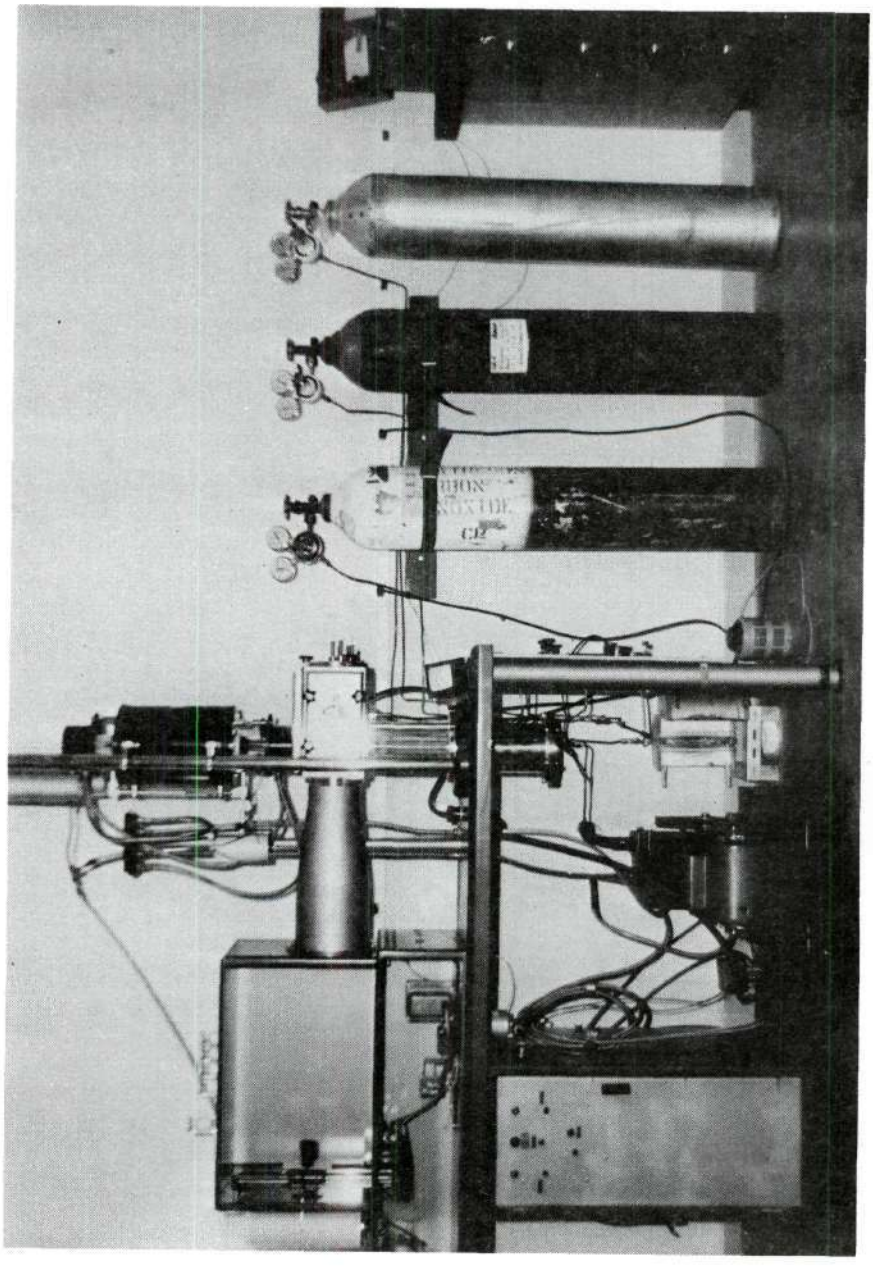

Figure 5. Thermobalance System

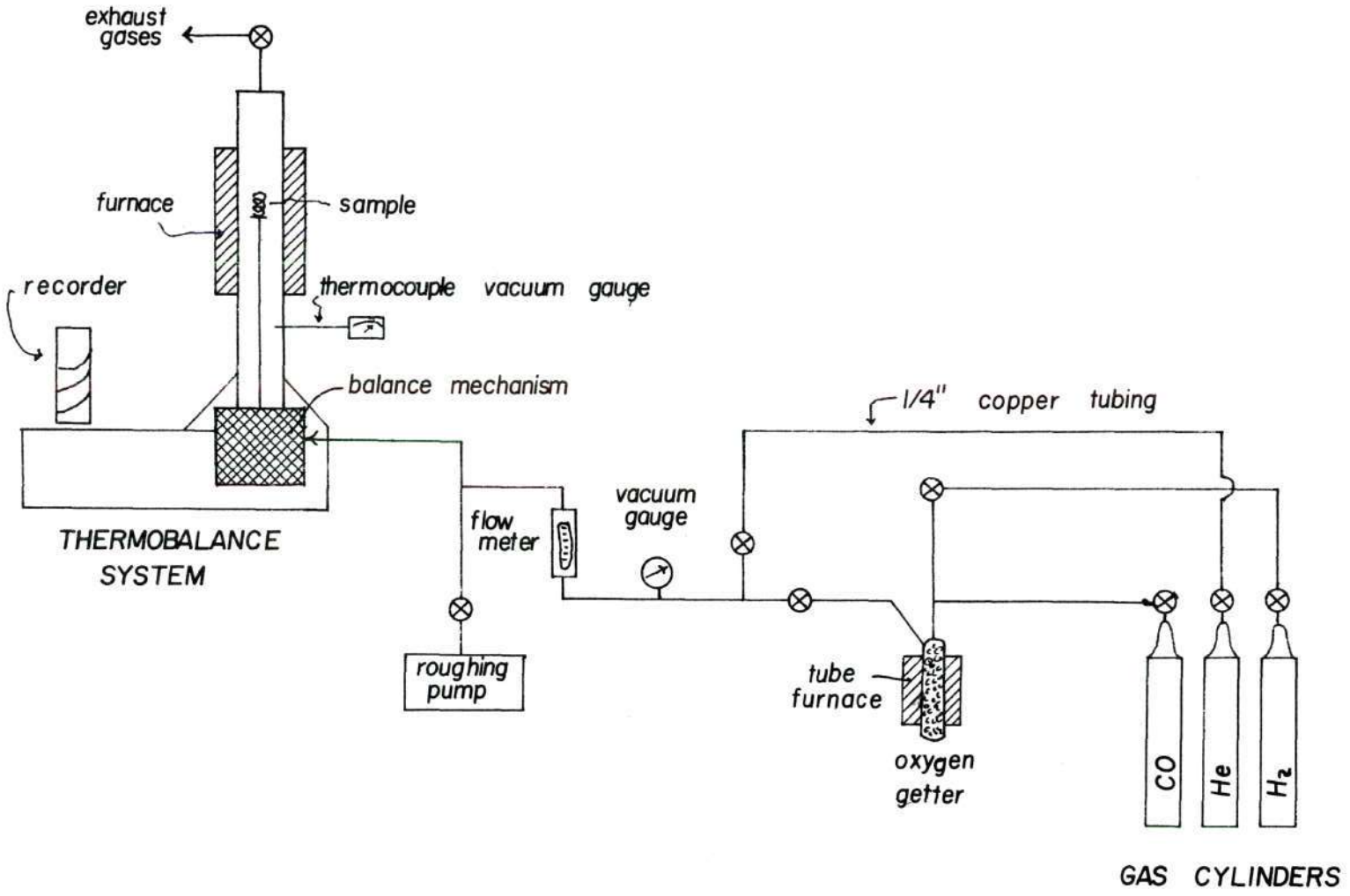

Figure 6. Schematic Diagram of Thermobalance System

The minimum guaranteed purity for the gases as given by the supplier was: carbon monoxide 99.5 molecular per cent, helium 99.995 molecular per cent, and hydrogen 99.8 molecular per cent. Typical analyses for these gases provided by the supplier, The Matheson Company, are tabulated in Table 6. Computations also show that at 20 microns of pressure, if oxygen is present in the same ratio to other molecules as at atmospheric pressure, its concentration will be 5 ppm. The concentration of oxygen in the carbon monoxide was stated as 195 ppm. A copper getter was installed to remove the oxygen and to decompose any carbonyls which may have formed during storage in the steel cylinder. During operation the copper was maintained at 350°C; at this temperature it is a widely-accepted oxygen remover. Thermodynamic calculations indicate an equilibrium pressure of 10^{-20} atmosphere of oxygen at 600°K. Although the actual amount of oxygen removed cannot be calculated, a major concentration reduction can be expected. It has been observed (19) that copper at 400°C does not have any influence on the Boudouard equilibrium. This was further substantiated by noting that there were no deposits in the trap after more than 1,000 hours of operation.

The oxygen trap was constructed from Pyrex glass consisting of a 1-1/2 inch OD glass tube, sealed at the bottom, containing concentrically a 1/4 inch glass tube extending 1 inch from the bottom (see Figure 33, Appendix A). It was similar to a common gas trap. Inside, the apparatus was lightly packed with high-purity copper gauze. Heating was accomplished with a tube furnace in a vertical position. A powerstat was used to control the power input, and thus a constant temperature could be maintained. In order to regenerate the copper, a cylinder

of dry hydrogen was installed so that the thermobalance could be isolated and hydrogen drawn through the gas trap, reducing the copper oxide to metallic copper.

To evacuate the system, a secondary positive displacement Cenco-Megavac vacuum pump from Central Scientific Company was used. The ultimate vacuum of the pump was 0.1 micron. Typical pumping curves for the pump and system are shown Appendix A, Figure 34. Under normal conditions, the system pressure would be lower than 20 microns after pumping for 10 minutes. With continued pumping the ultimate vacuum was 7 microns.

Pressure measurements were read from two gauges: a rough gauge on the line which had a range of 0 to 30 inches of mercury, and a Hastings thermocouple gauge, which was installed in a room temperature portion of the thermobalance system.

The possibility of using a diffusion pump to obtain lower pressures was considered; however, previous work had shown that the diffusion oil contaminated the balance mechanism. The calculation on the purity of the reactants shows that the secondary pump alone will accomplish concentrations lower than the reactants, obviating a quest for lower pressures. Furthermore, with the geometry and complexity of the system, it is questionable if such pressures could actually be obtained and maintained in a practical situation.

The gas lines of the system were constructed of 1/4 inch copper tubing with Swagelok fittings. The glass-to-metal fittings at the copper oxygen getter were Swagelok fittings with special plastic and Teflon seals.

Flow Rate

Flow rate measurement was made by a calibrated Airco model 09-1011 rotameter. The rotameter contained both glass and stainless steel floats to accommodate large variations in flow rates. However, the majority of experiments were done at the same flow rate. The flow meters were factory calibrated and air curves were furnished. Since absolute flow rate was not a variable in the experiments, no attempt was made to check the curves. Small variations were found not to have a significant affect on the results.

Thermobalance

The thermobalance operation, although simple in principle, is complex in design, and allows continuous accurate weight change measurements from an isolated system. Only the salient features will be discussed here; the reader is referred to Appendix A for further details.

In essence the thermobalance is a vertical tube furnace capable of reaching temperatures to 1050°C. The heated section of the system consists of a quartz tube with a 4.4 centimeter outside diameter and a 0.3 centimeter wall thickness. The quartz tube is 56 centimeters in length and has water-cooled jackets at each end. The heating furnace is 30 centimeters in length and heated with Nichrome resistance wire. The furnace is insulated by four centimeters of asbestos packing.

The unheated metallic body and most of the internal mechanism is constructed of aluminum because of its passive nature to most atmospheres. Previous unpublished work in this field has shown that aluminum is not reactive with carbon monoxide in the region of concern.

The suspension mechanism consists of a 30 centimeter long hollow tube of alumina which extends from the room temperature suspension apparatus into the heart of the furnace. The thermocouple wires are held in the center of this stem with the junction at the top. A small table, two centimeters in diameter, sits on the top of the rod with a small hole in the center for the thermocouple to protrude.

In the base section are a counterweight, balancing weight (to adjust the sensitivity), a small platform to hold calibrating weights, a concave reflecting mirror, thermocouple connecting wires, and three support wires. Beneath this mechanism and attached to the balance section is a damping mechanism. The above equipment is supported by three extremely thin pieces of metal ribbon. The concave mirror is in a position to reflect a beam of light from a source to a photocell. The thermocouple connecting wire is hair-fine and of the same composition of the wires in the stem (platinum-platinum 10 per cent rhodium). They are essentially weightless so as not to affect the measurement (for detail, see Figure 11).

The suspended mechanism can be secured by the use of two locking mechanisms: (1) a light duty arm which merely supports the mechanism in a position against the bulwark, (2) a screw-clamp which tightens securely the entire suspension and removes tension from the delicate metal ribbons. It is only in this latter position that adjustments may be made on the equipment.

Recording the weight gain or loss is accomplished by reflecting a light beam from the concave mirror attached to the suspension mechanism and then measuring the deflection, $rd\theta$. The value of r is one

meter. Because of this relatively large value, it is possible to record very small changes of angle, $d\theta$. This is done using a photocell attached to a small motive unit which runs on a vertical track. The motor, which raises and lowers the photocell unit, is activated by the photocell crossing the reflected beam. While operating, the photocell mechanism will traverse a path of approximately 1.5 centimeters, continuously cycling. A recording pen is aligned exactly in the center of the path so that an increase in deflection will move the recorder. A change in mirror position will cause a $d\theta$ for the reflected beam. Thus, weight changes are measured by the deviation of the equilibrium path of the photocell and are recorded by the pen. The recordings are made on a rotating cylindrical chart, giving the weight change as a function of time.

Temperature control is by expansion of a metal rod which passes through the furnace, secured at the top and attached to a lever arm which activates the furnace through current adjustment. By setting the rod at a position, a temperature is maintained using a mercury relay and a transformer. The temperature observations from operations have shown that the temperature will not vary more than one degree from a setting. From the construction of the furnace, it can be assumed that the temperature will be constant in the region of the sample at low flow rates. Although operationally it is difficult to achieve exact predetermined temperatures, once a setting is made, the temperature obtained is held very accurately by the control mechanism.

The temperature of the sample is measured by a platinum-platinum 10 per cent rhodium thermocouple which runs up the hollow center of the

sample support. The junction is directly beneath the sample and slightly above the center of the furnace. At the base of the support stem (room temperature) the wires are connected to the outside by very fine wires of their respective composition, and then both outside terminals are connected to the potentiometer with six-foot copper lead wires. Although the thermocouples have been tested by the manufacturer for accuracy, several standards were used to verify the readings obtained. Boiling water and melting potassium chloride were used as standards for the thermocouple. Details are found in Appendix A. A Leeds and Northrup portable precision potentiometer was used to measure the potential of the thermocouple. The standard cell of the potentiometer was calibrated with one which had been checked at the National Bureau of Standards and this was used as an internal reference junction after measurement of the ambient temperature.

Horizontal Tube Furnace

A separate system using a horizontal tube furnace was constructed as an auxiliary apparatus. It consisted simply of a one-inch diameter quartz tube connected with a carbon monoxide gas cylinder and a flow-meter. The reaction chamber was provided by a Lindbergh Heavi-Duty 54000 tube furnace. The furnace provided a heated zone of one-foot length. Temperature was measured with a Platinel II thermocouple.

High-Temperature X-ray Apparatus

Several temperature examinations with x-rays were made to verify that phases seen by room temperature analyses, or postulated to exist at reaction temperatures, are indeed part of the reaction phenomena. A high-temperature x-ray camera built by Fleming, Johnson, Boland, and

Bomar (107) was modified and used for this experiment.

A Siemens Crystalloflex IV x-ray generator, a Philips diffractometer, and a molybdenum x-ray tube were used.

The furnace was constructed from fused silica with eight cubic inches of heated space. Two Mylar windows in the sides allowed the x-ray beam to pass through. Temperature of the reaction chamber was controlled by a variable transformer. Temperature was determined by a platinum, platinum-13 per cent rhodium thermocouple placed close to the sample. Figure 7 shows the apparatus. Details are given in Appendix A.

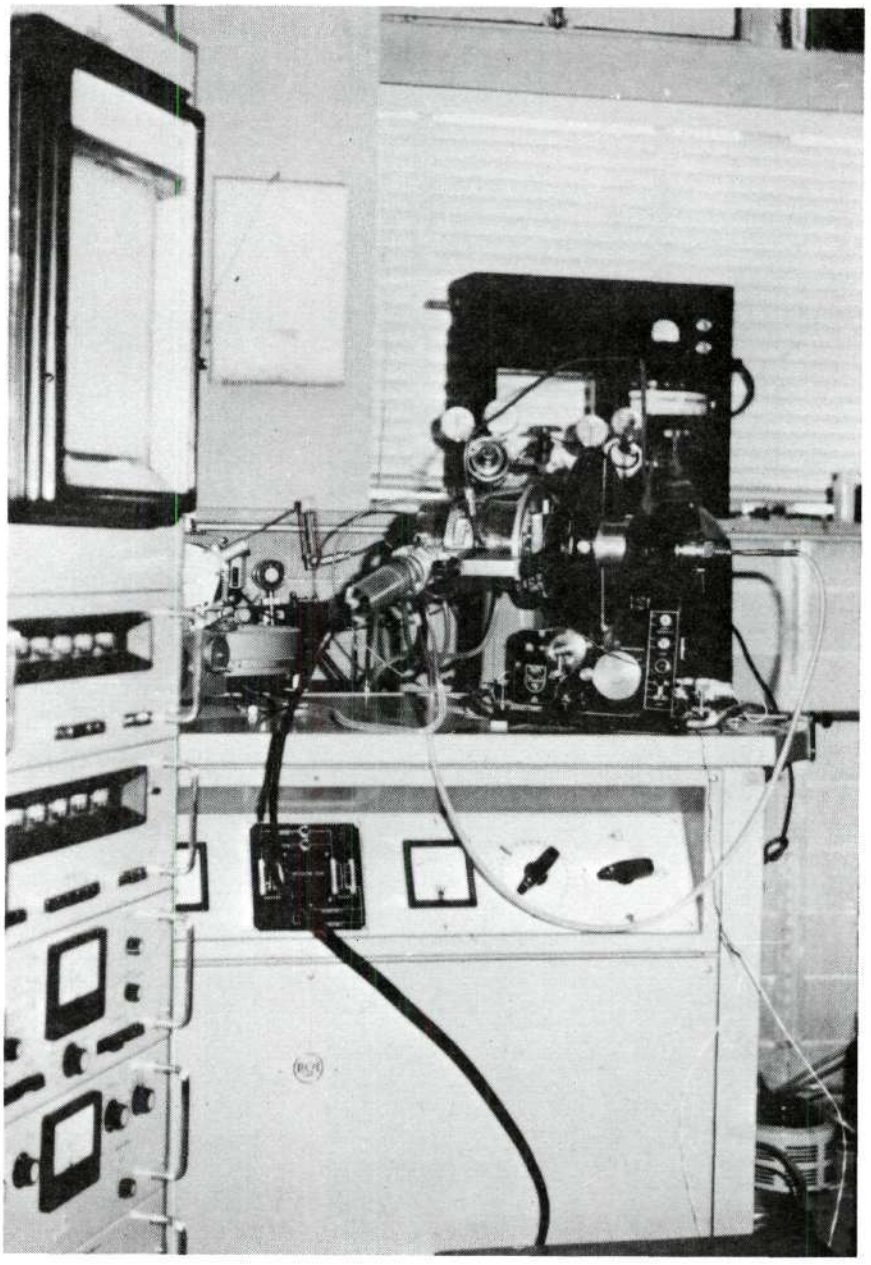

Figure 7. High-Temperature X-ray Apparatus

CHAPTER III

EXPERIMENTAL PROCEDURE

Thermobalance Operation

Preparation of the Specimen

For the experiments wire specimens were used because they were easy to work with, they best simulated practical industrial conditions in a controlled laboratory environment, and most important, the wires offered a consistent nominal surface area. Originally, powders were tried as a reaction material, but difficulty was encountered in determining the surface area and developing uniform and reproducible sample preparations. Furthermore, subsequent analysis of the reacted substance would be hindered since there is no structure to the powder, and each handling alters the relative orientation.

The iron wire used in the thermobalance studies was ultra-high purity iron produced by Material Research Corporation, Orangeburg, New York. This wire had been triple zone refined and possessed an overall purity of 99.995 per cent. In the course of the experimental work, wires of different heats from the above source in some cases resulted in different reactivities under the same experimental conditions. This is accounted for in the experimental results.

The iron wire was received from the manufacturer with a diameter of 0.020 inches and in 100-foot lots, rolled on a 3-inch spool. The wires were covered with varying amounts of a heavy clear hydrocarbon

described by the manufacturer as Vaseline, which was used as a drawing lubricant, and to protect the surface from subsequent corrosion. The standard procedure for preparing a sample was to cut a length of the 20 mil wire to 64.5 centimeters, corresponding to a surface area of 10 square centimeters. This wire was then firmly rubbed about ten times with a Kimwipe saturated with trichloroethylene (solvent recommended by Materials Research) to remove the lubricant, taking extreme care not to touch the wire with the hands. (Figure 8 shows the wire surface as received and then after solvent treatment described.) The specimen was then coiled on a 1/2 inch diameter rod of Teflon. The resulting sample coil was 3/4 inch in diameter and approximately 1/2 inch in length. After a gravimetric weighing, the sample would be ready to be placed in the thermobalance.

Surface Treatments

Various surface treatments were made to determine their effect on the reactivity of a specimen. Figure 8 shows the surface of the wire as received and after wiping with trichloroethylene. Although the surface does appear fairly rough, it is one of the best which can be obtained with a wire, and certainly better than powder surfaces. A program of surface preparations included: ultrasonic cleaning with alcohol and trichloroethylene, electrolytically cleaning with a commercial electrolyte using the sample as the cathode, cleaning with dilute nitric acid, oxidizing the surface, rubbing with fine emery cloth, and cleaning with a commercial etching solution. (Details and results of the above investigation are documented in Appendix B). No significant difference in specimen reactivity was observed except for

AS RECEIVED

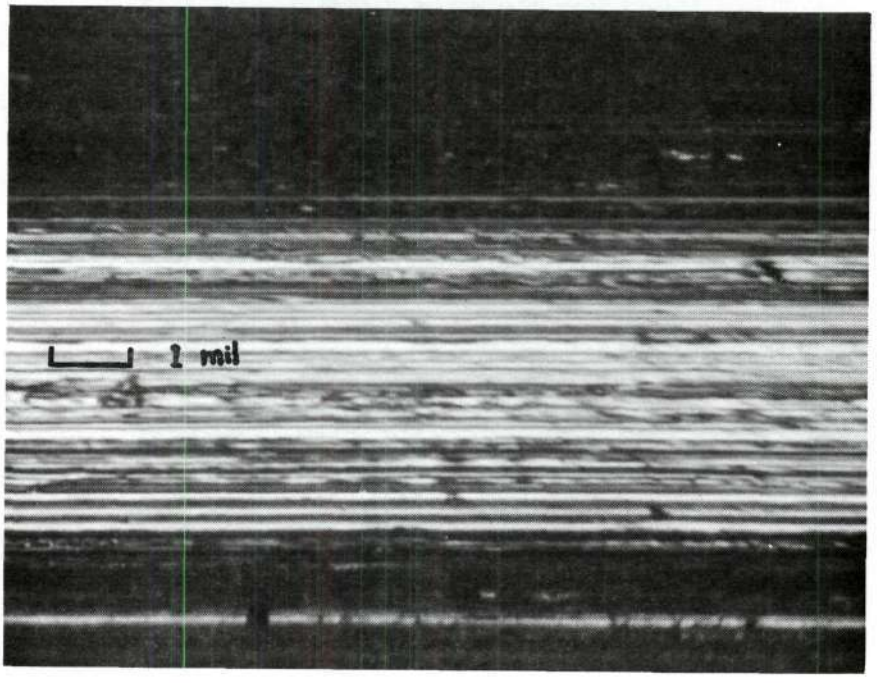

WIPED WITH TRICHLOROETHYLENE

Figure 8. Photographs of High-Purity Iron Wire Surfaces

an oxidized sample which had a period of weight loss (corresponding to oxide reduction), followed by the usual weight-gain curve. This finding is consistent with the results of Pettit, Yinger and Wagner (67) who studied the oxidation of iron in carbon monoxide-carbon dioxide mixtures. They stated that no significant difference in oxidation rate was detected between chemical, electrolytic, or mechanical polish, or nitric acid etch. It is thus concluded that the surface preparation, once a uniformly clean surface is obtained, has little influence on the final result. Thus, the most elementary technique of merely wiping the sample clean with trichloroethylene was adopted, so as not to overcomplicate the experimental procedure and to best simulate practical conditions.

Experimental Operating Procedure for the Thermobalance

By raising the furnace and quartz tube apparatus, the prepared wire sample can be placed on the sample holder. The furnace is then lowered and secured. The system is purged with helium for two minutes and then vacuum pumped for at least 15 minutes. The system is then filled with helium, the pump is restarted, and the furnace is activated (see Appendix B, Figure 34).

During the heat-up period, the thermobalance is momentarily isolated from the remainder of the system, and hydrogen is introduced to regenerate the copper getter. The pump draws the hydrogen through while maintaining a vacuum of 20 inches of mercury. The getter furnace is held at 450°C during this operation.

After the furnace reaches thermal equilibrium (about an hour) (see the heating curves, Figure 45 in Appendix B), the pump is stopped,

and the apparatus is rapidly flooded with carbon monoxide. The volume of the system is approximately four liters, and it takes about one minute to reach atmospheric pressure. When a slight over-pressure is reached, the flow is reduced to 30.8 cc/min, the exit valve is opened, and the photocell is activated, and recording begins. At any time during the run, the sensitivity of the balance can be determined by adding a calibrated weight and measuring the deflection.

Terminating the run is done by closing the exit valve, turning off the carbon monoxide and evacuating the system. The furnace is turned off and allowed to cool to about 70°C (see cooling curves, Appendix B), at which time the sample is removed. The system is always brought to pressure by back-filling it with helium in order to eliminate the possibility of contamination with oxygen and water vapor.

Horizontal Tube Furnace

Samples for the Lindbergh Hevi-Duty furnace were prepared in the same manner as previously discussed, except that a lower quality of iron wire was used. This wire was purchased from Gallard Schlesinger and had a stated purity of 99.99 per cent. The sample or samples were placed in the tube and centered in the furnace. The system was purged for ten minutes with helium, carbon monoxide flow was started, and then the furnace was turned on. Runs were spaced at 50° intervals and lasted three days (72 hours). The flow rate was 70.0 cc/min. On completion, the samples were removed, taking care not to disturb the carbonaceous deposits, and weighted. Due to the length of the experiment and high flow rate, in some cases it was possible to remove the sample without

dislodging significant portions of the deposits. In such cases, the weight of these powders was added to the sample weight. The cooling and heating curves for the Linbergh furnace are presented in Appendix B, Figure 48.

Methods of Analysis

Inherently, each run had the initial-terminal weight gain as one indication of the reactivity. The thermobalance results also had a curve to examine the kinetics. Representative runs were also chosen and were examined: (1) optically through metallographic techniques, (2) with the electron microscope, both by replicas of the surface and replicas of the etched cross sections, (3) with the electron microprobe, (4) x-ray diffraction of wire segments at room temperature, and (5) x-ray analysis of iron carbonyl powder reacting with carbon monoxide in a high-temperature camera.

Metallographic Analysis

Initially, standard metallographic laboratory techniques (100) were used to examine the sample microstructure and were found to be unsatisfactory. Samples mounted in Quickmount, wet-ground on the standard papers and polished on a lap wheel with chromium oxide and alumina all possessed edges which were markedly rounded, preventing observation of the important surface area. Incorporation of a vibrating polishing technique did little to ameloriate this problem and also seemed to cause a spurious structure.

A new procedure was developed specifically for this work. Samples were mounted in a much harder thermal-setting powder, Diallyl

Phthalate (Metallurgical Supply, Houston, Texas), which hardness tests indicated was about four times harder than Quickmount, and one and one-half times harder than Bakelite. Blanks were first prepared and four vertical 0.041 inch diameter holes were drilled. Segments of a reacted sample were placed in the mounting apparatus with additional powder at the end to be polished. A small amount of powder admixed with some copper powder was placed on the other side to give a conducting seal.

Samples were initially ground with a belt grinder until the wire cross sections were completely circular. An automatic grinding unit was used for the 220, 320 and 400 abrasive papers, and consisted of revolving nine-inch emery disks with a holder which moved the samples in an arc across the rotating paper. Normally, water is used as a lubricant, but for the microprobe samples, Johnson's No. 140 Stik-wax and kerosene were used to avoid any oxidation which may be caused by the water. Although the hard mount does produce good edge results, it was found that the matrix resin was too hard or tough for the number 600 grinding paper and after only one minute of grinding, the emery would be expended. With the samples to be etched for optical metallography and electron microscopy, water was used as a lubricant, and the final grinding on the 600 paper was done by hand to insure the best possible surface.

For fine polishing of the specimens, diamond dust was used, since it will give the cleanest cut. Progressive grade sizes of 6, 3, 1 and 1/4 micron were employed in the process. An automatic unit similar to that described for the grinding operation was used. Kerosene served as

a lubricant for all samples. Drying was done with ethyl alcohol and a heated air blast. A special hard lap cloth, Buehler's Teximet polishing cloth, was used as another aid to obtaining the best edge possible.

To develop the microstructure, two etchants were utilized: (1) a 2 per cent nitric, 2 per cent picric acid in ethanol, and (2) alkaline sodium picric etch (see Appendix B).

High-Temperature X-ray Procedure

Samples for the examination were prepared by placing a small amount of carbonyl iron powder in a one-inch mounting press and applying 10,000 pounds per square inch pressure for about one minute.

For the reaction, the sample was placed in the center of the x-ray furnace. Furnace alignment was then adjusted so that the sample intercepted one-half of the incident x-ray beam. Aluminum foil was placed over the x-ray cavity to act as a radiation shield and to protect the Mylar. The stainless steel vacuum vessel was placed over the furnace and secured. The system was then evacuated with a primary pump for five minutes. Helium was run through the system while heating to the temperature of reaction (about 30 minutes). After the temperature had equilibrated, the system was evacuated, and carbon monoxide was introduced. A flow rate of 0.4 cubic feet per hour was maintained. For the duration of the run, temperature variation usually did not exceed more than ten degrees from the set-point. Samples would become distorted after about an hour, and the run would then be terminated. The length of time during which data could be taken varied inversely with the rate of reaction.

Traces were taken about every 30 minutes, and each trace lasted about 15 minutes. Angles investigated were 2θ values from 12° to 36°. The amount of noise below 12° made readings meaningless, while angles above 36° were eliminated for fear of disrupting the sample.

Operating parameters for the scintillation counter of Siemens x-ray diffractometer unit were:

Attenuation	=	10 volts
Detector voltage	=	570 volts
Pulse-height	=	18 volts
Channel-width	=	8 volts

A molybdenum x-ray tube was used for the source, with 35 kilovolts and 16 milliamps current. A zirconium filter was also used.

Electron Microscopy

Higher magnifications than possible with an optical system were obtained by taking replicas of a mildly etched cross section. Replicas were made of parlodion (cellulose acetate). Difficulty was encountered in stripping; consequently very few edge portions were obtained.

Surface replicas were taken directly from several reacted samples, repeating the replication process until the carbon had been stripped off and portions of the surface could be observed.

Microprobe Analysis

A Siemens electron micro-analyzer was used to examine several samples as to the concentration of iron, carbon and oxygen. Traces were made at the rate of 180 microns per minute. On several samples, counts were taken over the entire sample. Quantitative results were not very conclusive due to a high background.

X-ray

Reacted wire samples were x-rayed in a Debye-Scherrer powder camera using a Siemen's x-ray diffractometer with a chromium tube. The specimen, a one-inch length of reacted wire, was placed in the camera and rotated at one revolution per minute for a half-hour.

CHAPTER IV

RESULTS AND DISCUSSION

Introduction

The experimental data is centered around pure iron wires which have been exposed to a carbon monoxide atmosphere in a microbalance for 20 hours at constant temperatures ranging from 500°C to 1000°C. Continuous weight gain measurements were made during the reaction to define the kinetics. After cooling, the wire samples were subjected to x-ray analysis, electron microprobe analysis, and metallographic analysis to determine reaction products and structure of the iron: from this information the reaction mechanism is deduced. Ancillary investigations were also made to verify and support conclusions made from the thermogravimetric samples: (1) prolonged exposure of iron wires to carbon monoxide in a horizontal tube furnace (Appendix E), (2) at-temperature, 500°C to 900°C, x-ray studies of carbon monoxide reacting with iron powder (Appendix F), (3) diffusion computations to study the theoretical weight gains accompanying the dissolution of carbon in iron (Appendix C).

The review of previous work reveals the enormous amount of data amassed concerning this system. The majority of research has been directed at narrow portions of a reaction due to the myriad of significant parameters. Some of the variables include: (1) composition of the solid catalyst (metallic iron, alloy steels, oxides, carbides, and

commercial iron base catalysts), (2) composition of the reacting gases (pure CO, CO-CO_2 mixtures, prepared mixtures of CH_4, H_2, CO, and CO_2, addition of inhibitors, and undefined industrial gases), (3) temperature of reaction, (4) history and geometry of the sample, and (5) flow rate of the gases. Almost all prior experimental techniques required a separation of the specimen from reaction conditions before recording any data. The most common method has been reacting for a period of time, removal, and then recording initial-terminal weight changes and analyzing the reaction products.

For this research ultra-high purity iron wires were reacted in pure carbon monoxide over the temperature range of significant reaction, 500°C to 1000°C. The pure components were chosen to avoid perplexing and incongruous results of some of the above mentioned complex systems. Since iron and carbon monoxide are fundamental to the reaction, a thorough knowledge of their interaction is a requisite to the understanding of the complex systems. It is hoped that the results obtained from this study can be extrapolated to aid in the solution of the multicomponent phenomena.

The basic apparatus chosen allows continuous weight-change measurements to define the kinetics. The reacted samples were then cooled and examined at room temperature. A high-temperature x-ray camera was also used to qualitatively examine phases present during the reaction of carbon monoxide with pure iron powder, and verify that phases considered to exist at reaction conditions are in fact present.

The literature survey indicates wide acceptance of some maximum in the reaction curve at about 550°C. Hochman (93) briefly studied

this system in the same basic equipment used for this research. He observed a maximum in the reactivity at 550°C followed by a minimum at about 700°C and increased reactivity at temperatures above 700°C. The results of the present work are in good agreement with those of Hochman.

Experimental Results

High-purity iron wire coils with a surface area of ten square centimeters were reacted in carbon monoxide at constant temperatures, and the sample weight gain was continuously recorded. Figure 9 gives some typical weight-gain curves. The complete data are found in Appendix D. These curves show that after an initial transient period of varying length, the weight gain tends to be a linear function of time. Above 723°C the non-linear portion of the curves appears to be parabolic, with the parabolic portion decreasing as the reaction temperature increases. Most of the reaction curves below 723°C have a hyperbolic-concave-upward portion of considerable length.

There is a major difference in the type of weight gain at temperatures below 723°C and those above this eutectoid transformation. Carbon is essentially insoluble in the ferrite, so almost the total weight gains are due to a sooty surface carbon deposit. At temperatures between 675°C and 730°C the samples appear unreacted. Above 730°C there is a gray-silvery surface deposit which increases in thickness as the temperature of reaction increases. Since carbon is soluble in austenite (0.8 to 2.0 per cent), these samples soon became saturated with carbon.

At temperatures below 800°C, a certain "dead time" was observed

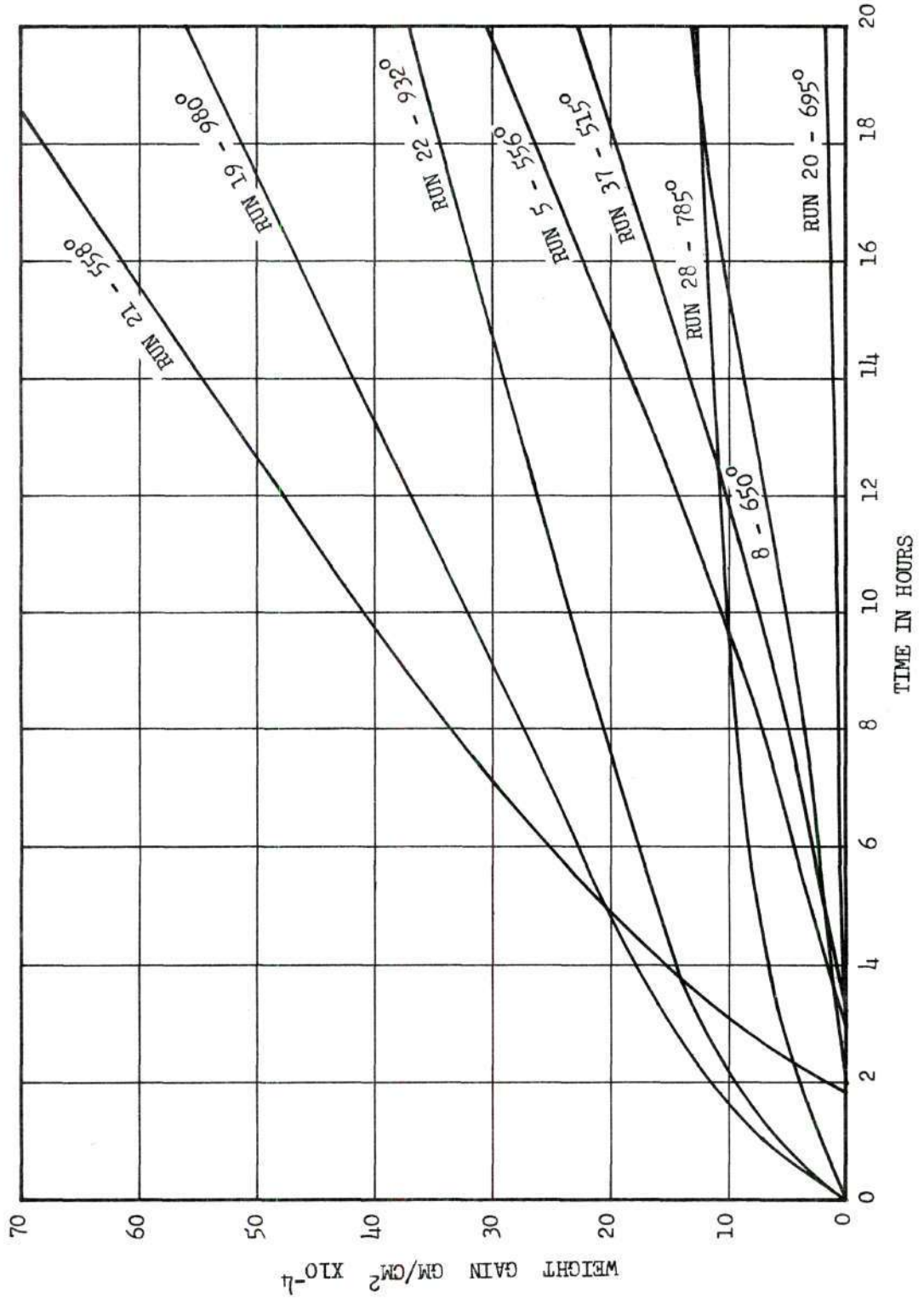

Figure 9. Typical Weight-Gain Curves for a 20-Hour Period

to exist before an observable weight gain is recorded. This is termed the "incubation period" and can be observed in Figure 9. The incubation time is plotted against temperature in Figure 10.

In the process of the research, three separate shipments of the iron wire were used in the experiments (Wire I, II, and III); all were obtained from the same supplier and had identical specifications. Above 723°C no significant variation in reactivity was observed. However, wire II was found to have considerably greater reactivity at the lower temperatures than the other two wires. This discovery was completely fortuitous and turned out to be beneficial, since it helps to explain a portion of the mechanism and possibly differences in previous works. The meaning is discussed later in the text.

The difference is shown in Figure 9 by Run 5 (wire I) and Run 21 (wire II). The variation seems to be predominantly in the initial reaction: after a slightly longer incubation period, Run 5 has a slowly increasing hyperbolic-concave-upward curve, while Run 21 begins with a rapid concave-downward curve--a weight gain characteristic of the parabolic high-temperature reaction curves. After an extended time, however, the slopes of curves are approximately equal. This phenomenon was observed in the range of 525°C to 625°C. Several samples of the wire (Runs 30 and 36) were annealed at 950°C for an hour, cooled to about 550°C and reacted in the normal manner. After this pretreatment, these wire II samples exhibited the same kinetics of reaction shown by the other lots.

Figures 11 and 12 show the slopes of the weight-gain curves plotted against reciprocal temperature. For Figure 11 the slopes are taken

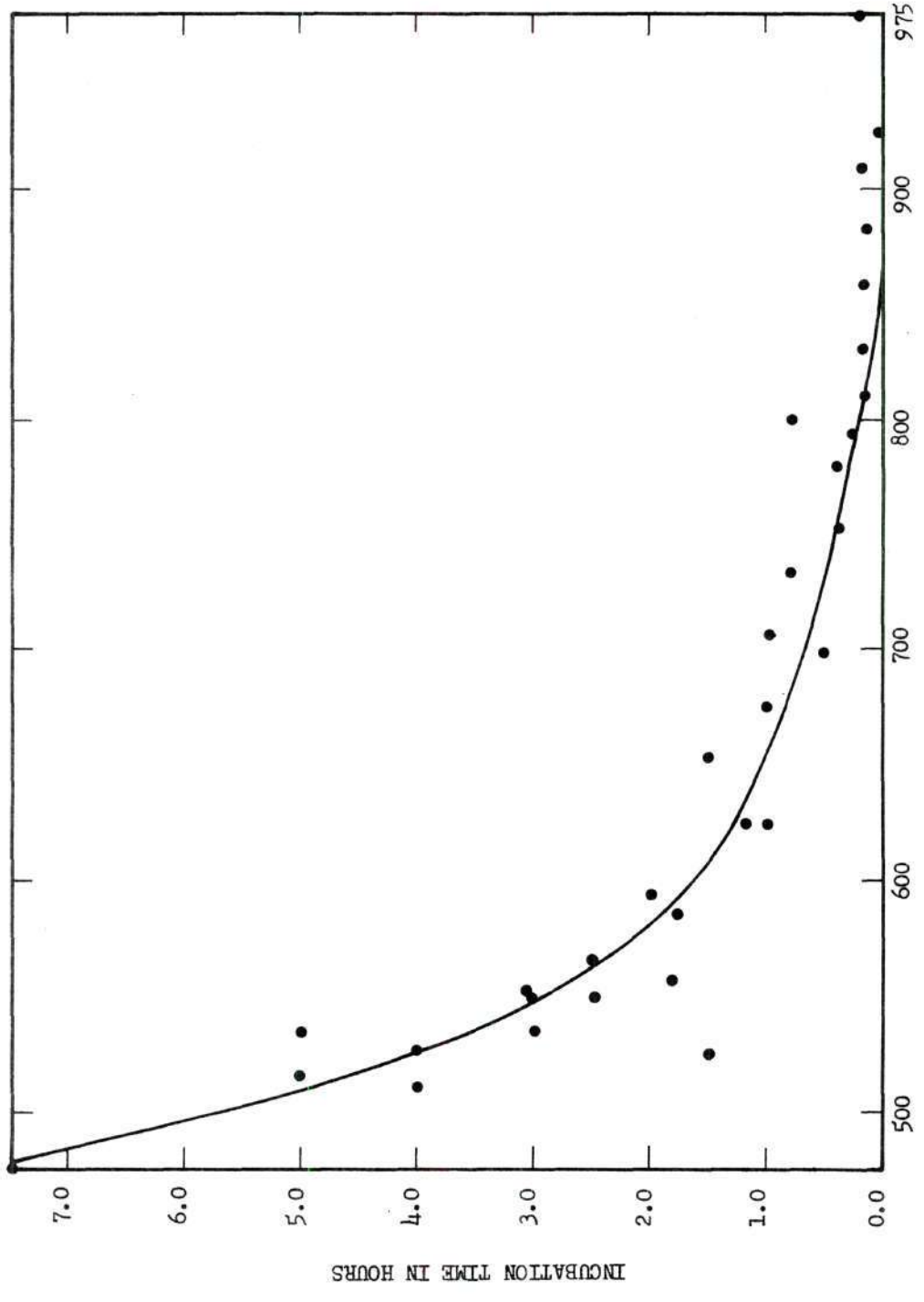

Figure 10. Incubation Period

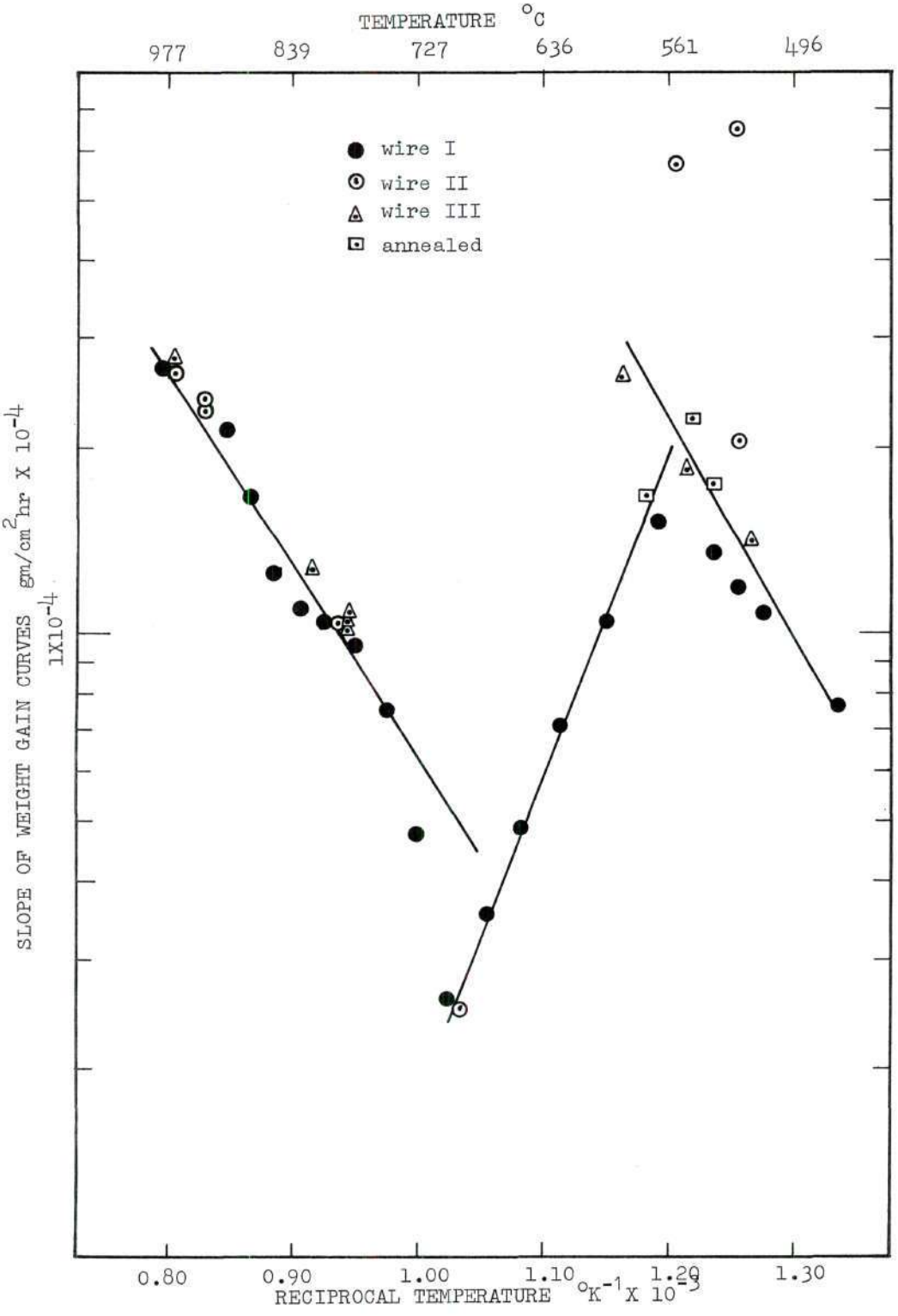

Figure 11. Reactivity at a Time of Incubation Plus Three Hours

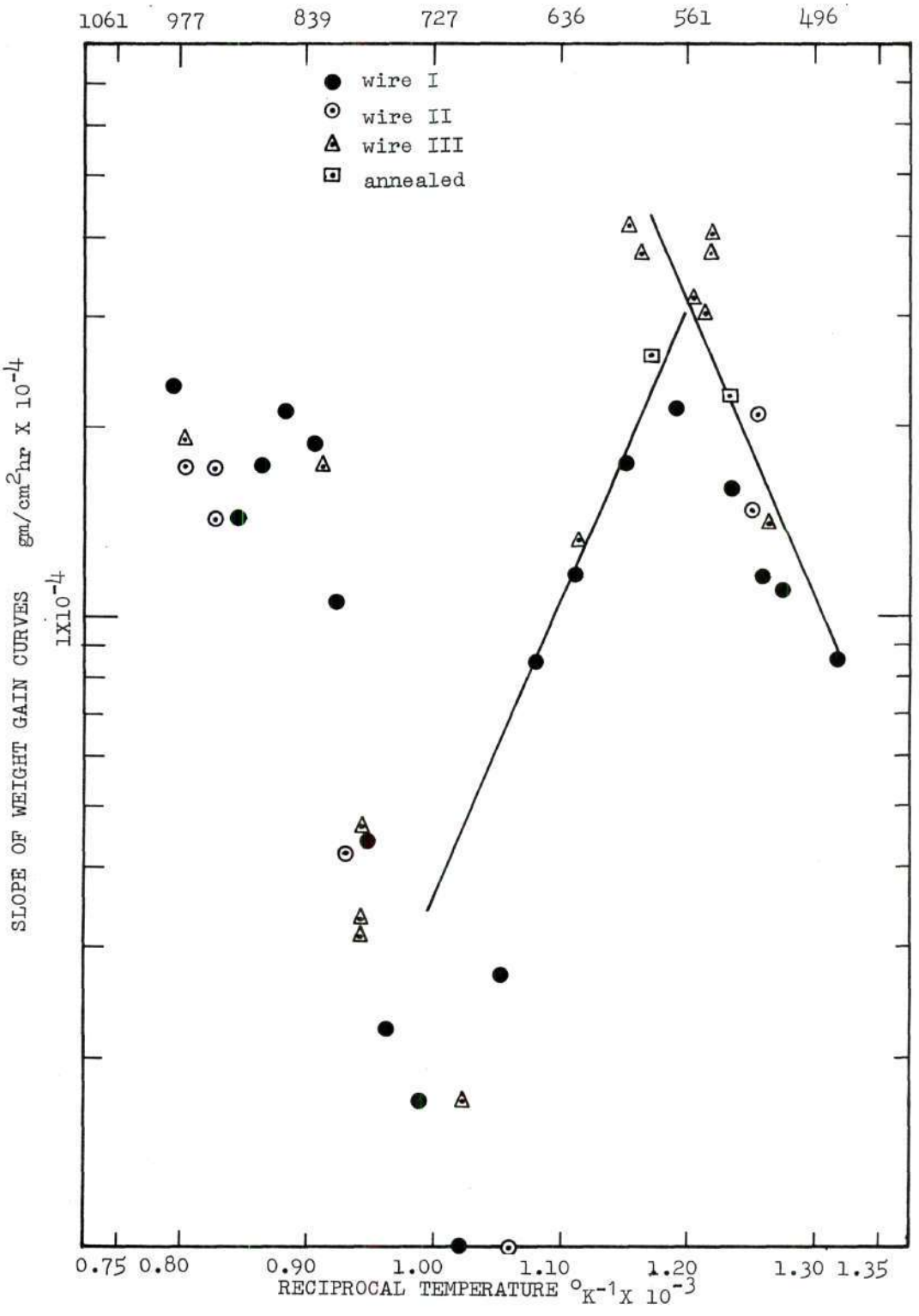

Figure 12. Reactivity after 16 Hours

at three hours following the incubation period, while those for Figure 12 are calculated after a total exposure time of 16 hours. Three hours after incubation most points fall on three straight lines, the exceptions being wire II samples which have the rapid initial reactivity. After 16 hours of reaction (Figure 12), the lower temperature wire II points fall on the line, but scatter is found at the higher temperatures.

With constant concentrations of the reactants, or a zero order reaction, the rate constant can be represented by the Arrhenius form.

$$\frac{dw}{dt} \propto \exp\left[-\frac{Q}{RT}\right]$$

where

w = sample weight

t = time

T = absolute temperature

Q = activation energy.

The activation energy of each temperature range may be calculated from Figure 11 and 12, and is tabulated below.

Table 3. Computed Energies of Reaction

Temperature Range °C	Activation Energy, Q, kcal/mole Incubation Plus Three Hours	16 Hours
500 - 570°C	+18.5	+22.0
570 - 700°C	-23.4	-24.5
700 - 1000°C	+18.0	*

* Results are scattered.

Weight gains for periods of 4, 8, 12, 16, and 20 hours are calculated from the experimental data and are plotted against temperature in Figures 13-17. These figures show the relative progression of the reaction. The reaction increases from either temperatures above or below 710°C. Also shown is the weight gain which would be equivalent to the maximum solubility of carbon in austenite. The dotted lines on each of the graphs indicate that some samples of ostensibly the same material result in a markedly different reactivity, as mentioned previously, and which will be explained later. Intermediate values could probably be obtained with some other theoretical sample.

After four hours, the reaction has barely begun at the lower temperatures. At high temperatures the maximum solubility of carbon in the matrix gamma-iron has already been exceeded. The unusual shape of this curve is due to the influence of the incubation period.

After eight hours, there is a definite maximum at about 570°C and a minimum at 710°C. As the reaction time increases to 20 hours, the weight gains at high temperatures continue to increase, while the minimum at 710°C remains virtually constant. The carbon saturation point (maximum solubility of carbon in iron) does not seem to be distinguished in the weight-gain curves.

After 20 hours of reaction, the weight gain versus temperature plot agrees well with the findings of Hochman (93).

Several samples were reacted at temperatures of 300°C, 350°C, 400°C and 450°C to determine the exact status of the reaction at these temperatures. Only a trace weight gain was observed at 450°C, and there was no evidence of reaction at the other temperatures.

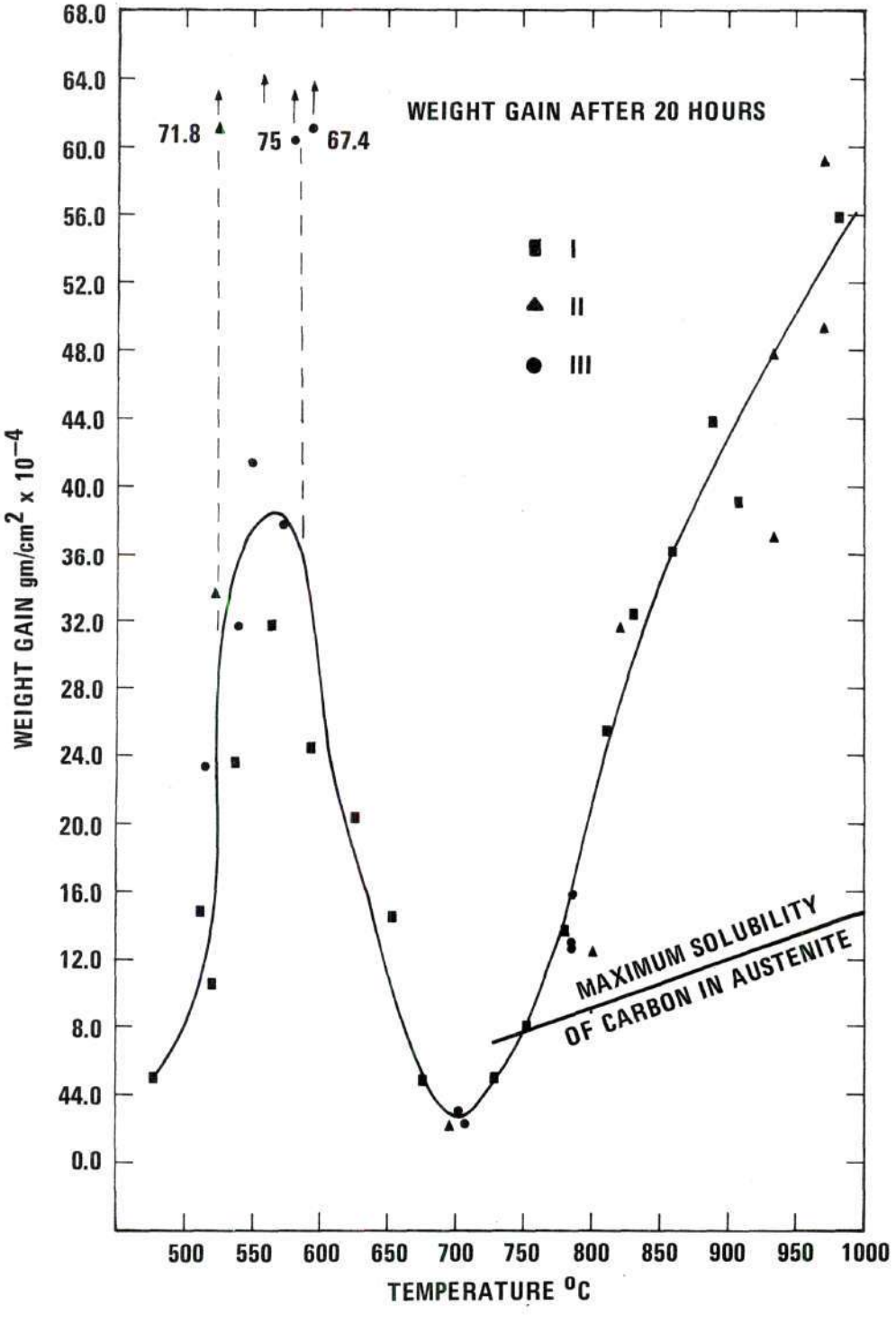

Figure 13. Sample Weight Gains after 20 Hours of Reaction

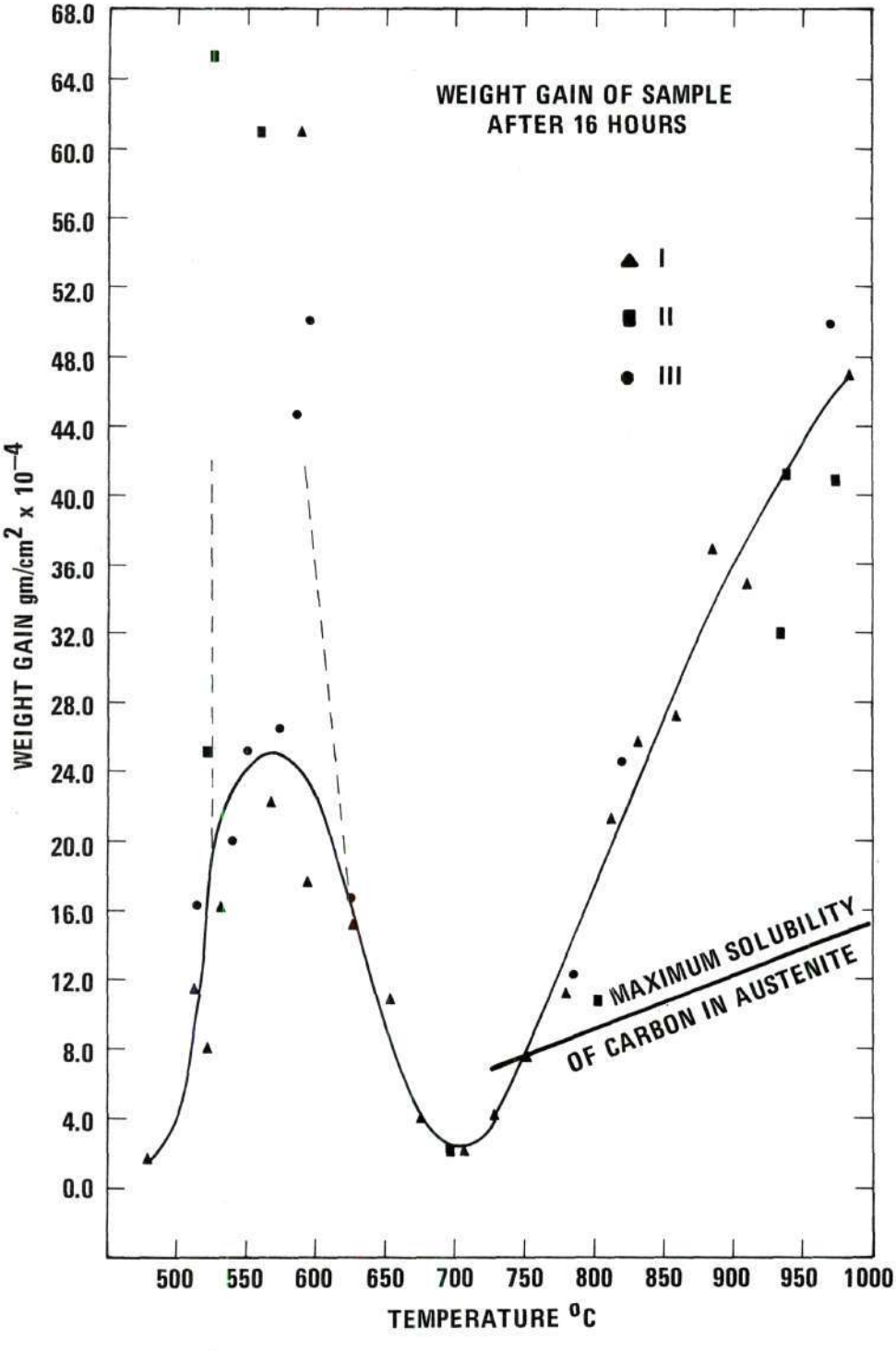

Figure 14. Sample Weight Gains after 16 Hours of Reaction

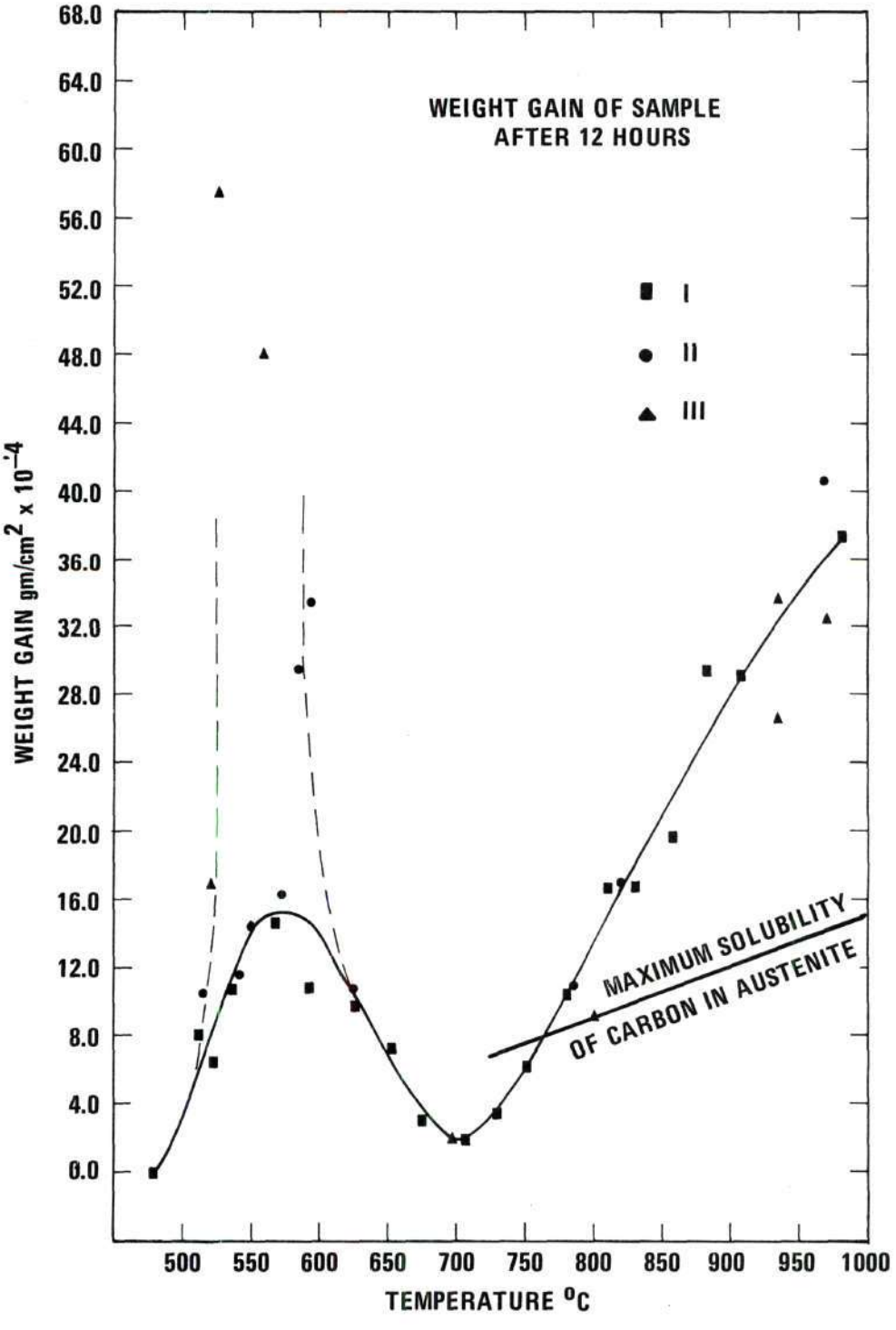

Figure 15. Sample Weight Gains after 12 Hours of Reaction

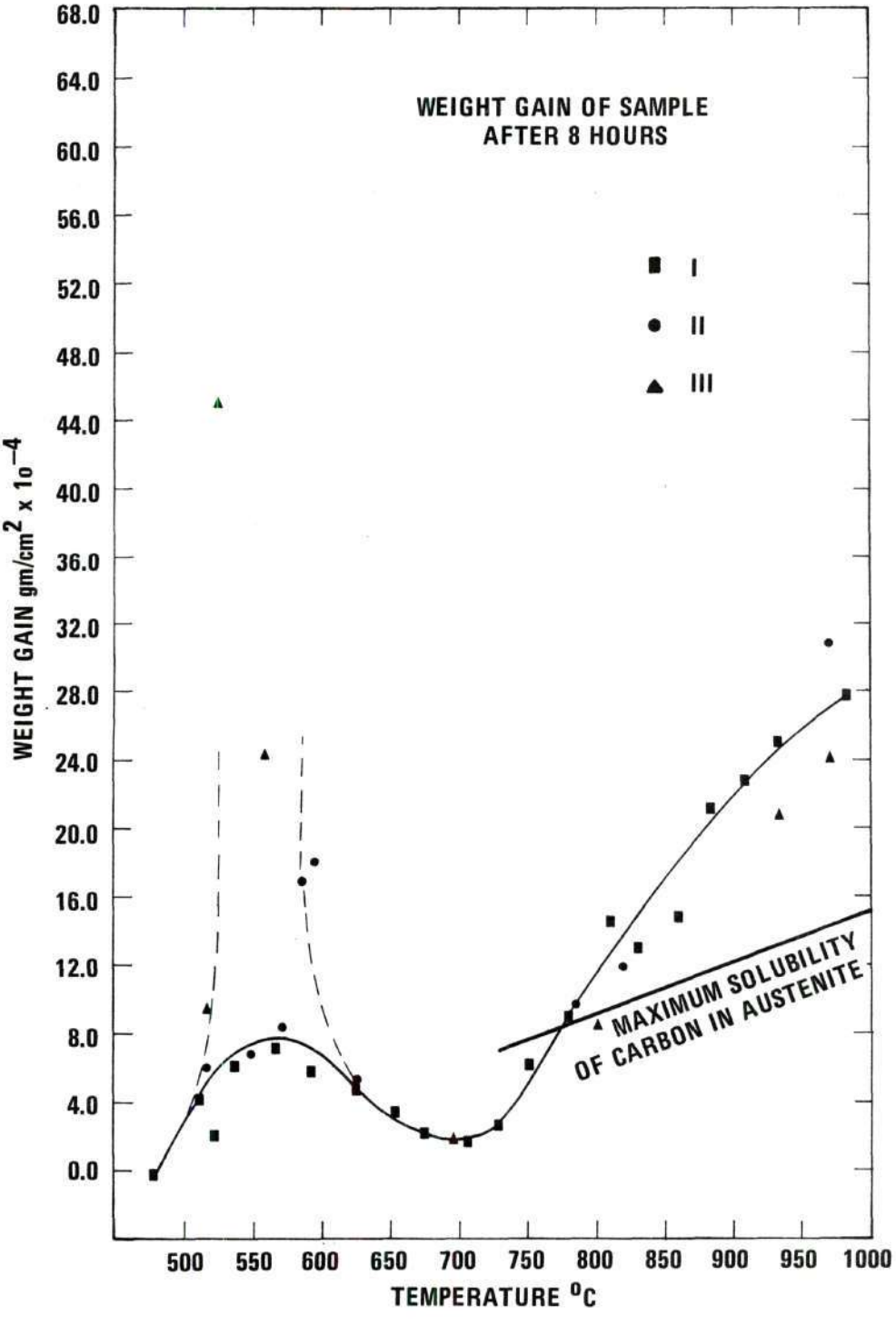

Figure 16. Sample Weight Gains after 8 Hours of Reaction

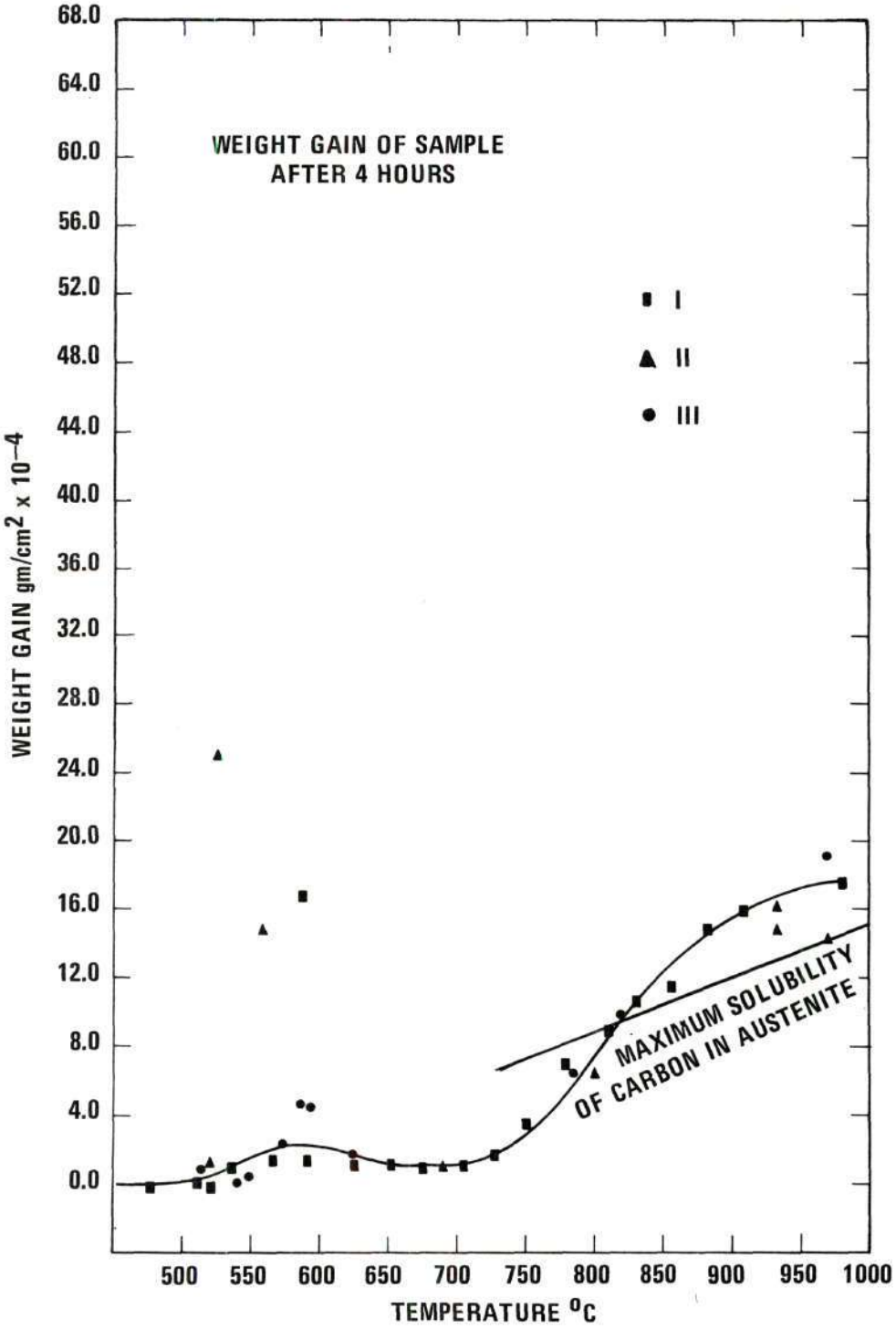

Figure 17. Sample Weight Gains after 4 Hours of Reaction

1/16/25 Missing page has been noted. Cannot determine whether missing page or misgeneration.

The horizontal tube furnace was used to measure the effect of longer reactions. Experiments were run at 50° intervals, at high flow rates for 70 hours. Gravimetric initial-terminal weight measurements were made to determine the extent of the reaction. The samples were from another iron source, but the surface area of each sample was maintained constant at ten square centimeters. The guaranteed purity of the iron was 99.995%. The grain size was much smaller in the reacted samples than the high-purity iron. The reaction product at low temperatures was a uniform dense soot carbon which fell off easily. At temperatures of 850°C and higher the samples crumbled upon handling. These samples appeared slightly more reactive and had a tendency to pit. The results of these experiments are shown graphically in Figure 18. The broken line is the 20-hour run in the thermobalance. Note that at temperatures in the gamma region, the weight gain is approximately proportional to the time of reaction. At the lower temperatures decidedly more carbon is deposited than one would expect from extrapolation. This could be caused by higher reactive samples (same phenomenon as wire II), or might be due to increased flow rate, or both. Detailed results are found in Appendix E.

Metallographic Analysis

Metallographically polished cross sections of some representative samples were prepared to examine the variation in structure following the reaction. The specially designed procedure described earlier was used to obtain the best possible specimens. A nital-picric acid etch was used. Several of these samples are shown to illustrate the variation. Figure 19 shows Run 34 (T = 546°C) cross section at magnifications

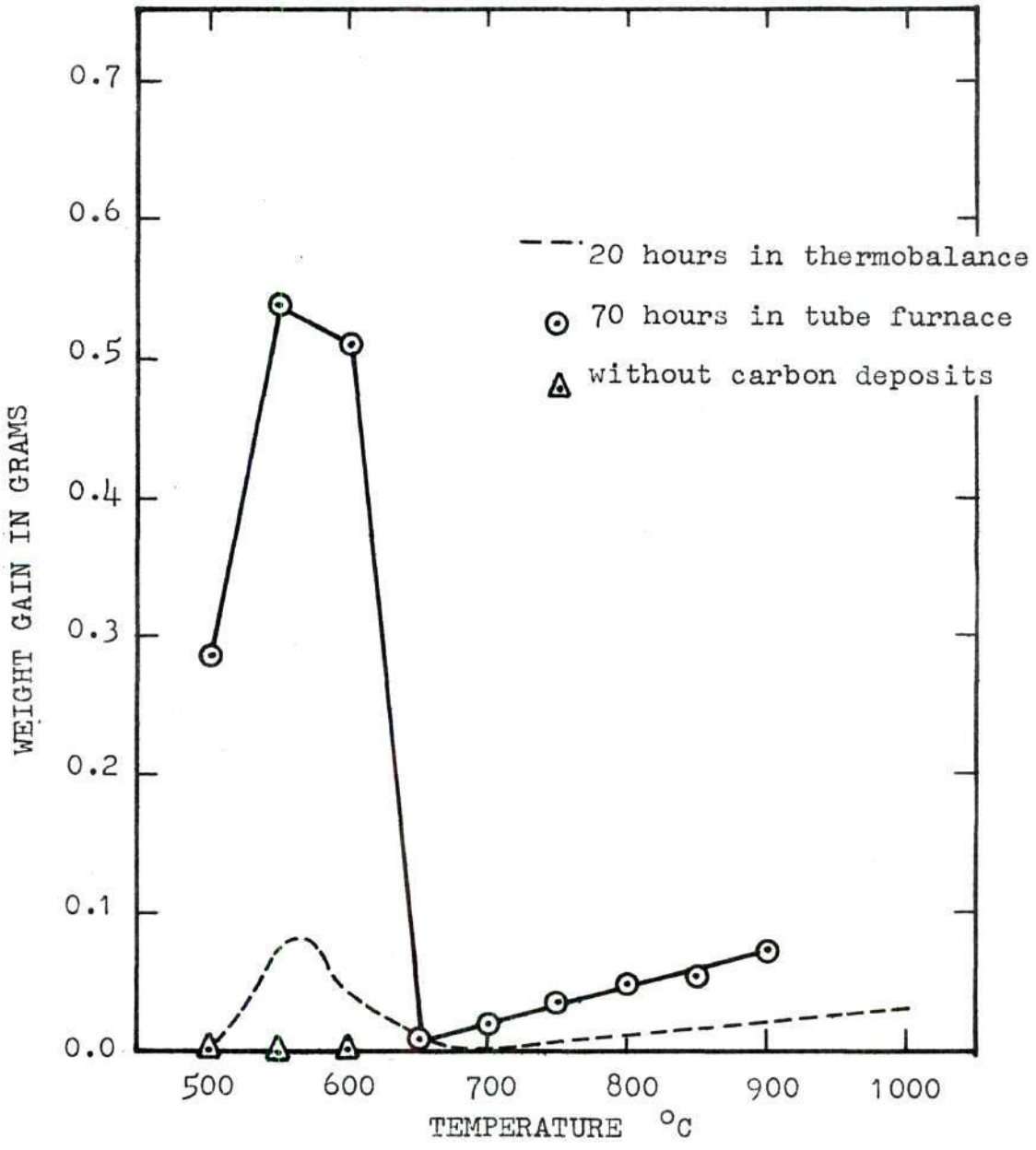

Figure 18. Prolonged Exposure Results

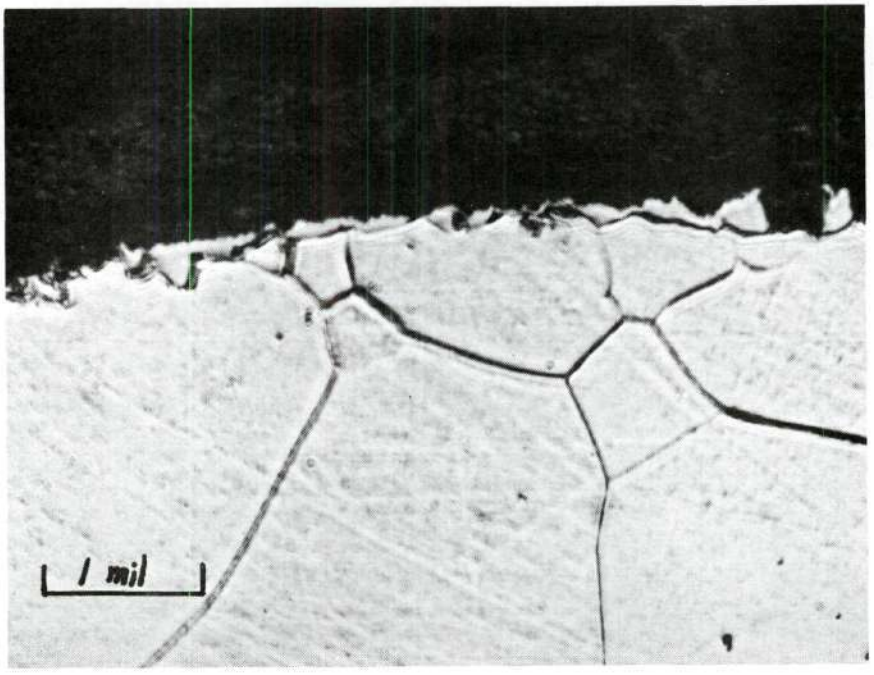

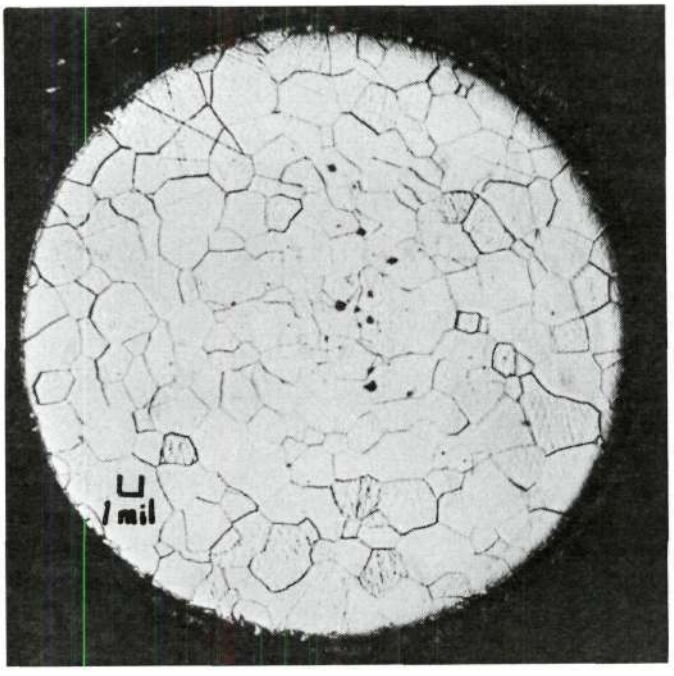

Figure 19. Polished Cross Section of Run 34 (T = 546°C) (Nital-Picric Etch)

of 100X and 600X. Figures 20 and 21 are Runs 40 (T = 702°C) and 38 (T = 969°C), respectively, with magnifications of 150X and 800X. The grain size increases from temperatures of 546° to 702°C due to the variation in rates of grain growth at the two temperatures. The outer boundary of samples 34 and 40 is cementite. A distinguishing fact is that these grains (especially in Run 40) are smoothly polished compared with the ferrite matrix, indicating that the boundary is of a harder material, implicating cementite. X-ray results and additional metallographic procedures, which will be presented later, confirm that these portions are cementite. Run 38 should be saturated with 1.4 weight per cent carbon in the interior. The light portions of Figure 21 are ferrite with parts of the center being cementite as illustrated in Figure 21. The dark areas in the interior are pearlite, and deposits outside the light border are composed mainly of carbon and cementite. This structure is formed on cooling. When the reaction is completed, the interior of the sample is saturated with carbon. Referring to the iron-carbon diagram (Figure 1), we see that on cooling, cementite precipitates out first. Since we are cooling relatively slowly (Figure 46), the cementite grains grow large, depleting surrounding areas of carbon and leaving them as ferrite. This fact is graphically shown by cementite particles in the center matrix. The outer edge consists, at least partially, of cementite. The scratches on the lighter portions indicate that it is softer than the surrounding structure (pearlite and cementite). Portions of the exterior deposits can be seen on Run 38. The sooty low temperature deposits could not be retained on the surface since they were too easily removed in the mounting and polishing procedure.

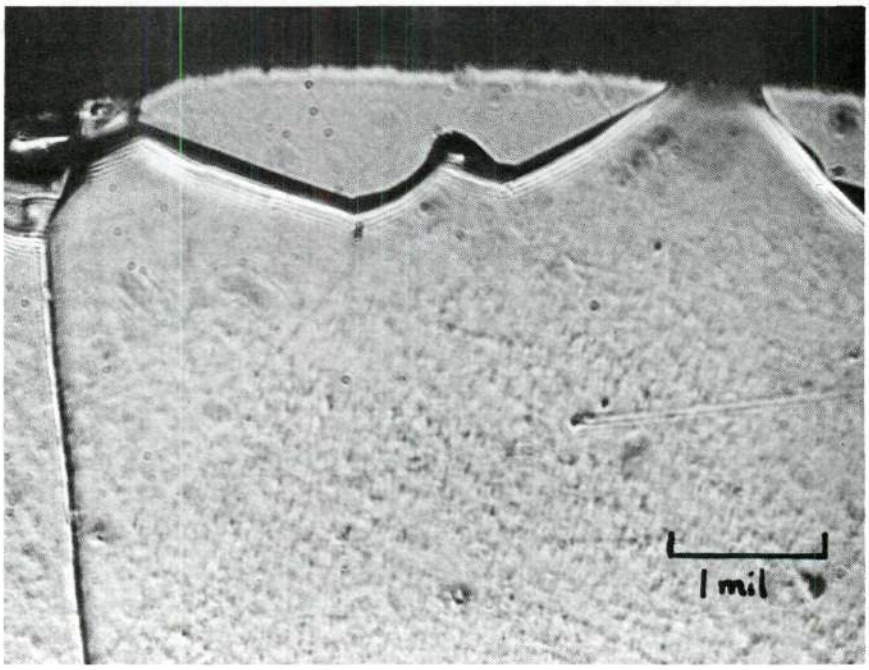

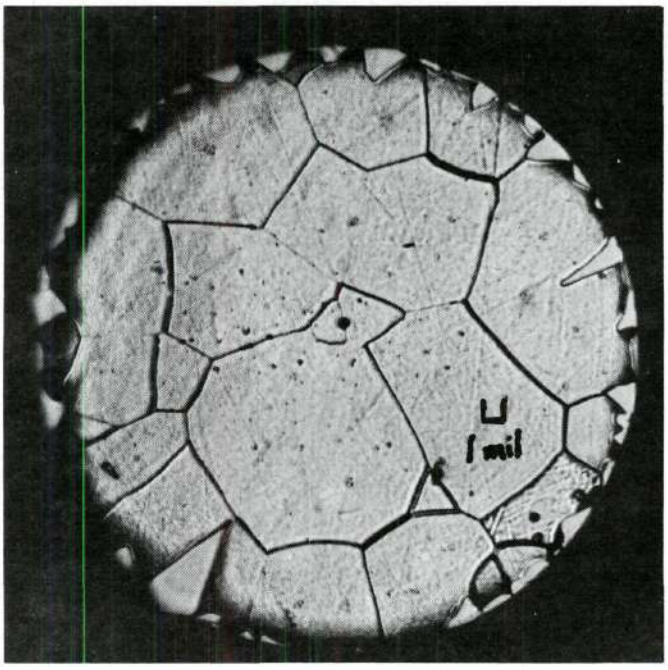

Figure 20. Polished Cross Section of Run 40 (T = 702°C) (Nital-Picric Etch)

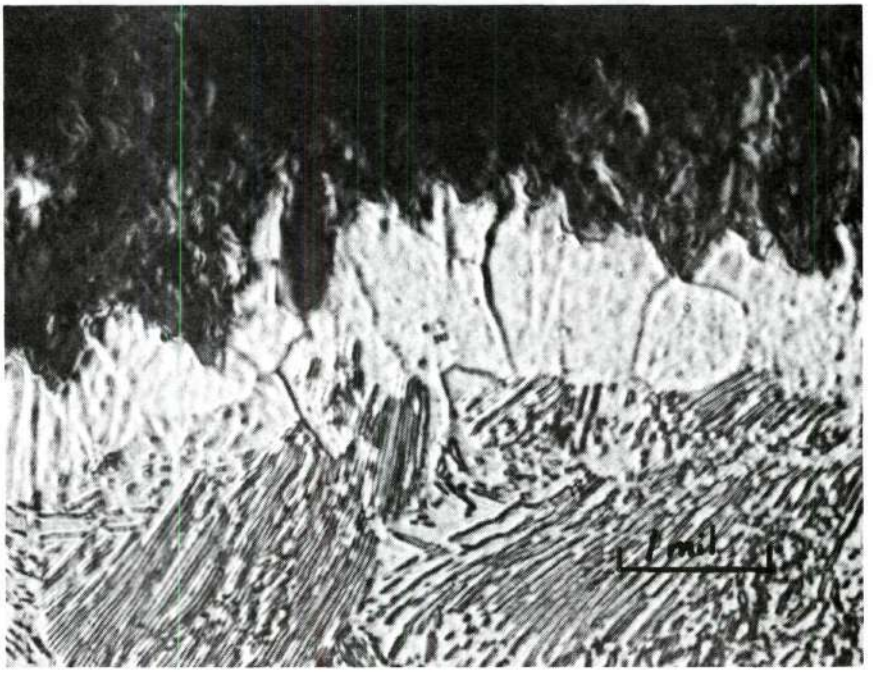

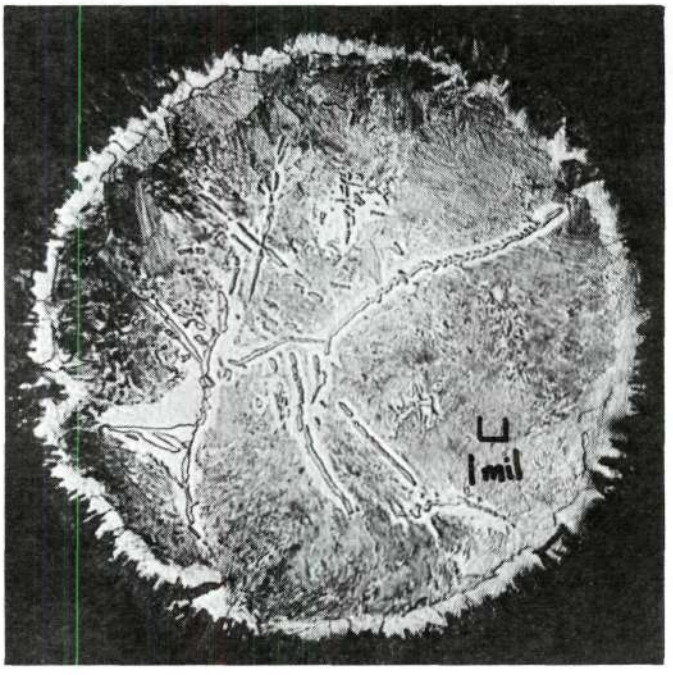

Figure 21. Polished Cross Section of Run 38 (T = 969°C) (Nital-Picric Etch)

To support the above conclusions from the metallographic data, several samples were etched with alkaline sodium picrate. After this treatment cementite will appear black. Figure 22 shows the surface of sample 38 at 1000X. The dark lines in the matrix are cementite in the pearlite. The ferrite on the surface is still observed light, while dark roots of cementite can be seen extending outward. Figure 23 shows similarly etched samples of Runs 34 and 40 at 600X.

Nature of the Carbon Deposits

The sooty carbon surface deposits from several samples reacted at about 550°C were observed in the electron microscope. Two fundamental structure formations were observed: (1) a filamentary type of growth, (2) bulk or flake forms. Photographs of each kind are shown in Figure 24. It is important to notice that the filamentary formation, although abundant, is considerably smaller in size and mass than the bulky flakes. Figure 25 shows two typical aggregates of the deposits; one is composed of a filamentary growth while the second gives a large flake structure with some small filaments growing off the surface. This also illustrates the relative size of the two types of carbon.

The above observations on carbon structure are completely consistent with those of previous works. Filamentary carbon growth has been reported repeatedly in the current literature (14,64,72,92,93). Ruston and co-workers (92) also have distinguished two different surface carbon deposits at 550°C.

Walker, Rakszawski, and Armington (102) state that carbon deposits on iron from carbon monoxide have been evaluated as both 100 per cent

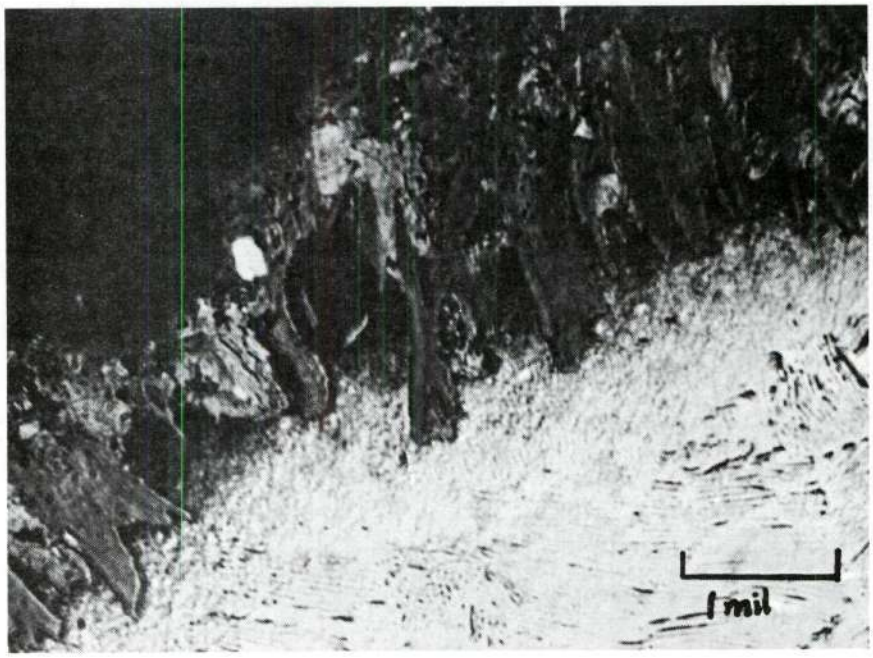

Figure 22. Polished Cross Section of Run 38 (T = 969°C) (Alkaline Sodium Picrate Etch)

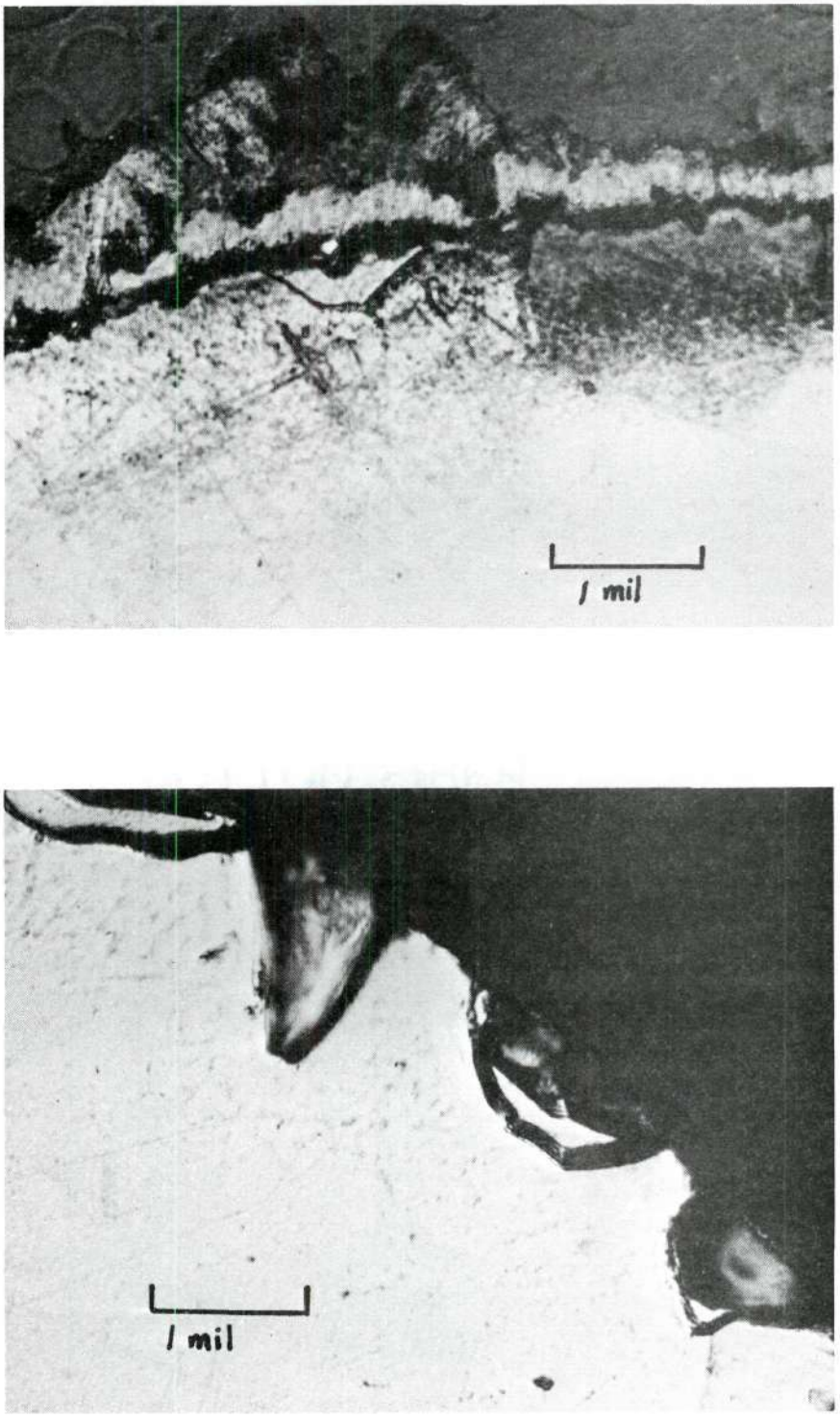

Figure 23. Polished Cross Section of Run 34 (T = 546°C) and Run 40 (T = 702°C) (Alkaline Sodium Picrate Etch)

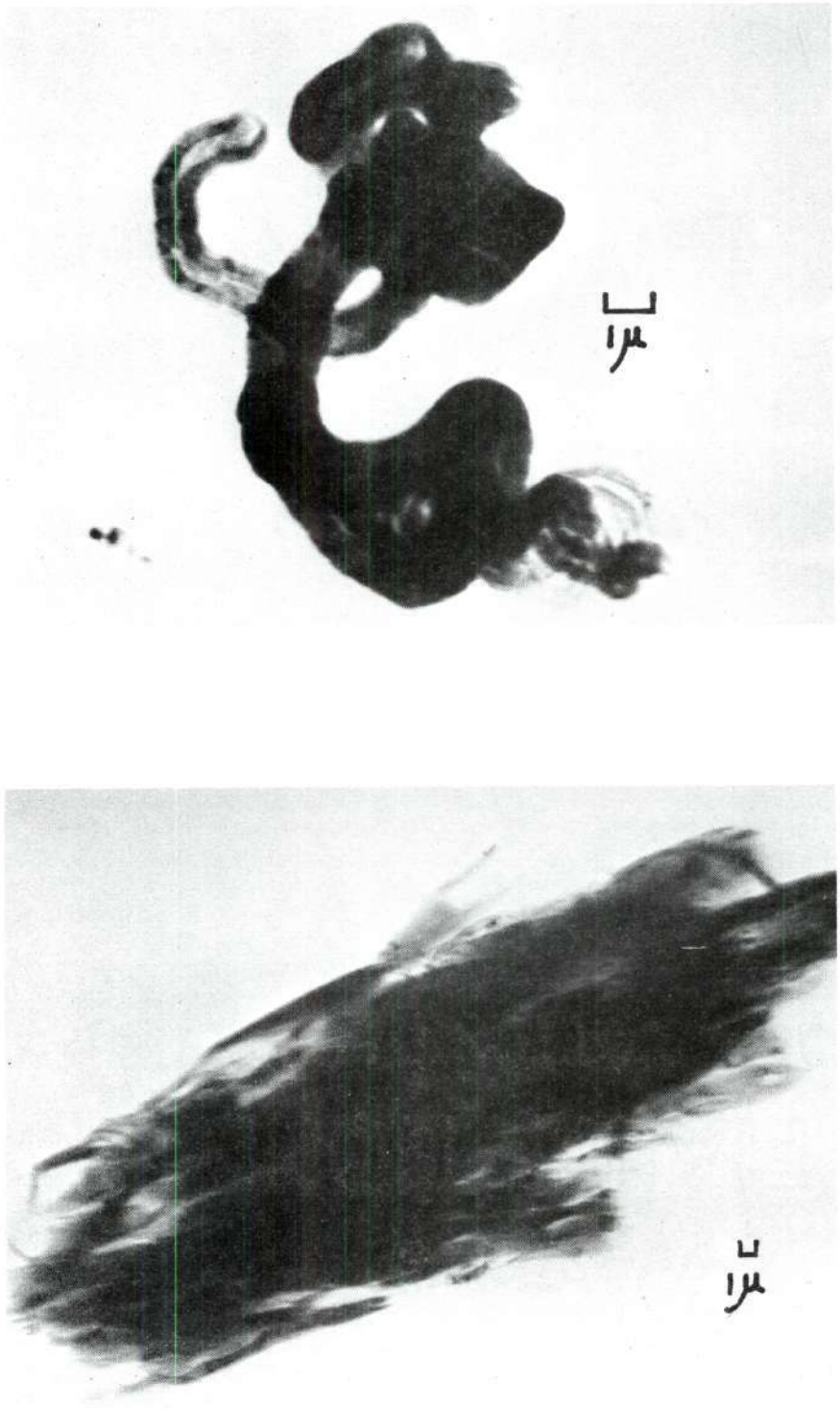

Figure 24. Filamentary and Flake Structures of the Carbon Deposits at 550°C

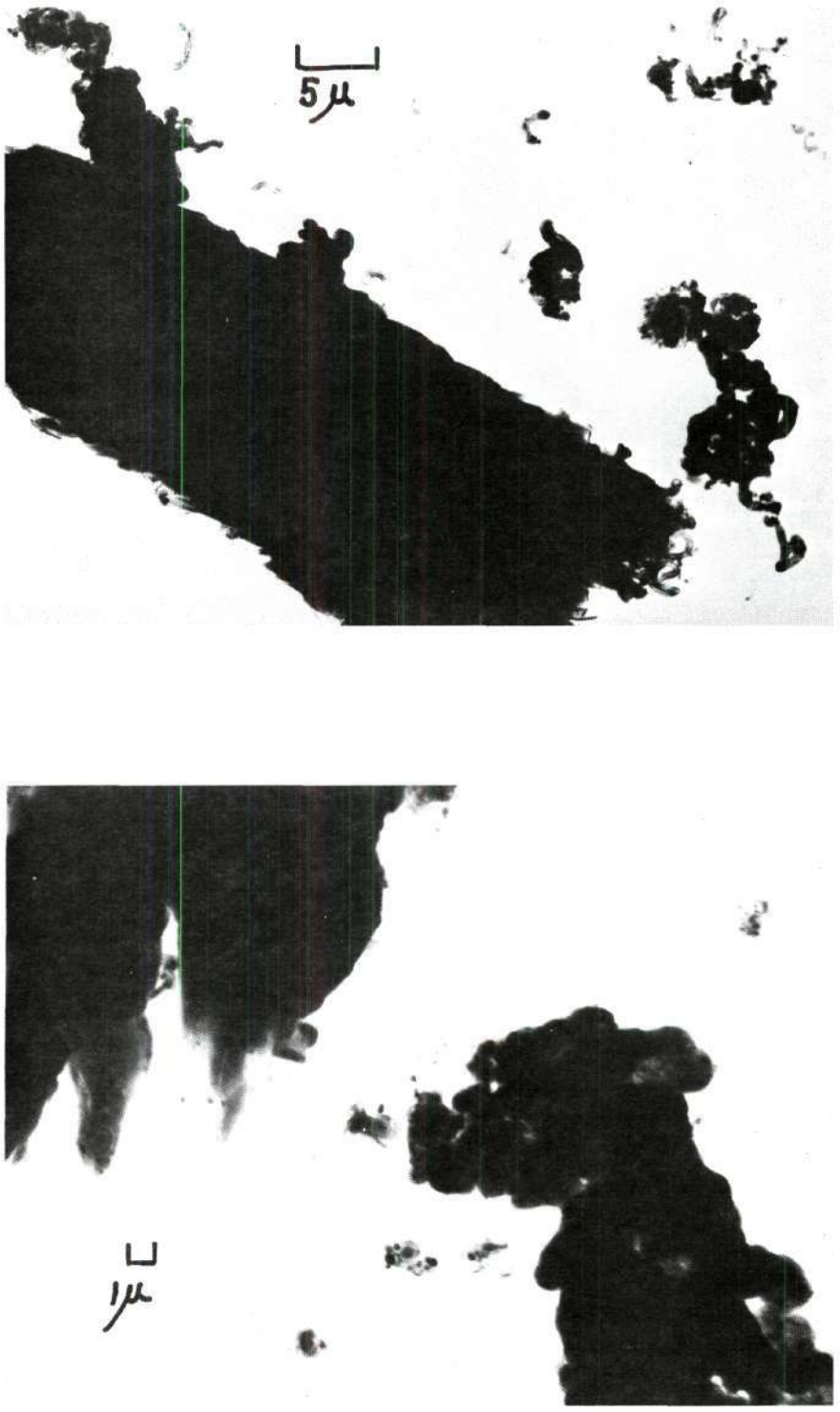

Figure 25. Typical Carbon Deposit Formations

graphitic and 100 per cent amorphous using the ASTM "Float and Sink Test" for graphitic carbon (71). This test was made on the sooty reaction deposits and indicated 100 per cent graphite. Walker and co-workers (102) have shown by x-ray analysis that these carbons are in reality composed of partially graphitic and partially amorphous structures. This could be due to the two types of carbon growth.

X-ray Analysis of Reacted Samples

Powder patterns of the reacted wires were made with a Debye-Scherrer camera to determine the phases present. The results are summarized in Table 4. In all the samples only carbon (graphite), alpha-iron, and cementite were found. Although it is difficult to make quantitative assessments from these data, it clearly verifies the judgments made from the metallographic observations. Cementite is present in increasing amounts to about 700°C, and then tends to decrease. A pattern of Run 38 (T = 696°C) was made after removing surface deposits, and only alpha-iron was indicated; thus the light ring on the exterior of the sample in Figure 21 is definitely ferrite. At the lower temperatures the diffuse line characteristic of carbon seemed much broader than at the high temperatures. Walker, Rakszawski and Armington (102) have shown that this is indicative of amorphous carbon.

High-Temperature X-ray Reaction Studies

A high-temperature x-ray camera was employed to study phases actually present during the reaction. The main purpose was to verify that phases observed at room temperature were correctly related to those at experimental conditions. The results are given in detail

Table 4. X-ray Analysis of Reacted Samples

ASTM Card (101)			Iron Wire	Run 37 T=515°C	Run 33 T=546°C	Run 35 Annealed T=536°C	Run 43 T=586°C	Run 40 T=702°C	Run 39 T=820°C	Run 38 T=969°C	Carbon from T=546°C	Run 101 550°C	Run 107 850°C	Run 36 T=594°C
α-Fe	Fe_3C	C(gr)												
1.17(30)			1.17(S)	1.17(S)	1.17(S)	1.17(S)	1.17(S)	1.17(X)	1.17(S)	1.17(S)		1.17(S)	1.17(S)	1.17(S)
	1.19(M)*				P	P		1.19(VL)			P	1.19(VL)		1.19(VL)
	1.22(M)*			1.22(VL)	1.22(VL)	1.22(VL)	1.22(L)	1.22(L)	1.22(L)		1.22(L)	1.22(M)	1.22(L)	1.21(L)
$1.28K_\beta$1.17			1.28(VL)	1.28(XL)	1.28(XL)	1.28(XL)	1.28(XL)		1.26(XL)	1.28(XL)			1.28(XL)	1.28(XL)
	1.32(M)*				1.33(XL)	1.33(XL)	1.33(L)	1.33(VL)			1.32(XL)	1.33(XL)		1.33(L)
1.43(19)			1.43(M)	1.43(M)	1.43(M)	1.43(M)	1.43(M)	1.43(M)	1.43(M)	1.43(VL)		1.43(M)	1.43(M)	1.43(M)
	1.58(20)			1.60(XL)		1.58(VL)	1.59(VL)	1.58(XL)				1.59(VL)		
		1.68(8)		P	P		1.68(XL)	1.68(XL)		1.67(M)	1.68(XL)	1.68(XL)		1.67(XL)
	1.85(40)			1.84(XL)	1.85(XL)	1.85(XL)	1.85(VL)	1.84(XL)	P		1.84(VL)	1.83(L)		1.85(XL)
	1.97(55)			1.97(XL)	1.97(XL)	1.97(VL)	1.97(L)		P		1.97(L)	1.83(L)		1.85(XL)
	2.01(100)			2.02(S)		2.02(S)					1.97(L)	P		1.97(VL)
	2.02(60)			2.02(S)		2.02(S)					2.01(L)	2.01(M)	2.01(L)	
2.03(100)			2.025(S)	2.02(S)	2.03(S)	2.02(S)	2.03(S)	2.02(S)	2.02(S)	2.03(S)	2.07(L)	2.03(M)	2.03(M)	2.03(S)
	2.06(70)			2.06(VL)	2.06(VL)	2.06(L)	2.06(L)	P	P		2.07(L)	2.06(VL)	P	2.06(L)
	2.10(60)			2.09(VL)	2.10(VL)	2.10(L)	2.10(L)	2.10(XL)	P	2.10(XL)	2.07(L)	2.10(VL)	2.10(XL)	2.10(L)
	2.20(25)			2.20(XL)	2.20(VL)	2.20(VL)	2.21(VL)	2.20(XL)	P	2.20(XL)		2.20(XL)	P	2.21(VL)
	2.26(25)				2.26(VL)	2.25(VL)	2.26(VL)	P				2.26(XL)		2.25(VL)
	2.38(65)			2.36(XL)	2.37(XL)	2.37(VL)	2.38(VL)	2.37(XL)			2.36(XL)	2.38(VL)	P	2.37(VL)
		3.35(100)		3.34(XL)	3.34(XL)	3.34(XL)	3.32(M)	3.31(XL)	3.33(L)	3.30(L)	3.35(S)	3.30(L)	3.30(L)	3.35(M)

*Hofer, et al. (61)

S = Strong L = Light X = Extremely
M = Moderate V = Very P = Possible
Relative intensities in parentheses.

in Appendix F.

Samples consisted of carbonyl iron powder compressed into a disk the size of a quarter and placed in the furnace. The Mylar x-ray windows could not be totally sealed, and some oxygen leaked in. After an hour the samples distorted and the runs were terminated; thus, long exposures could not be evaluated.

The results confirmed previous experimental data. At 550°C, the oxide was reduced from Fe_3O_4 to FeO to iron and cementite was formed. On visual inspection the sample was covered with carbon. At 680°C a good cementite pattern was obtained and the sample had no soot deposits. A reaction at 890°C for two hours gave a pattern only of austenite. On cooling while reacting, cementite was formed. No unusual lines were observed to indicate the formation of another carbide or phase. The oxide present was discounted as an impurity resulting from experimental procedure; it had not been observed in x-ray studies of reacted samples, and was reduced by the carbon monoxide.

Microprobe Studies

A comprehensive program of analysis was performed with the electron microprobe. Polished cross sections of reacted samples were analyzed. Unfortunately, the results had to be considered inconclusive due to a low sensitivity and a fairly high background. Details of the investigation have been deleted since they do not add to the conclusions.

Discussion

The mechanism of the reaction is logically divided into two

portions: the alpha region, below 723°C, and where gamma-iron can exist, above 723°C. In the latter, significant carbon concentrations are obtained in iron.

Alpha Domain (723°C and Under)

Mechanism. From the experimental results, a mechanism is postulated for the alpha region: (1) adsorption of carbon monoxide on the ferrite surface, (2) Boudouard reaction ($2CO \rightarrow C + CO_2$) releasing the carbon, (3) formation of cementite, (4) decomposition of cementite crystals to alpha-iron and graphite. Carbon deposits are built up on the surface by a continuous cycle of the above steps. Variation of the rate of reaction with temperature is caused by the change in the stability of cementite. At lower temperatures cementite is more unstable; hence, less will be formed and subsequently decomposed.

Nucleation. From a study of the adsorption data, Podgurski, Kummer, DeWitt, and Emmett (70) have deduced that cementite forms at nucleation sites and not uniformly over the entire surface. Ratliff (97) has seen cementite form at dislocations of single iron crystals at temperatures as low as 350°C. His observations further substantiate the conclusion that grain boundaries and imperfections are the sites for initial cementite growth. Numerous accounts of carbide formation below 500°C have been cited earlier; however, a reaction could not be detected by the thermobalance below 450°C.

The rate of formation of a critical nucleus at temperatures below 475°C is so slow that no bulk reaction was observed in the thermobalance. A critical nucleus is necessary for the stable formation and subsequent decomposition cycle. The time required for a critical nucleus to form

follows the Arrhenius form. The activation energy of formation for the critical nucleus is calculated from the incubation data (Figure 10). A linear function with reciprocal temperature is obtained and the activation energy is calculated to be 19.0 kcal/mole. This value is comparable to the 18.5 and 22.0 kcal/mole values obtained from the kinetic data in the 500°C to 570°C range. The limiting factor of the reaction in this range is the formation of cementite crystals on the ferrite surface. The cementite produced decomposes into ferrite and graphite faster than it is formed.

Cementite. Podgurski and co-workers (70) have shown that carbon monoxide is strongly chemisorbed on ferrite at temperatures below 100°C. Above this temperature, experimental difficulty is encountered due to carbide formation. Their experiments show that carbon monoxide is not adsorbed by Hägg carbide at 200°C. This implies that cementite would also have only weak chemisorption, since Fe_3C and Hägg carbide have similar ferro-magnetic moments and the outer d-orbitals of the iron are occupied. Since cementite is more stable than Hägg carbide, it is logical to label cementite as an inactive substance and probably more passive than χ-carbide. The formation of a stable layer of the carbide on the iron surface accounts for the declivity in reactivity.

As the temperature is increased from 500°C, cementite becomes more stable. Figure 26 shows the free energy of formation of cementite, the free energy of reaction from iron and carbon monoxide, and the free energy of the Boudouard reaction as a function of temperature (75, 96). Unfortunately, the stability of cementite cannot be determined exactly because it is relative to the environment. In steels it is well known

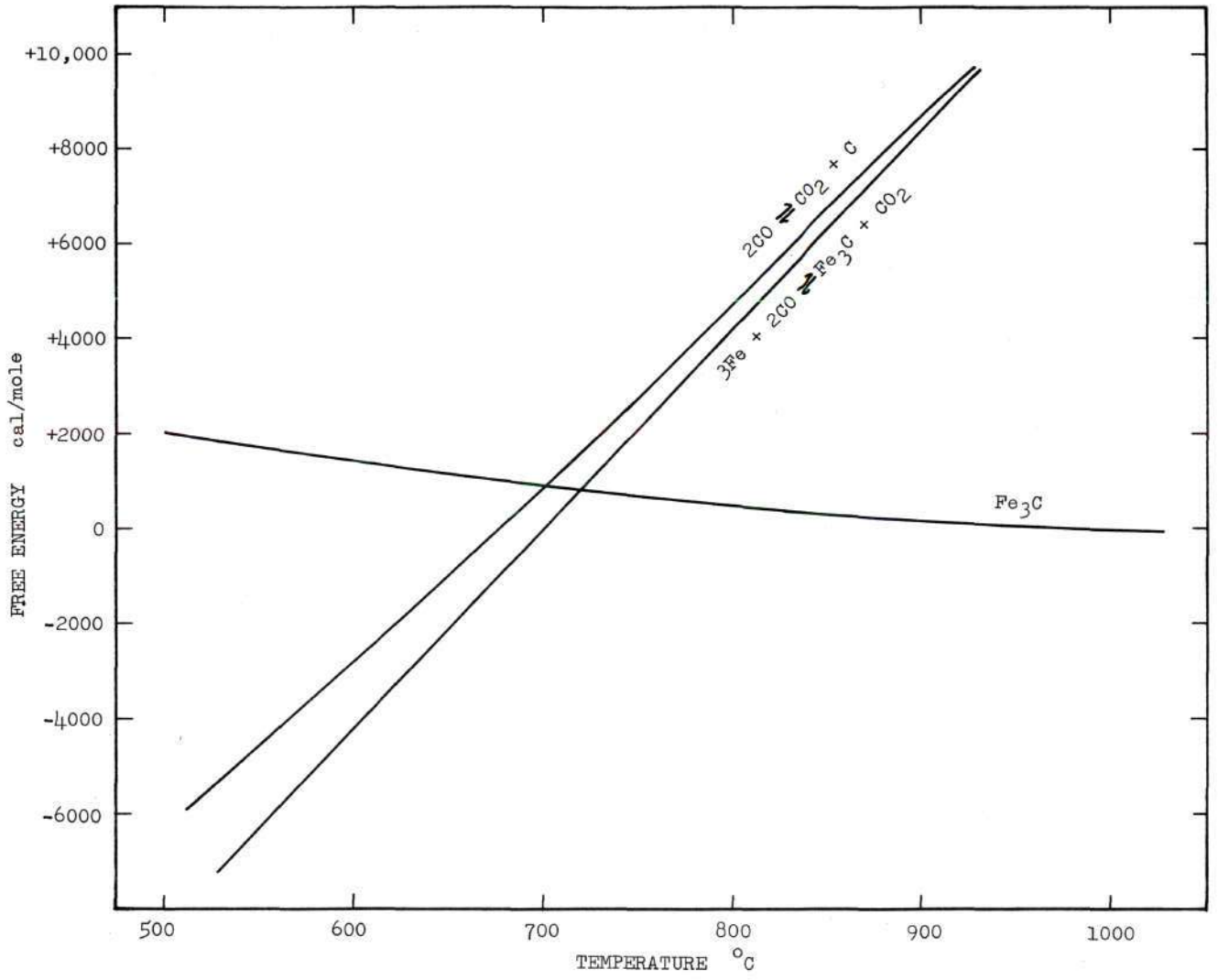

Figure 26. Free Energy of Formation of Cementite

to exist indefinitely at room temperature where it is decidedly unstable. Cementite has been extracted from samples of iron reacted with CO and then heated to the reaction temperature where it decomposed in a brief time (92). It is possible to form significant amounts of cementite on the surface of reacting iron at 600°C.

Epsilon and chi iron carbides in the literature survey were found to decompose rapidly at a temperature of 500°C, forming cementite and graphite (72). Since the conditions for the above statements were arbitrary, the results do not specifically evince that given different surroundings a higher carbide could not exist. However, when isolated, such a compound would be unstable. Due to the instability of the pure compounds and the transitory nature, limited concrete data about the iron carbides are available.

The metallographic observations show that there is an increase in cementite thickness at the minimum reactivity, 700°C. The above proposed mechanism agrees with the deductions of Walker, Rakszawski, and Imperial (36) from their work with carbon monoxide-hydrogen mixtures reacting over iron catalysts.

Nature of the Accelerated Reactions. Ruston, Warzee, Hennaut, and Waty (92) have performed an in-depth investigation on the reaction of carbon monoxide on polycrystalline films at 550°C. They report observing carbon formation by two distinct processes, decomposition of cementite and the formation of ε-carbide crystals which catalyze elementary carbon deposition on the surface. Originally, these crystals are formed on the surface, but the carbide is lifted from the surface and carried at the tip of the formation. Different orientations have

more reactivity, but rates equalize in the extended reactions. Ratliff (98) also has observed variation in grain reactivity of polycrystalline iron films reacting in carbon monoxide.

The present experimental work observed no carbide other than cementite. This could be due to carbon whiskers, hence the ε-carbide, being dislodged before analysis. It is also possible that minute ε-carbide particles in the filaments escaped detection by x-ray analysis. Selected area diffraction with the electron microscope was impossible because of the small size of the filaments. The carbon reaction products did contain the carbon whiskers like those reported by others (14, 64,36,92,93). The two forms of carbon formed in the reaction deposits at 550°C indicate two mechanisms of carbon growth.

Two explanations are possible for the rapid initial reactivity in the wire II samples: (1) a higher energy state consisting of an abnormal amount of dislocations, and imperfections and grain boundaries, or (2) a preferred orientation of the crystals which would give rise to a more rapid reaction. The amount and nature of the cold work and the heat treatment history of the sample control both of these variables. The shift in curvature of the initial weight-gain curves for wire II suggests a mechanistic change. Wire I and wire III samples were uniformly coated with carbon, but those samples with accelerated weight gain (wire II) had numerous blunt protrusions from the surface. The foregoing information indicated that wire II was in a more activated state and had a substantial amount of filamentary growth occurring in the first eight hours. After heat treatment, recrystallization eliminated the high energy state and normal reaction curves resulted.

Equilibrium Limitation. The equilibrium of carbon monoxide over iron (shown in Figure 3) decreases markedly and could operate locally to slow the reaction at higher temperatures. Evidence to the contrary is the rapid reaction at much greater temperatures. Furthermore, even at the reaction peaks, overall conversion of carbon monoxide barely approaches 99 per cent.

Synopsis. The lack of observable reaction below 475°C and the increasing amounts of carbon deposits up to about 570°C is controlled by the formation rate of critical cementite nuclei. An excess of alpha-iron is available for reaction. The ferrite surface supports the reaction, while the cementite is passive. At about 570°C the production rate of cementite surpasses the decomposition rate and a maximum occurs in the weight gain at this temperature. As the temperature approaches 710°C, the cementite becomes more stable, forming a passive surface and prohibiting further reaction. Carbon is deposited either in the form of bulky flakes or as a filamentary growth. The amount of filamentary formation is dependent on the cold work and microstructure of the iron sample and will occur mainly during the initial portion of the reaction.

The two aspects of the reaction are illustrated in Figure 27. Using the activation energies in Table 3, two limiting exponential curves are plotted. The reaction is bound by the lowest curve. The first curve represents the rate of critical nucleus production, while the decreasing exponential represents the rate of cementite decomposition, which limits the amount of carbon deposited at temperatures from 575°C to 710°C. The broken line represents a theoretical weight-gain

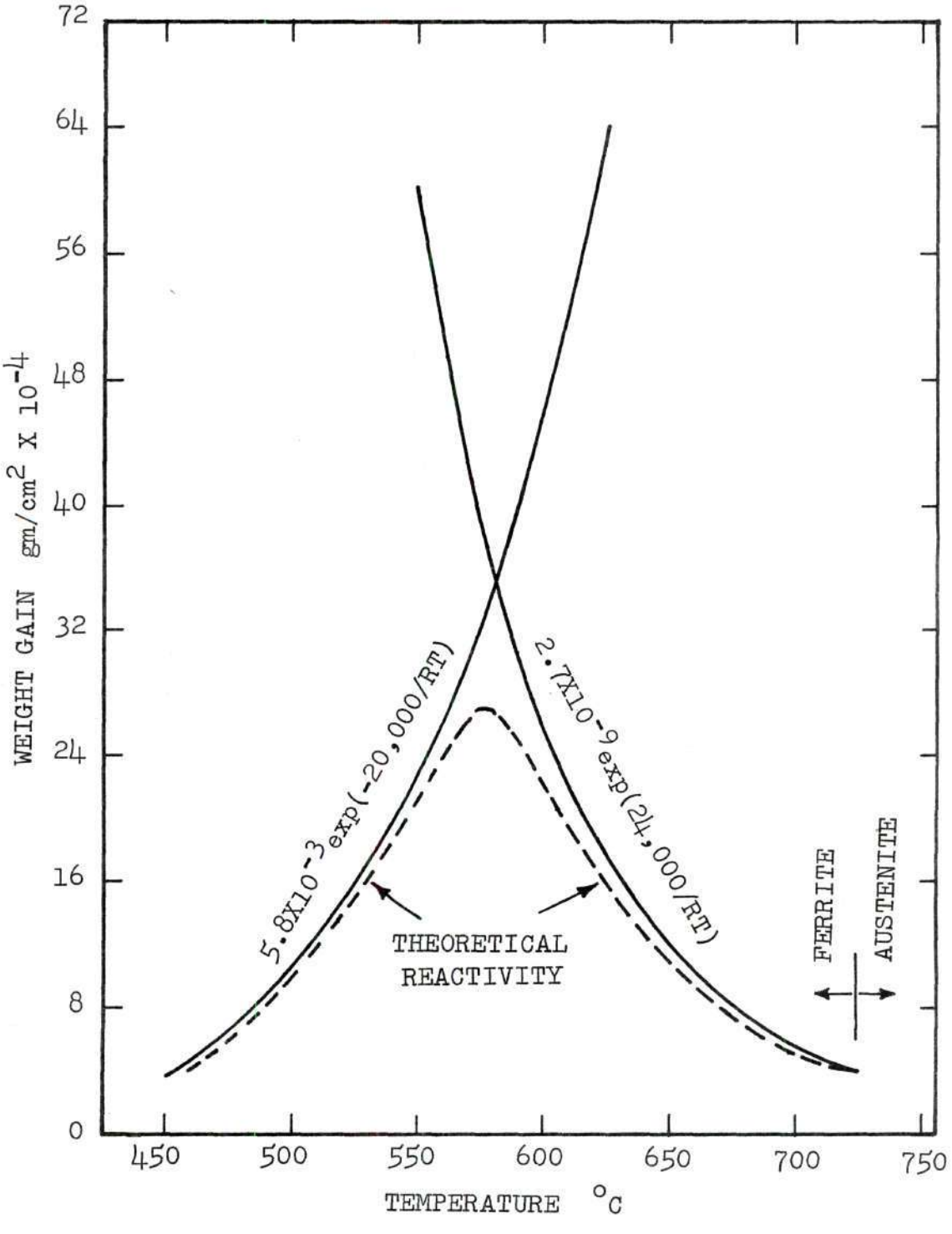

Figure 27. Calculated Theoretical Reactivity in the Alpha Domain for 20 Hours

curve for 20 hours reaction. It agrees well with the experimental curve. The maximum occurs at 575°C. Weight gains in the vicinity of the maximum are slightly lower than the experimental results. This is due to the filamentary growth which occurs during the initial stages and which is in addition to the cementite decomposition.

Mechanism Above 723°C

Diffusion. By noting the temperature where the maximum solubility of carbon in austenite intersects the reactivity curves at the different times in Figures 13-17, one will find that these times represent approximately the end of the hyperbolic portion of weight-gain curve (Figure 9). Diffusion, therefore, is related to the controlling factor, until the carbon saturates the austenite.

Duffusion equations for a cylindrical system, with boundary conditions of surface concentration constant for all time greater than zero, and initially free of solute, are developed in Appendix C. In the case of carburizing pure iron isothermally between 723°C and 910°C, a two-phase region will be encountered. It can reasonably be postulated that a saturated alpha structure with essentially no carbon will exist in the center since the diffusivity of carbon in ferrite is much greater than in gamma, as illustrated in Table 12. When carbon is deposited from the carbon monoxide, an outer layer of austenite will form on the outside and encompass the ferrite. The time required to accomplish this will depend on the diffusivity of carbon in austenite, availability of carbon, and the mobility of the two-phase interface.

From equations in Appendix C, approximate times required for the center of the wire to reach the minimum concentration necessary for

austenite to exist are calculated and presented in Table 5.

Table 5. Calculated Time Required for Concentration in Wire Center to Become Minimum for Austenite

T°C	C_H	C_L	C_L/C_H	D cm^2/sec	Time to Reach C_L/C_H at r=0 Hours
750	0.76	0.54	0.71	1.5×10^{-8}	3.5
800	0.90	0.29	0.32	3×10^{-8}	0.91
850	1.05	0.14	0.13	6×10^{-8}	0.32
900	1.20	0.002	0.0016	1.5×10^{-7}	0.05

D = approximate average diffusivity of austenite at given temperature.

C_H = maximum concentration of carbon in austenite at given temperature (this should be the constant surface concentration during reaction).

C_L = minimum concentration of carbon in austenite at given temperature.

For these calculations diffusion is assumed to be the limiting factor and the sample is assumed to consist entirely of austenite. If the phase transformation is more rapid than the rate of diffusion, the concentration profiles for the system with a phase change will be similar to that of a homogeneous medium when the concentrations at r = 0 are the same. This case is illustrated in Table 5. If the rate of transformation from ferrite to austenite is significant, relative to

diffusion, the gamma phase will approach homogeneity.

Two wires reacted in carbon monoxide for 20 hours at 728°C and 735°C are shown in Figure 28. The difference in contrast is due to the degree of etching and not necessarily carbon content. Note the uniform appearance of the pearlite structure, indicating the existence of a relatively homogeneous austenite phase during the reaction. For these temperatures a minimum period of five to six hours was calculated for the time required for the sample to become entirely austenite. The homogeneity of the pearlite indicates that the conversion of ferrite is slower than the diffusion. Samples reacted at higher temperatures possessed an entirely uniform cross section.

Some concentration-time curves calculated from Equation 10 (Appendix C) are given in Figure 29. Since the concentration is graphed as C/C_H (C_H is the surface concentration), the curves apply equally to all temperatures when there is a reduction of time to offset any increase in the diffusivity. Note that even at a temperature of 730°C, slightly above the minimum of 723°C for austenite, after 20 hours the computed concentration at the center reaches 94 per cent of that at the surface.

The increase in the weight-gain curves at temperatures above 723°C can be attributed to a saturation of the lattice with carbon, and then the formation of a carbide on the surface. As the temperature increases the stability of the carbide relative to austenite and graphite (Figure 2) decreases. This is indicated by the room temperature x-ray data where decreasing amounts of cementite were observed as the sample reaction temperature increased. At-temperature x-ray analysis at 890°C did not detect cementite.

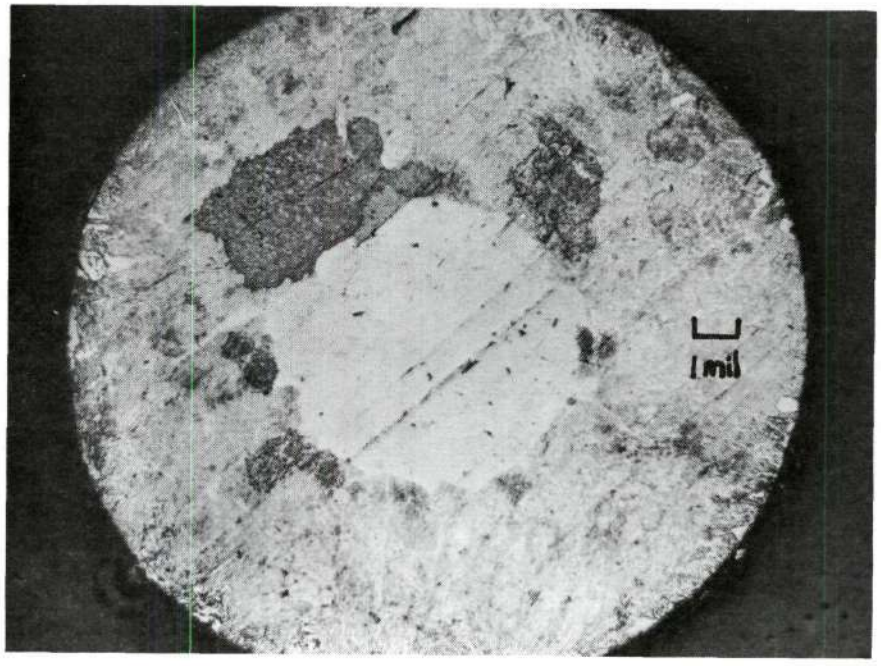

T=728°C

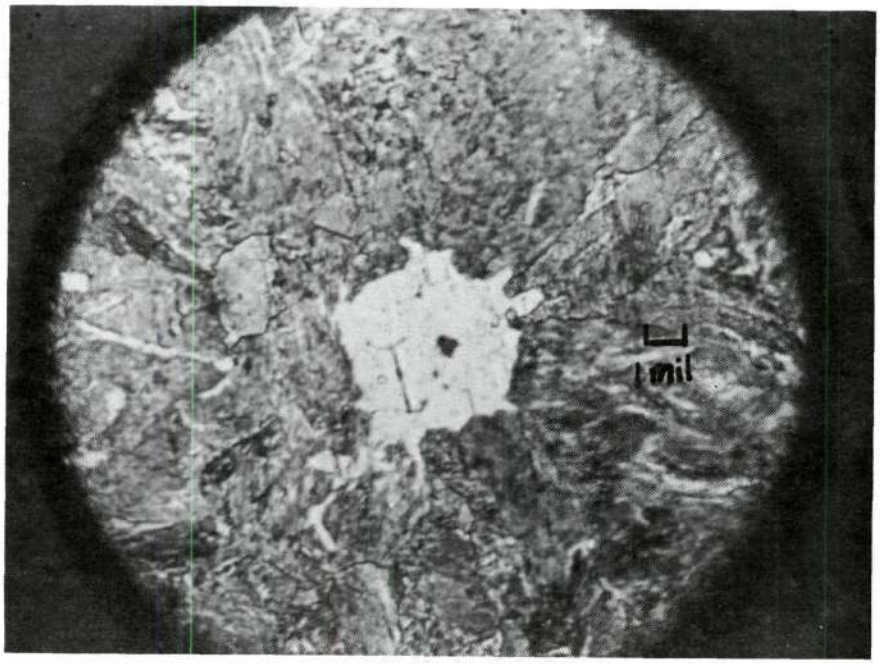

T=735°C

Figure 28. Polished Iron Cross Section after Reaction in Carbon Monoxide for 20 Hours

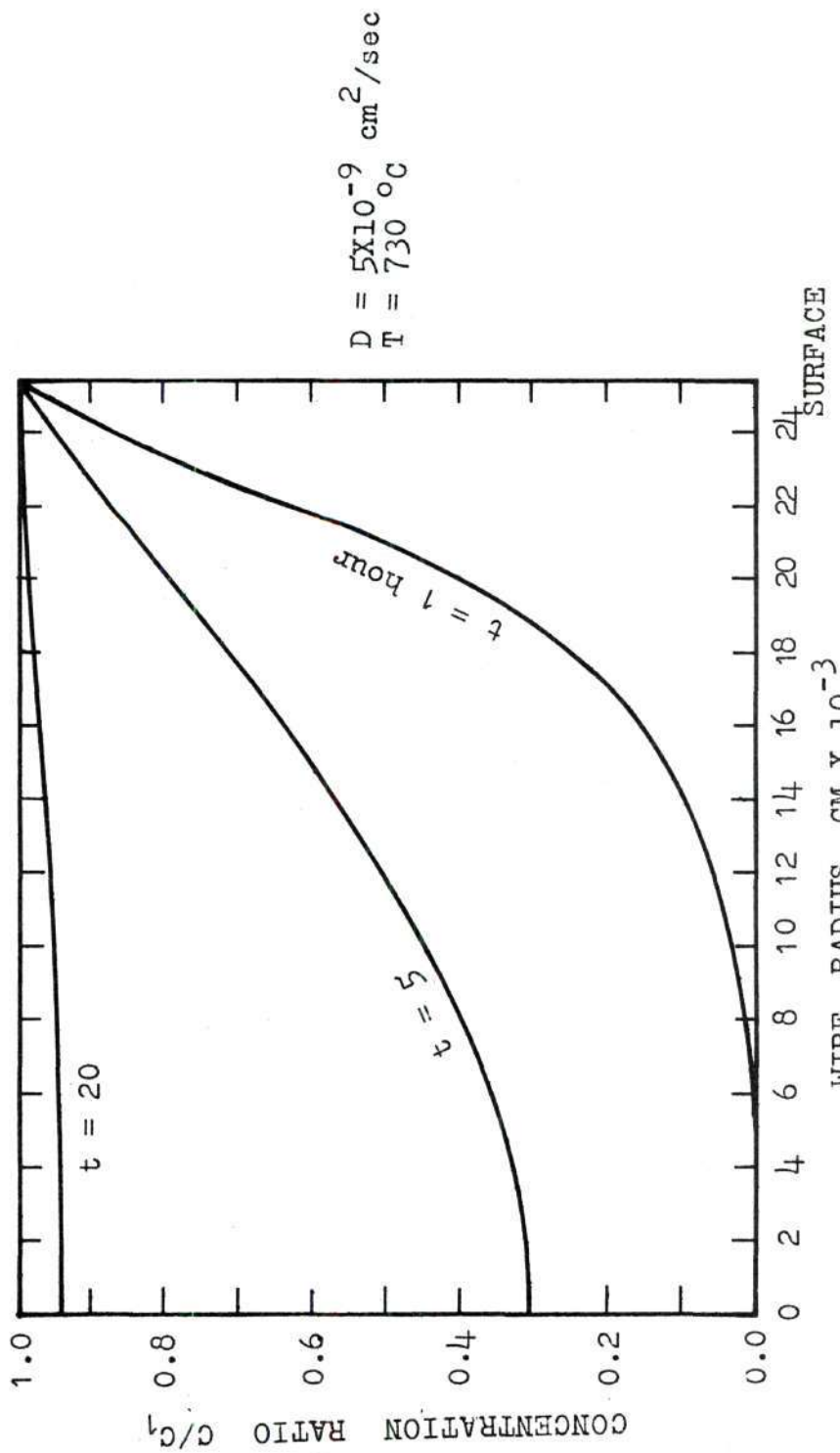

Figure 29. Diffusion Profile Curves for 730°C

The rate of diffusion of carbon into the iron is the controlling factor for samples reacted above 723°C. Figure 30 shows the parabolic portions of the weight-gain curves plotted against the square root of time. The linear relationship is indicative of diffusion in an infinite slab, and is approximated by the experimental samples at short times. The slope of these curves, which represent the reactivity, is plotted against temperature in Figure 31. The computed activation energy of diffusion is 35.4 kcal/mole, the exact value calculated by Asimow (103) for austenite with no carbon. Austenite saturated with carbon will have an activation energy of about 37.0 kcal/mole. Until the iron becomes saturated, carbon diffusion is deemed the controlling factor.

Formation of Surface Deposits. After the sample is saturated with carbon, it is possible that at high temperatures graphite is formed directly from free carbon, released by the Boudouard reaction, on the surface of austenite. Retarding the reaction would be any cementite present on the surface. X-ray results showed lesser amounts of cementite on the surface as the reaction temperatures increased from 710°C. Figure 2 showed that cementite becomes less stable in the austenite-graphite-cementite system. The amount of cementite formed decreases with increasing temperature, exposing greater amounts of reactive austenite.

Metal Dusting

The results of this study give several clues to the mechanism of metal dusting encountered in ferrous alloys in industry. At temperatures below the eutectoid (723°C), uniform removal from the surface is accomplished by the gradual formation of cementite and the mechanical

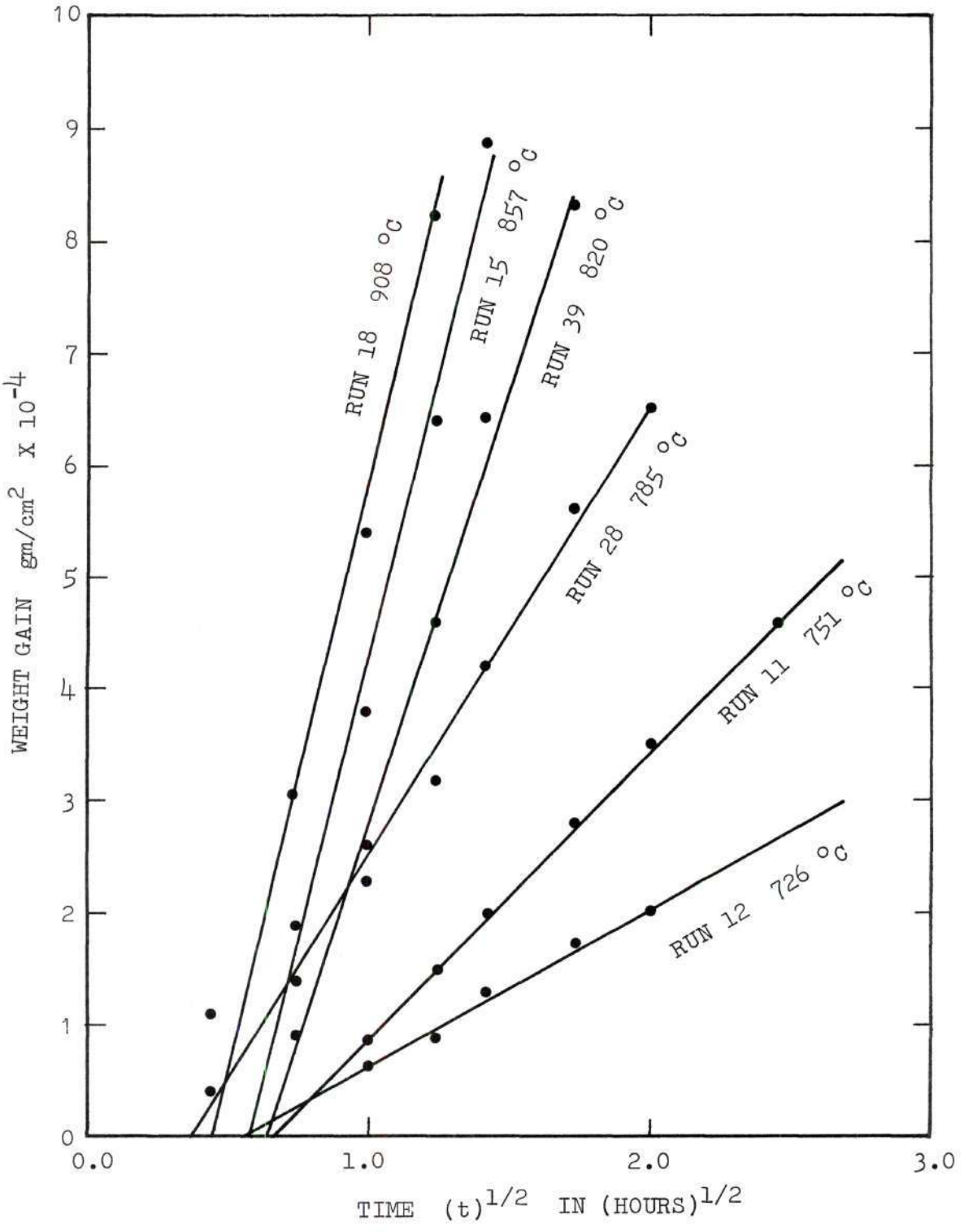

Figure 30. Initial Weight Gain of Austenitic Samples Versus Square Root of Time

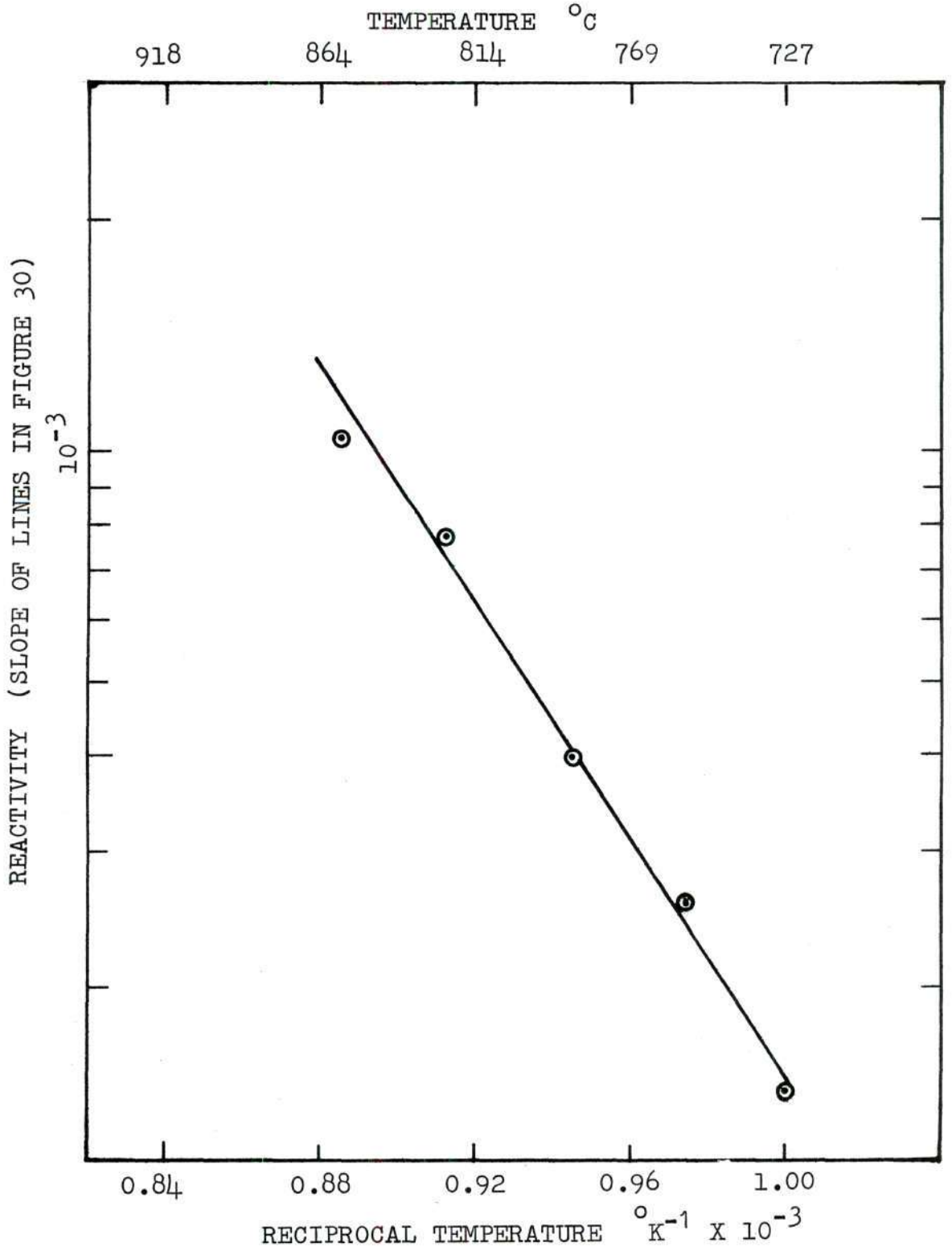

Figure 31. Calculation of Activation Energy of Initial Segments of the Austenitic Samples

removal of the cementite, which does not firmly adhere to the surface. Figure 32 shows an example of how the cementite layer might be removed from the surface. Pitting at the lower temperatures could be attributed to reactivity caused by the grain orientation in the Fe_7C_3 reaction found by Ruston and co-workers (92), in addition to industrial flow rates and passive films. At the higher temperatures, unexplained examples of catastrophic corrosion might be caused by temperature cycling with the formation and subsequent mechanical removal of cementite, leaving an exterior band of reactive ferrite. When austenite cools rapidly, the carbon in the lattice will produce compressive stresses on the surface, which will cause cracking and possibly the removal of entire grains.

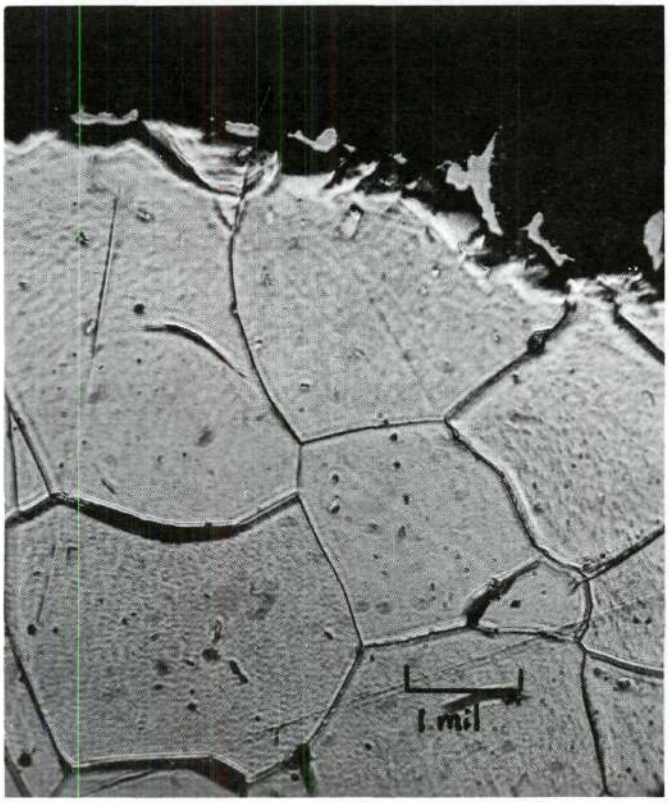

Figure 32. Polished Cross Section of Run 36 (T = 594°C) (Nital-Picric Acid Etch)

CHAPTER V

CONCLUSIONS

From this research, the following can be concluded:

1. When pure iron reacts with pure carbon monoxide at constant temperatures, carbon is deposited on the surface in the 500°C to 720°C temperature range. A maximum rate of carbon production occurs at 570°C. A minimum, with very slight reactivity, occurs at 710°C. A gradual increase in reaction follows as the reaction temperature is increased beyond 710°C up to 1000°C.

2. The bulk of the carbon deposits in the alpha-iron region (below 723°C) is caused by the carbon monoxide reacting with the ferrite to form cementite, and the subsequent decomposition of the cementite into graphite and alpha-iron. Cementite is relatively unreactive with carbon monoxide.

3. The increase in the amount of carbon deposits in the 500°C to 570°C span is due to an increased rate of cementite attaining a critical nucleus for decomposition. The activation energy for nucleation is 19.0 kcal/mole. An excess of alpha-iron is available for continuing the reaction; the controlling factor is the formation of the carbide nucleus.

4. The carbide phase becomes thermodynamically more stable with respect to ferrite and carbon as the temperature increases. The decrease in activity from a highly reactive state at 570°C to a virtually inert

state at 710°C is due to the formation of an unreactive surface of cementite which suppresses the reaction.

5. The diffusion rate of carbon into austenite, until saturation is attained, governs the reaction at temperatures between 723°C and 1000°C. The activation energy for carbon diffusion into austenite was calculated to be 35.4 kcal/mole.

6. The carbon deposited at the lower temperatures is composed of: (1) filamentary growths, and (2) flake or bulk deposits.

7. An accelerated reactivity will be encountered with samples containing an abnormal number of dislocations, imperfections, and grain boundaries, from plastic deformation, or a preferred crystal orientation at temperatures below the recrystallization temperature. This is caused by the selective nature of the filamentary growth. This phenomenon is predominantly part of the initial reaction and diminishes as steady-state is approached.

8. In ferrous alloys, "metal dusting" at low temperatures can be explained by the formation of surface cementite and subsequent mechanical removal. At higher temperatures, where temperature cycling has occurred, an exterior band of reactive ferrite will be formed on slow cooling. Rapid cooling of austenite containing carbon results in compressive surface stresses and possible cracking.

CHAPTER VI

RECOMMENDATIONS FOR ADDITIONAL STUDIES

It was the purpose of this research to investigate a reaction which is fundamental to many complex and compound phenomena. Analysis and understanding of the mechanisms have been hindered by the multitude of experimental possibilities. One of the goals of this work was to provide a foundation from which the more common and intricate reaction mechanisms could be examined. A natural extension, therefore, would be to expand gradually the system under investigation. Such an extension would take two paths: (1) the reaction of iron with various gas mixtures, and (2) the reaction of iron alloys with carbon monoxide. Once data are obtained from such studies, it would then be possible to combine the two, examining complicated systems of interest to obtain meaningful results.

Gas mixtures of interest include carbon monoxide with hydrogen, methane, and carbon dioxide. Also, examining the effect of additions of substances known to activate or inhibit the reaction is important. Variations in the composition of the solid catalyst would include many of the common steels which are exposed to such atmospheres in industrial processes. Other pure metals and their alloys could be studied.

Reactions of iron and assorted iron-containing substances with methane have been conducted at Georgia Tech. It is recommended that correlations be made between the kinetics and mechanism of iron

carburization in the two atmospheres.

One of the adventitious findings of this work was the different reactivity of apparently identical samples. The variation was attributed to the amount of cold work. A study of the variation of reactivity with controlled amounts of cold work would be a definite contribution.

One of the most interesting portions of this research was with the high-temperature x-ray camera--the examination of samples while the reaction was proceeding. The purpose of this apparatus was auxiliary in nature, but by refining techniques valuable quantitative data could be obtained. Difficulty encountered with the sample structure and purity of the gases could be mollified with extended effort, then definitive data could be obtained.

Further study of the carbon deposits is recommended. The basic types were defined in this report. It would be helpful to study variations with temperature. Such an examination would require a more sophisticated electron microscope than the one available for this research.

APPENDICES

APPENDIX A

DETAILS OF THE EXPERIMENTAL APPARATUS

The following pages exhibit the details of the equipment used in the experimental work.

Table 6. Gas Analyses

Element	Typical Analyses from Matheson			Actual Analysis of CO Used
	High-Purity He	Extra-Dry H_2	CO	
Minimum Purity	99.995	99.8	99.5	99.82 Actual
N_2	14 ppm	50 ppm	75 ppm	468 ppm
C_2	1	10	20	192
CO_2	1	5	200	1130
H_2O	12	10	8	7
H_2	1			<10
CH_4	1			< 5
Ne	14			
Ar	1			
CO		5	bal	bal

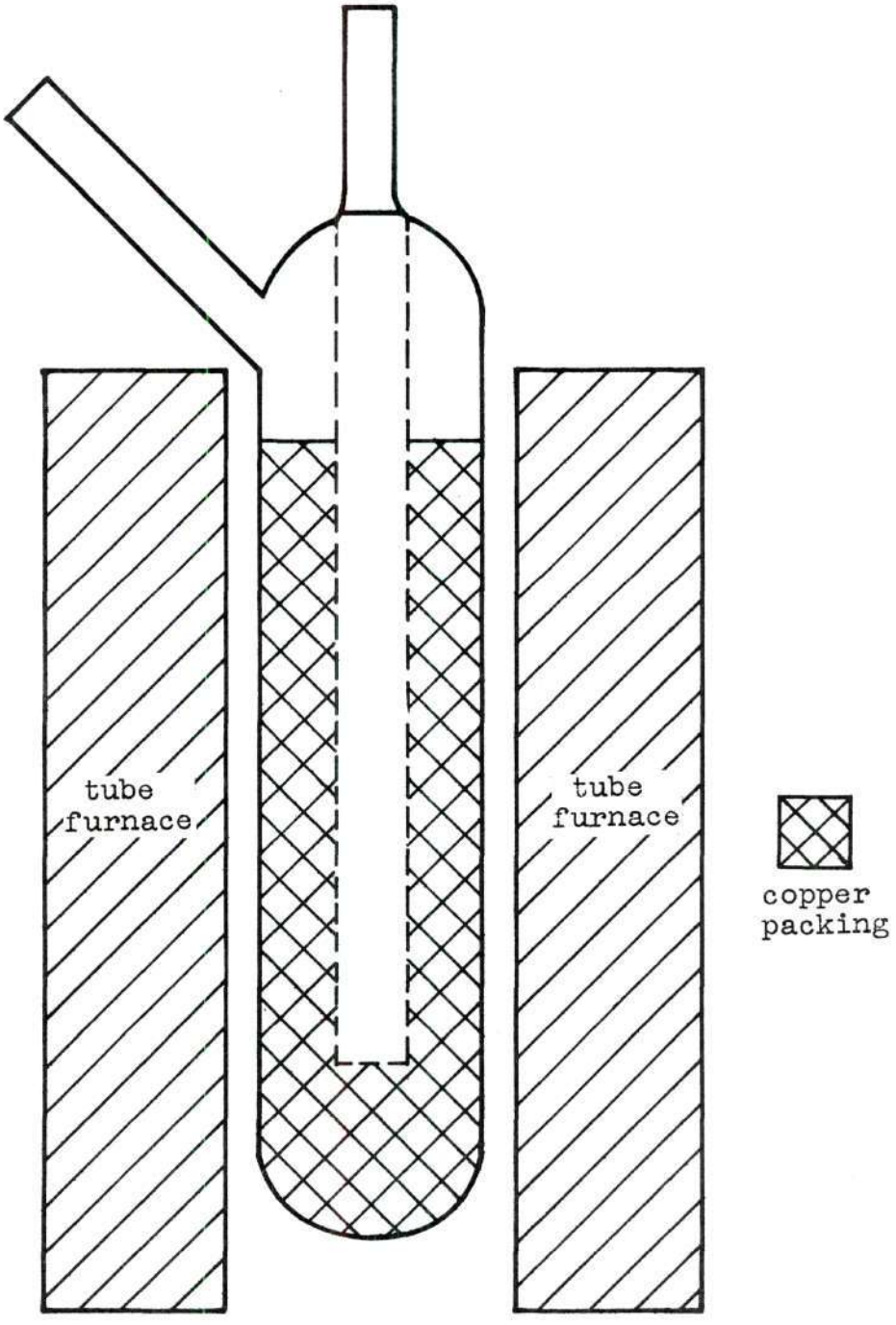

Figure 33. Diagram of the Copper Getter

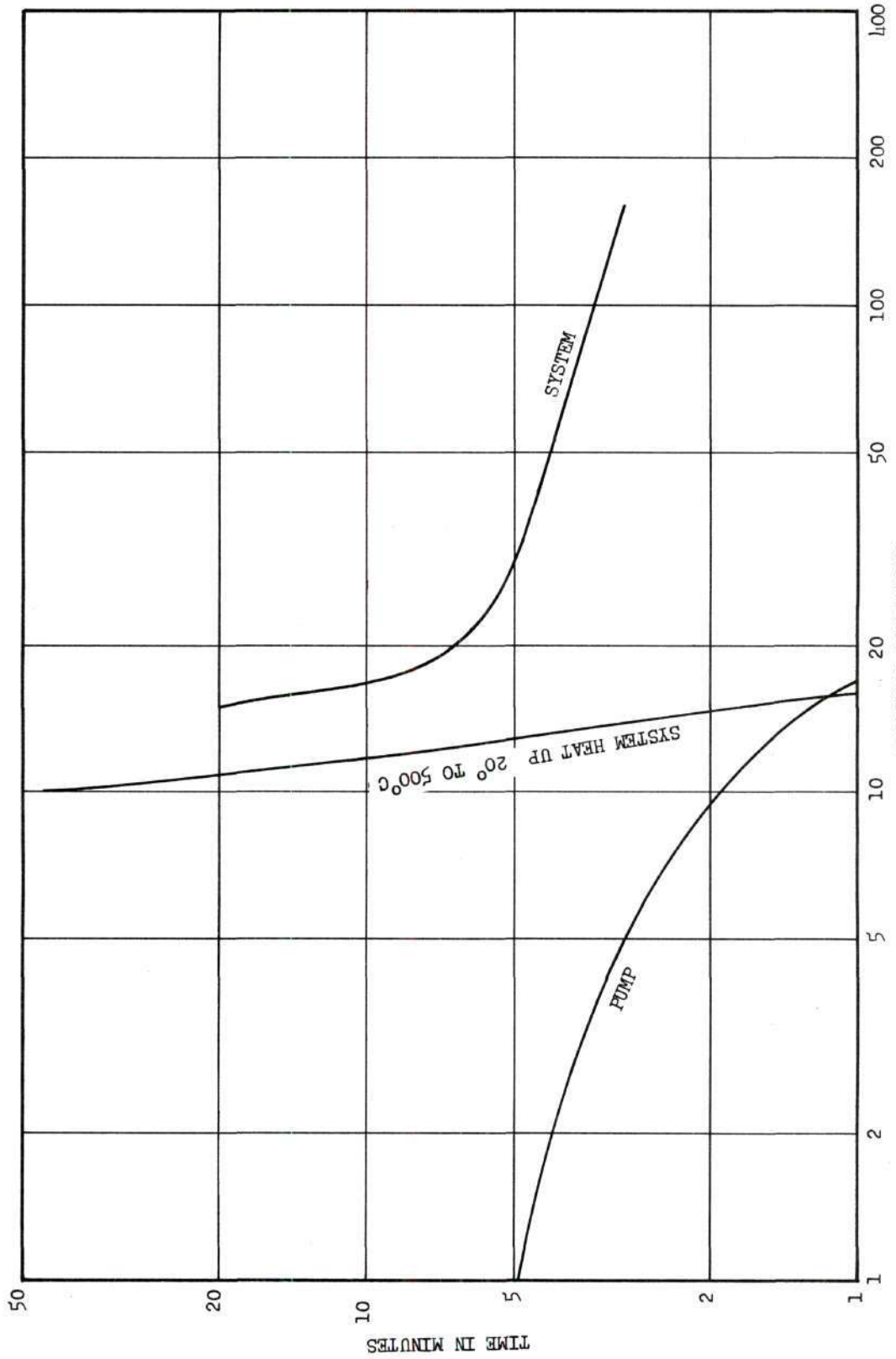

Figure 34. Thermobalance Pumping Characteristics

Computations of the Expected Impurity Concentration

Air Composition

Element	Molecular Per Cent at One Atmosphere	PPM Original Remaining at 20 Microns	PPM After Flush and Repumping to 20 Microns
N_2	76.09	20.7	550×10^{-6}
O_2	20.95	5.5	145×10^{-6}
Ar	0.93	0.25	6.5×10^{-6}
CO_2	0.04	0.01	$.3 \times 10^{-6}$
H_2O (21°-70%)	2.00	0.50	1.25×10^{-6}

The above table illustrates that simply pumping the system to 20 microns reduces the atmospheric impurities well below the level existing in the reaction gas. The practice of flushing the system with helium after an approximate pressure of 20 microns is attained allows the hypothetical values given in the right column. The above conclusions depend on the assumptions that the gases will be removed ideally, in their ratio of content, and leakage and adsorption are assumed zero. However, the concentrations after only pumping are considerably lower than those of the carbon monoxide, especially after the quartz and alumina is heated above 500°C. The actual oxygen content of the gas after passing through the copper getter could not be measured, but is estimated at about two ppm.

Table 7. Calibration of the Thermocouples

I. STANDARDS USED ON THE THERMOBALANCE THERMOCOUPLE

Boiling Water:	Recorded temperature	98.2°C
	Actual Water Temperature	98.2°C
	Atmospheric Pressure	746.2mm
Melting Potassium Chloride:	Melting Point	770.3°C
	Constant Temperature Reading	771°C

II. VARIATION OF THERMOCOUPLE READINGS

Present Thermobalance Pt - Pt 10% Rh	Old Thermobalance Pt - Pt 10% Rh	Horizontal Furnace
512°C	509°C	508°C
612	610	610
706	704	700
805	803	800
903	900	900
1005	999	1005

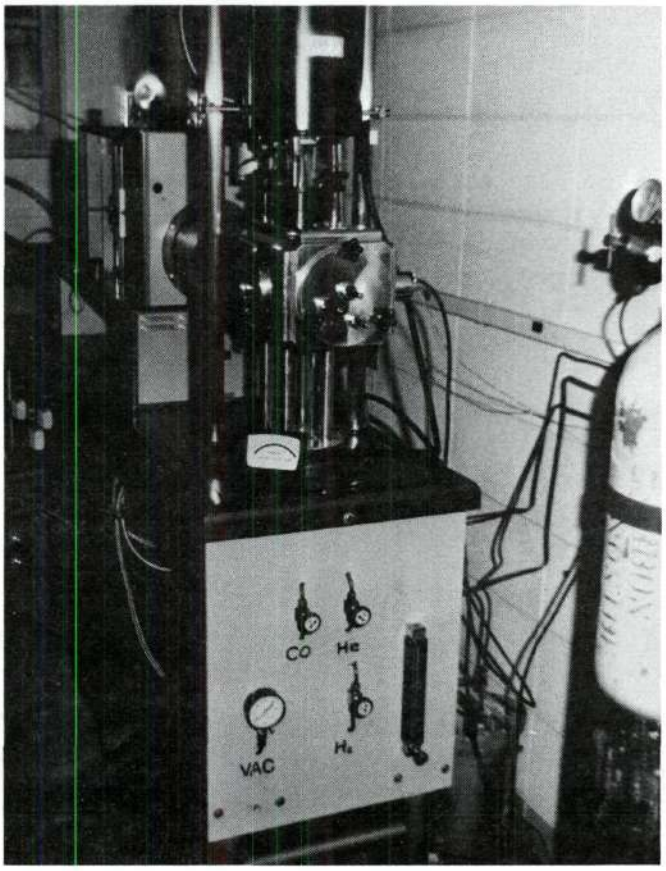

Figure 35. Side View of Thermobalance System

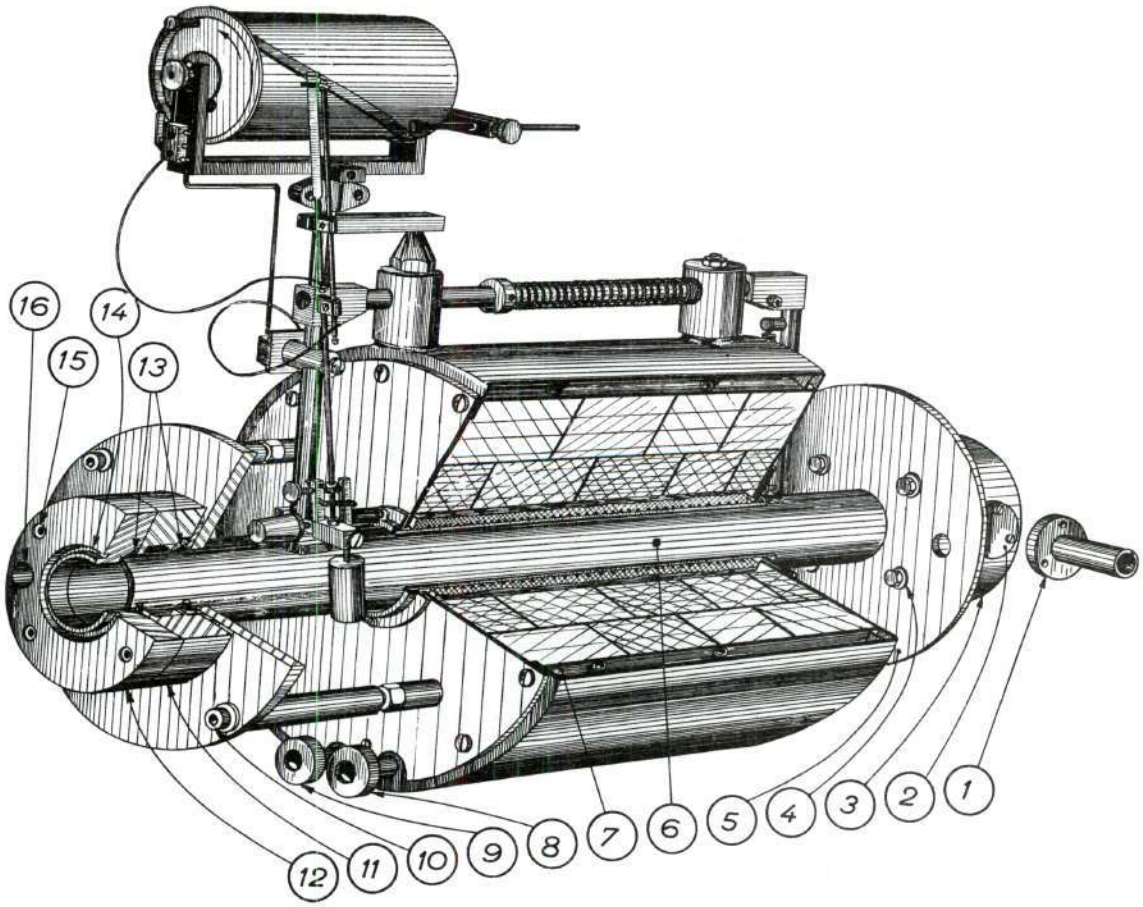

Figure 36. Furnace Diagram

Table 8. Key to Furnace Diagram (Figure 36)

Furnace

1.	Exhaust Port Attachment
2.	Plate Covering Exhaust Port
3.	Water-Cooled Head Piece
4.	Bolt to Hold 3 to 5
5.	Support Plate
6.	Quartz Tube Reaction Chamber
7.	External Furnace Cover
8.	Power Inlet
9.	Power Inlet
10.	Bolt
11.	Water-Cooled Jacket
12.	Bottom Portion of Water-Cooled Jacket
13.	O-Ring
14.	Groove for O-Ring
15.	Bolt
16.	Alignment Port

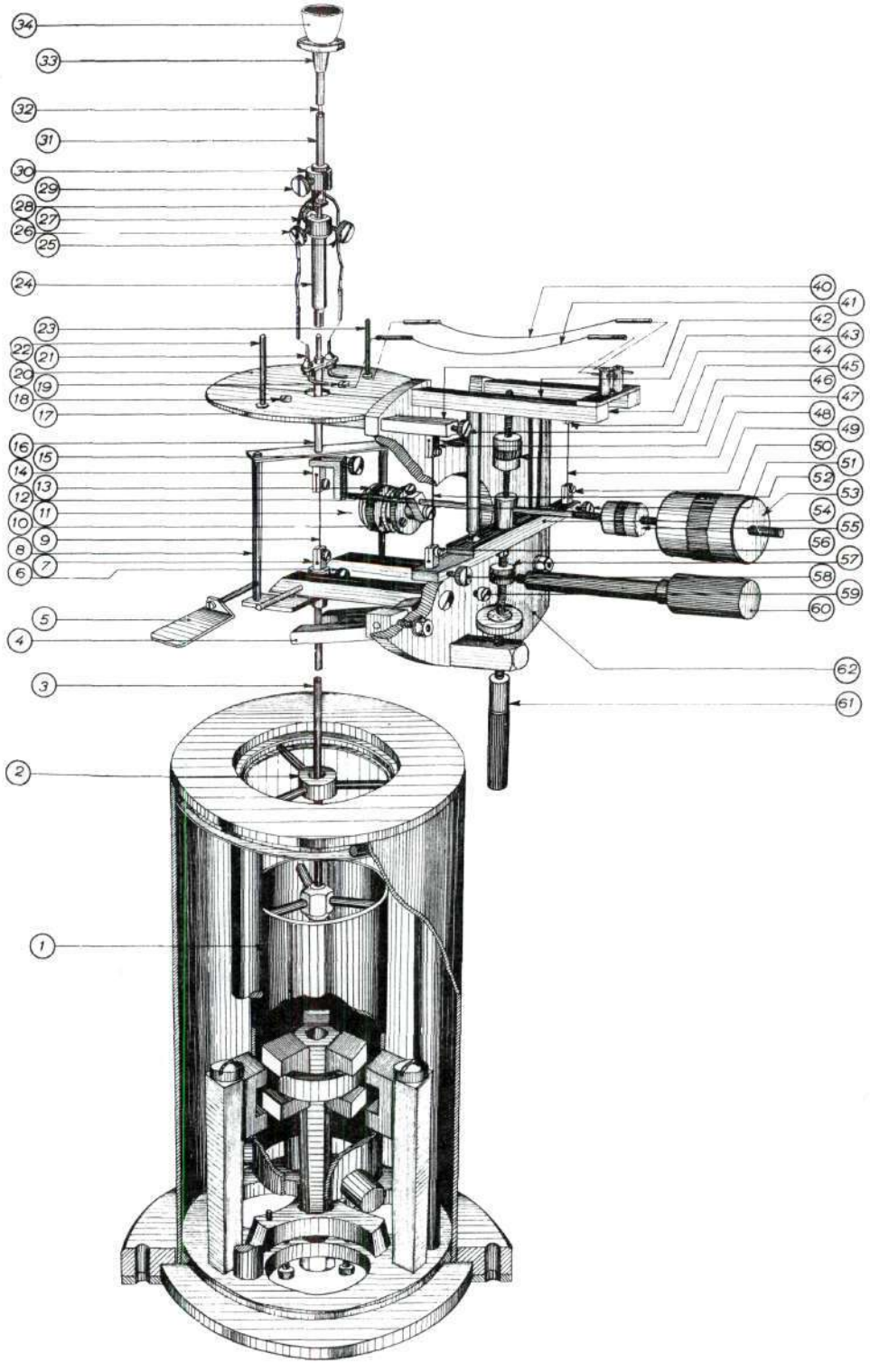

Figure 37. Suspension and Balance Mechanism

Table 9. Key to Suspension and Balance Mechanism (Figure 37)

1.	Damping mechanism
2.	Alignment support
3.	Connection rod
4.	Balance support to secure vertical motion
5.	Plate to hold calibrating weights
6.	Securing screw for ribbon clamps
7.	Ribbon clamp
8.	Frame
9.	Metal suspension ribbon
10.	Mirror adjustment
11.	Concave reflecting mirror
12.	Rod holding conter weights and mirror
13.	Mirror support
14.	Ribbon clamp
15.	Securing screw for ribbon clamp
16.	Connecting rod
17.	Plate to protect suspension mechanism from dirt particles
18.	Screw holding 17
19.	Screw holding 20
20.	Other half of 17
21.	Male junction for thermocouple wire
22.	Rod attached to 17 to facilitate handling
23.	Same as 22
24.	Metal fitting to join alumina sample-support rod
25. 26. 27.	Alignment adjustment screws for alumina rod
28.	Open base of alumina rod clamp
29.	Tightening screw for 30
30.	Alumina rod clamp
31.	Alumina rod
32.	Thermocouple rod
33.	Platform for sample
34.	Boat for liquid and powder samples
40.	Platinum wire
41.	Platinum - 10% rhodium wire
42.	Support bar for suspension equipment
43.	Support bar for thermocouple wires
44.	Securing screw for ribbon clamp (hidden)
45.	Ribbon clamp
46.	Securing screw for ribbon clamp
47.	Ribbon clamp
48.	Sensitivity adjustment weight
49.	Metal suspension ribbon
50.	Ribbon clamp
51.	Securing screw for ribbon clamp
52.	Metal suspension ribbon
53.	Counterweight
54.	Suspension cross bar
55.	Small counterweight
56.	Ribbon clamp
57.	Fine sensitivity adjustment
58.	Securing screw for ribbon clamp
59.	Clamp support screw
60.	External screw adjusting rod for 4
61.	External rod which locks entire suspension in tension-free position.

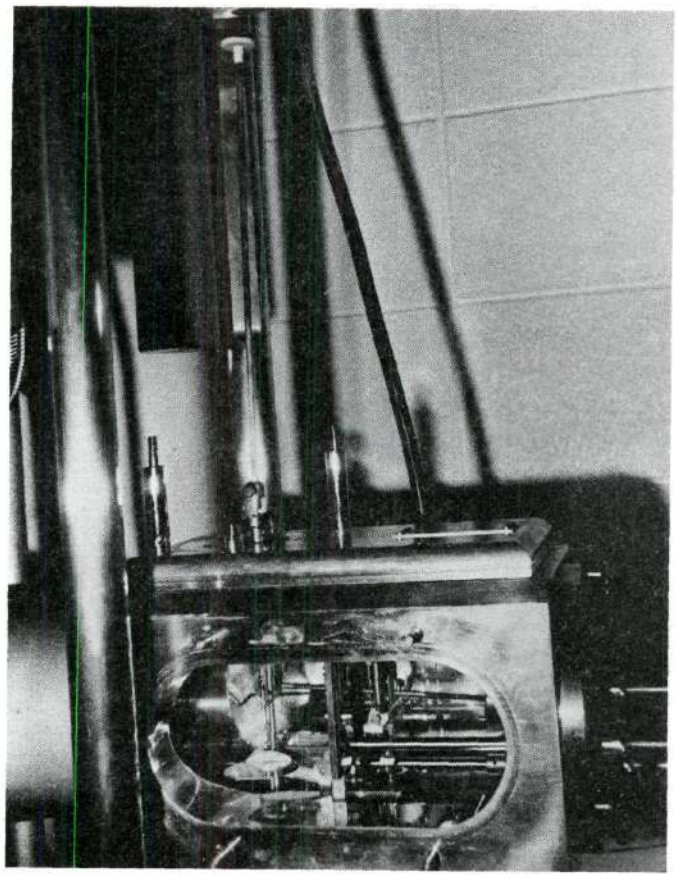

Figure 38. Photograph of Suspension Mechanism and Sample Support

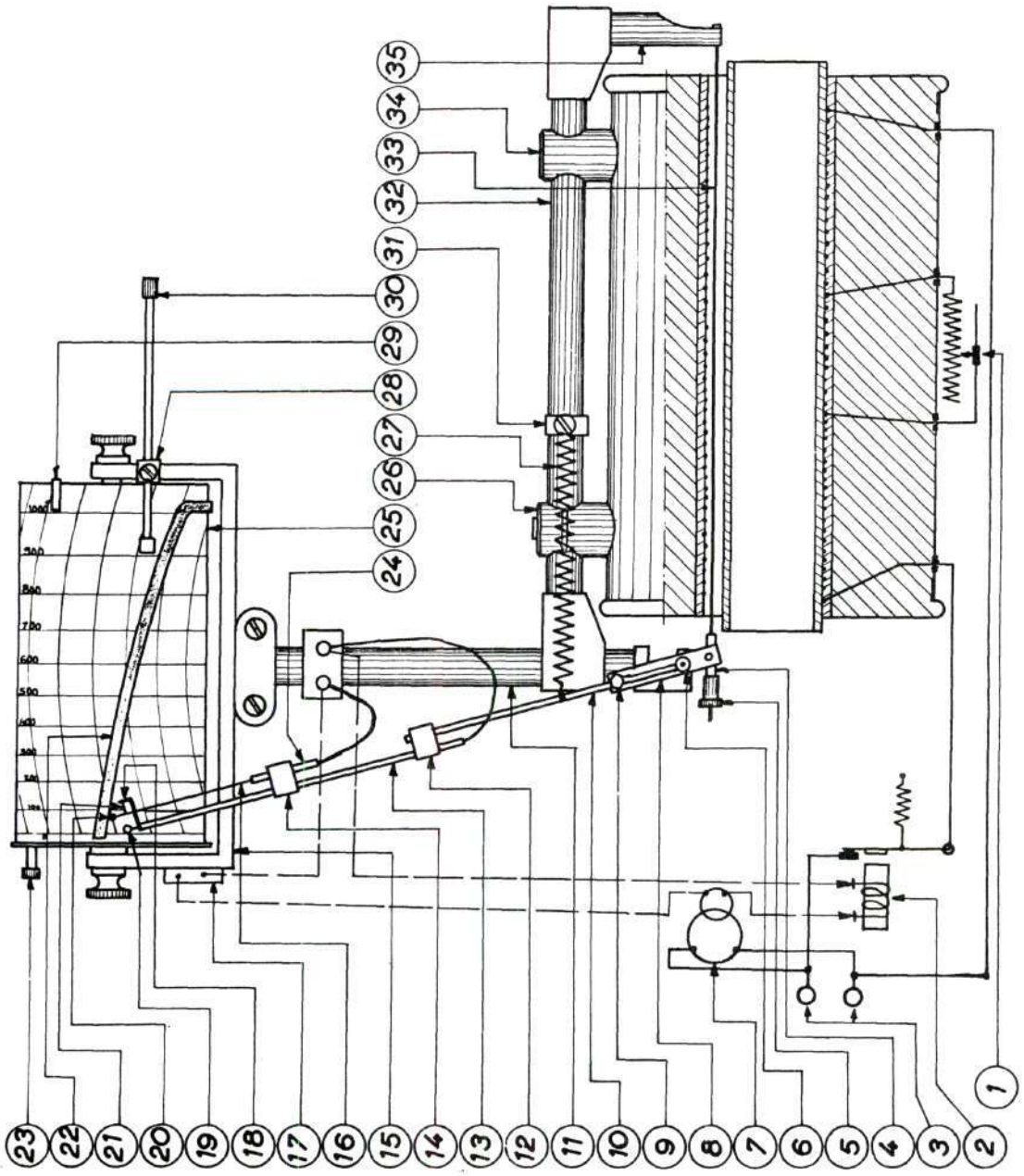

Figure 39. Temperature Control Mechanism

Table 10. Key to Temperature Control Diagram

1.	Variable resistor
2.	Mercury relay
3.	Power supply
4.	Attachment of rod assembly to expansion wire
5.	Tension adjustment screw
6.	Fulcrum point for entire rod assembly
7.	Transformer
8.	Metal support for rod assembly
9.	Stabilizing pin
10.	Metal rod
11.	Support for temperature chart
12.	Rod connector
13.	Rod with internal wire
14.	Rod connector
15.	Temperature chart support
16.	Conducting metal strip
17.	Circuit breaker to cut off power after run completed
18.	Conducting metal support for contact point
19.	Rest to prevent over tension on 13
20.	Temperature indicator
21.	Contact point
22.	Cardboard cut out to control temperature cycling
23.	Activator for 17
24.	Rod with internal wire
25.	Cylindrical temperature chart with internal clock
26.	Secure post for wire support bar
27.	Tension spring
28.	Adjusting screw
29.	Clip to secure paper chart to cylinder
30.	Maximum temperature control
31.	Spring adjustment screw
32.	Wire support bar
33.	Tension wire in furnace
34.	Secure post for wire support bar
35.	Wire support bar

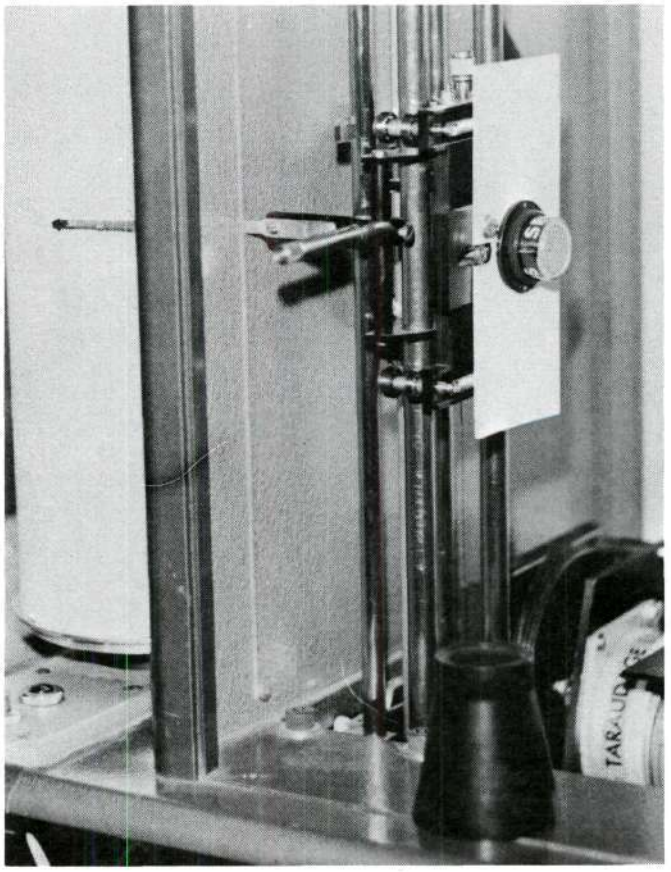

Figure 40. Picture of Recording Mechanism and Photocell

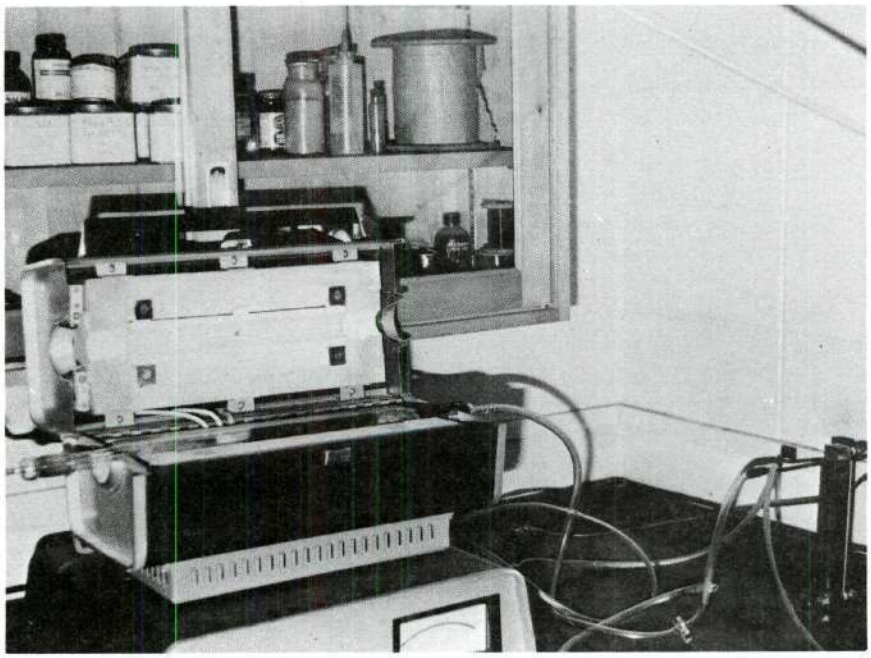

Figure 41. Horizontal Tube Furnace System

High-Temperature X-ray Apparatus (107)

The high-temperature furnace is illustrated in Figure 42. The furnace body is cut from foamed fused silica, and the heated cavity is a cube measuring two inches on a side. About 200 inches of Kanthal A-1 resistance wire (40 mil diameter) are coiled and placed around lengths of 3/16-inch diameter alumina spaghetti. The upper and lower halves of the furnace were fabricated separately, and the heaters in each half connected in series.

The high-temperature diffraction equipment consists of a Siemens Crystalloflex IV x-ray generator, a North American Philips Company diffractometer, a scintillation counter, and a Siemens counting equipment including a strip-chart recorder. A Philips and molybdenum x-ray tube was used as the source.

Two platinum, platinum - 13% rhodium thermocouples, prepared from 0.020 inch diameter wire and supported by alumina spaghetti, extend through the roof of the heated cavity, and are positioned very close to the specimen. These are connected to temperature compensated lead wires which extend through vacuum glands in the aluminum end plate. One thermocouple actuates a Wheelco Model 403 temperature controller, and the other allows accurate temperature readings from a potentiometer.

The stainless steel vacuum vessel is placed over the furnace body and sealed at the aluminum back plate with a neoprene gasket. The two x-ray windows on the side are covered with 0.001 inch thick Mylar and are held in place by aluminum clamps and sealed with neoprene gaskets. Cooling water is circulated through copper tubing attached to the outer wall of the furnace and the aluminum back plate where high

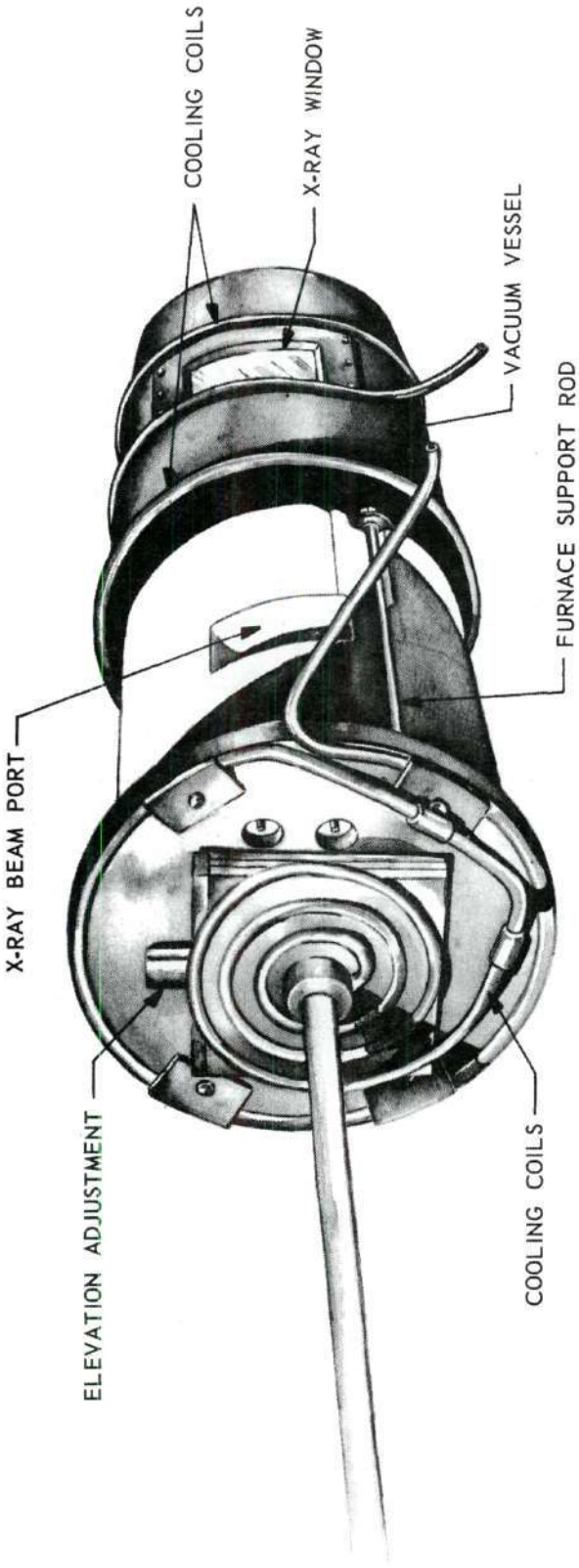

Figure 42. High-Temperature X-ray Furnace

temperatures are likely to be a hazard to the equipment.

The sample rests on a slip-cast and fired alumina platform supported by two 3/16-inch diameter alumina rods.

The carbon monoxide reaction gas is vented at the top of the furnace from a port in the side below the sample. Flow rates are measured by a rotameter.

APPENDIX B

EXPERIMENTAL PROCEDURE

Herein are contained the specific data on the experimental procedure of this work. The details of the surface preparation are included. Heating and cooling characteristics for the equipment are given. Flow calculations are made to demonstrate the amount and type of flow during the experiments. Also, variation of reactivity with flow rate is presented. The etching procedure is given in detail.

Surface Preparations

Initially, several surface treatments were used in an attempt to determine the one giving the most consistent results. The samples were reacted, following the various treatments.

The wire arrived coated with a greasy substance and was stored in a desiccator without treatment until ready for use. The "Vaseline" on the wire was first wiped off the sample using trichloroethylene as a solvent (recommended by the manufacturer). Figure 43 illustrates the wire in the raw state, and after removing the grease. Ultrasonic cleaning in alcohol and trichloroethylene was tried. A cathodic cleaning procedure was also employed by using a dilute commercial solution and a current of four amperes for one minute. Following this treatment, the specimen was dried in a hot air blast. Slight variations of this washing procedure were also used. The above cathodic preparation was used as a basic first step for additional treatments: (1) etching with

a 5 per cent nital, (2) etching with a commercial solution designed to remove any oxide, and (3) ultrasonic cleaning. Figure 44 shows the surface of a cathodically cleaned wire and the surface after etching with nitric acid, both at 500X. Although variation in the surface can be observed, no significant variation of reactivity was observed with any of the treatments, except for excessive oxidation, where reduction preceded the weight gain. This observation is consistent with Pettit, Yinger and Wagner (67), who also attempted several varied techniques of surface preparations, such as polishing, etching, and etectro-polishing coupon iron samples. They, too, observed no variation in reactivity from surface treatment. Their experimental work measured the oxidation of iron in CO - CO_2 mixtures.

Since no enhancement of experimental results was obtained, the procedure of only wiping with trichloroethylene was adopted as the standard method since it was uncomplicated and offered the least exposure of the sample to unknown and possibly varying conditions (commercial solutions and drying methods).

Flow Calculation

It has been shown by previous investigation (67,95) that the carbon monoxide reaction with iron is independent of the gas flow rate. This is applicable over a large range of flow rates and includes the experimental conditions of this work. Furthermore, it has been demonstrated by Decroly (57) that carbon monoxide is practically insoluble in the metal matrix.

For the experimental work with the thermobalance, the absolute volume rate of the carbon monoxide has been determined at 30.8 cc/min.

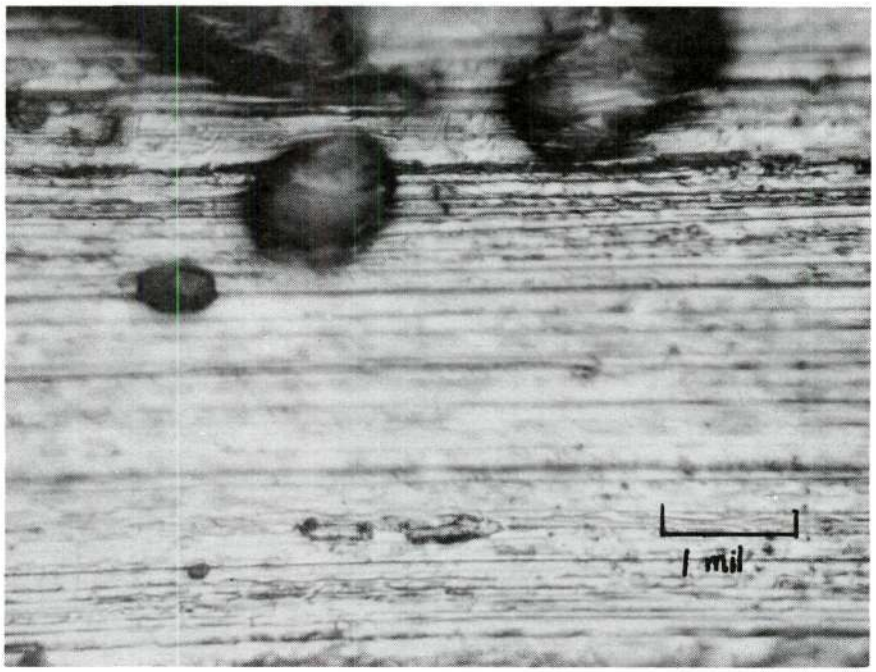

AS RECEIVED

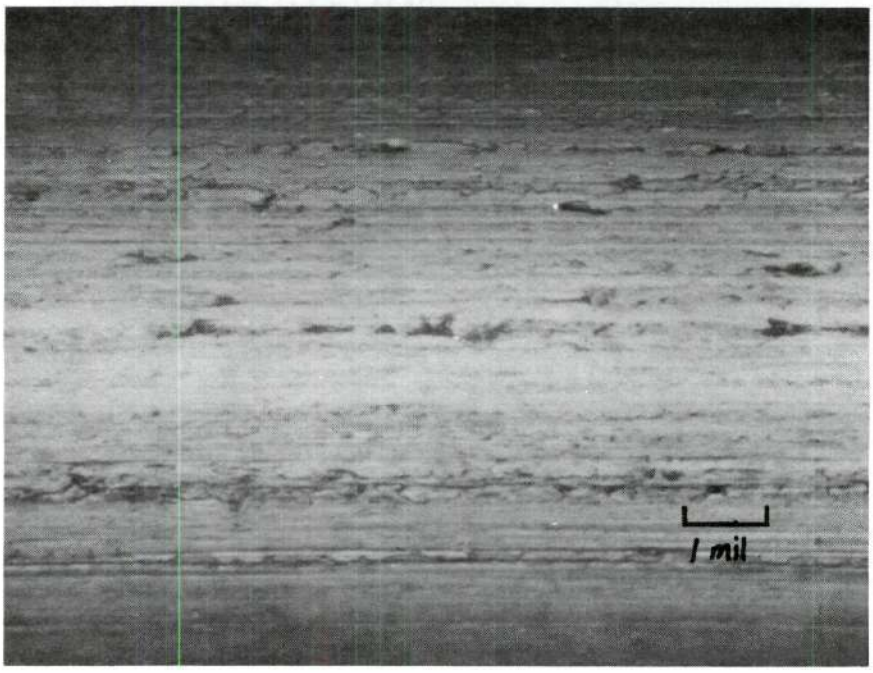

WIPED WITH TRICHLOROETHYLENE

Figure 43. Iron Wire Surface as Received and after Cleaning

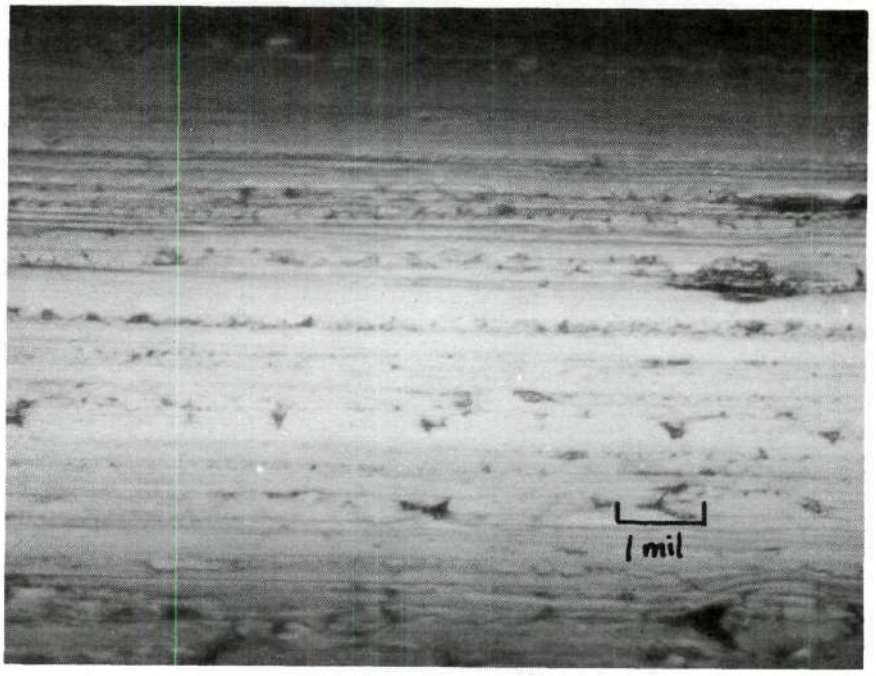

CATHODICALLY CLEANED

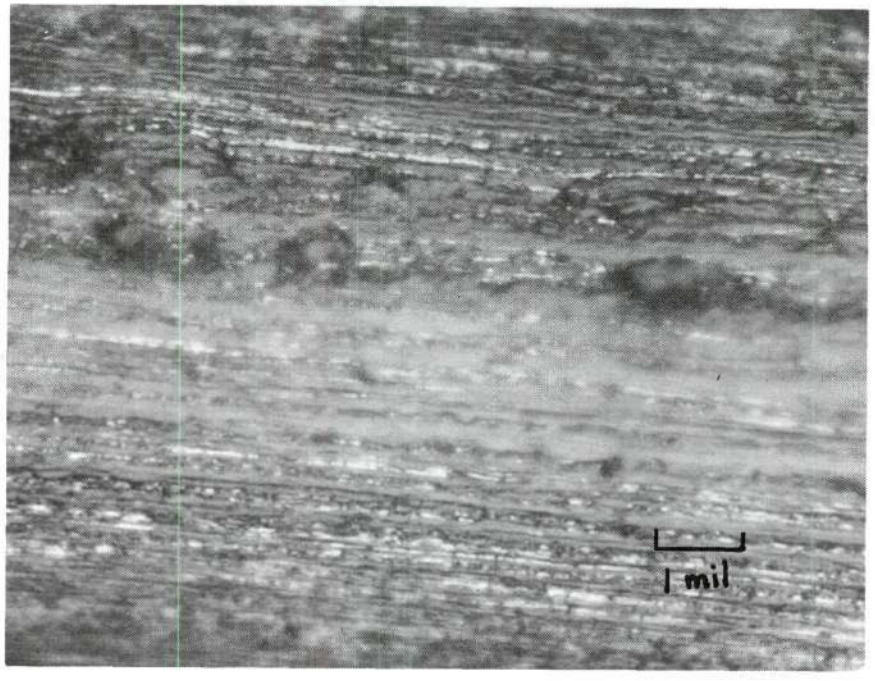

NITRIC ETCH

Figure 44. Iron Wire Surface after Cathodic Cleaning and after Etching

This value was obtained from the calibration curves for air furnished with the rotameter. Corrections were made for variation in density, pressure and temperature.

To determine the variation of reactivity with flow rate, experiments were performed at flow rates 17.4, 30.8, and 49.4 cc/min at both 545°C and 785°C. The results are illustrated in Figure 47. Although variations were observed, they did not correlate to the rate of flow. It is concluded that other variations in the sample will dwarf any change in reactivity due to the flow, and that reactivity is relatively independent of flow rate.

The prolonged exposure experiments were performed at a flow rate of 123 cc/min.

The Reynolds number for the reaction system was calculated to be of the order of 10^{-3}, which is known to be well in the region of laminar flow (99).

Etching Procedures

A picric acid-nitric acid in ethanol, which is a slight variation of the standard nital etch as used in Kehl (100), was the first etchant used. The mounted wire samples were polished using the rotor grind followed by a series (6,3,1, and 1/4 micron) of diamond polishes. Kerosene was used as a lubricant in the diamond polishing. The polished surface was swabbed with kerosene saturated cotton; a dry piece of cotton was placed over the sample and removed under a hot air blast. Immediately following, the sample was etched with a 2 per cent nitric-2 per cent picric acid in ethanol. A saturated piece of cotton was

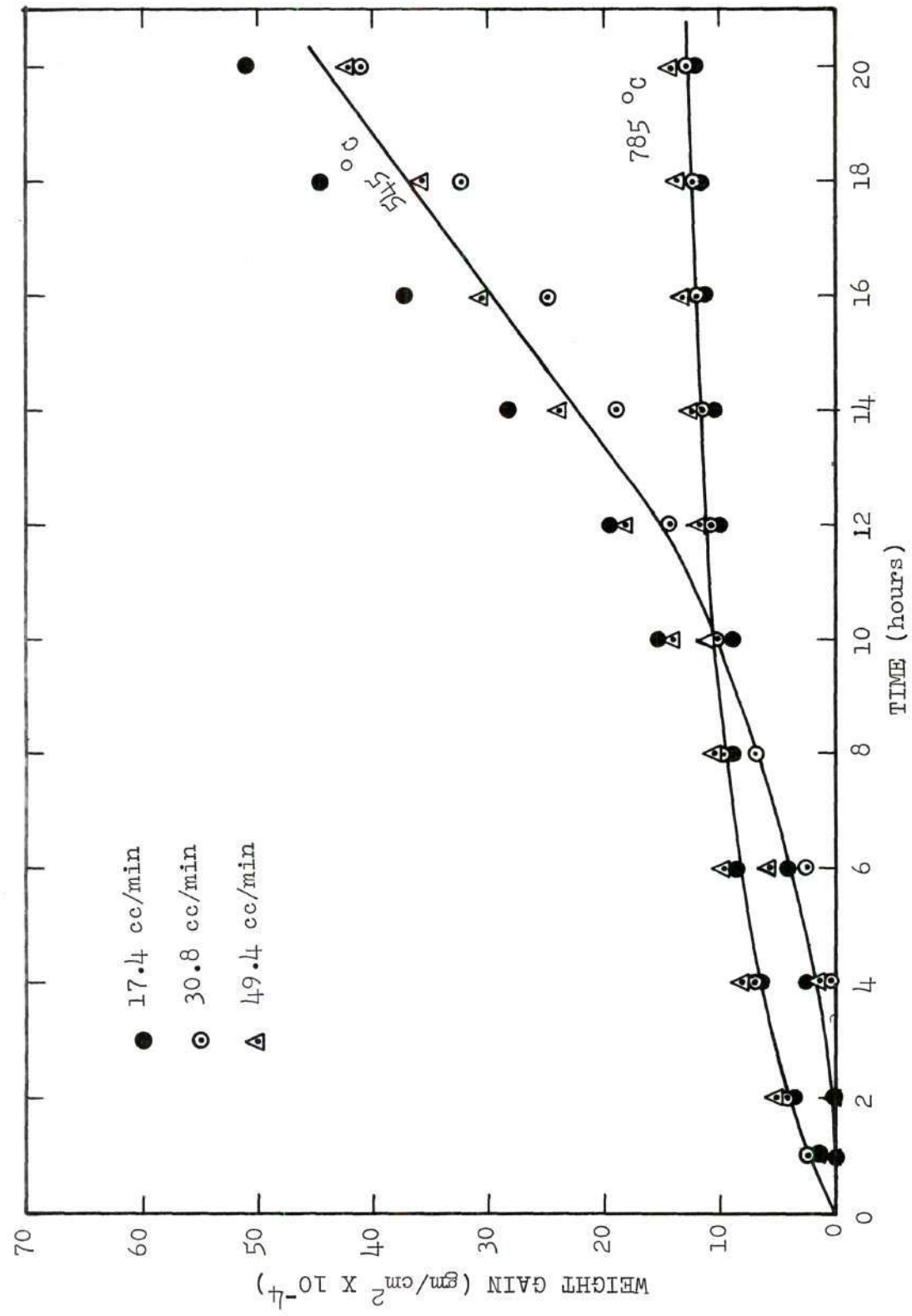

Figure 45. Variation of Reactivity with Flow Rate

placed on the polished surface; when fogging of the metal was observed with the unaided eye, the surface was flushed with methanol to remove remnants of the acid. The surface was swabbed with ethanol and dried by the standard method: applying a dry piece of cotton and then removing it in the presence of a hot air blast. The etching period was from 30 seconds to 2 minutes, depending on the sample. Several of the wires required longer etches and were severely pitted and showed little microstructure. This etch is designed to reveal the general microstructure and pearlite. Cementite will appear white.

A second etchant, alkaline sodium picrate, was used especially to ascertain the cementite structure on several of the samples; cementite has a dark appearance as a result of this etch. A solution of two grams picric acid, 25 grams sodium hydroxide and 100 grams of water was prepared. A circuit with a potential of 6 volts was made, using the sample as the anode and a stainless steel cathode. A wire was taped to the conducting copper reverse of the polished sample, and the obverse was immersed in the liquid for 40 seconds. A resistance of 0.4 ohms was observed. The etched sample was flushed with hot water and washed and dried with ethanol.

Table 11. Typical Mass Spectrometer Analysis by Battelle Memorial Institute of High-Purity Iron Wire

Impurity	Content (ppm)	Impurity	Content (ppm)
Li	0.004	Rh	<0.03
Be	0.005	Pd	<0.08
B	<0.0008	Ag	<0.04
C	8.0	Cd	<0.08
N_2	7.0	In	<0.06
O_2	7.2	Sn	<0.02
H_2	<0.1	Sb	<0.02
F	Interference	Te	<0.07
Na	0.8	I	<0.007
Mg	8.0	Cs	<0.006
Al	Interference	Ba	<0.04
Si	<0.5	La	<0.006
P	0.3	Ce	<0.006
S	1.2	Pr	<0.006
Cl	3.0	Nd	<0.02
K	0.2	Sm	<0.025
Ca	2.0	Eu	<0.012
Sc	<0.025	Gd	<0.025
Ti	0.5	Tb	<0.006
V	<0.1	Dy	<0.03
Cr	0.6	Ho	<0.01
Mn	<0.1	Er	<0.4
Co	0.3	Tm	<0.3
Ni	1.2	Yb	<0.02
Cu	<0.2	Lu	<0.006
Zn	<0.8	Hf	<0.025
Ga	<0.5	Ta	<1.0
Ge	<1.0	Re	<0.012
As	<0.1	Os	<0.02
Se	<1.0	Ir	<0.012
Br	<0.15	Pt	<0.025
Rb	<0.08	Au	0.4
Sr	<0.08	Hg	<0.03
Y	<0.04	Tl	<0.012
Zr	<0.06	Pb	<0.015
Nb	0.03	Bi,Th,V all	<0.008
Mo	0.2		
Ru	<0.1		

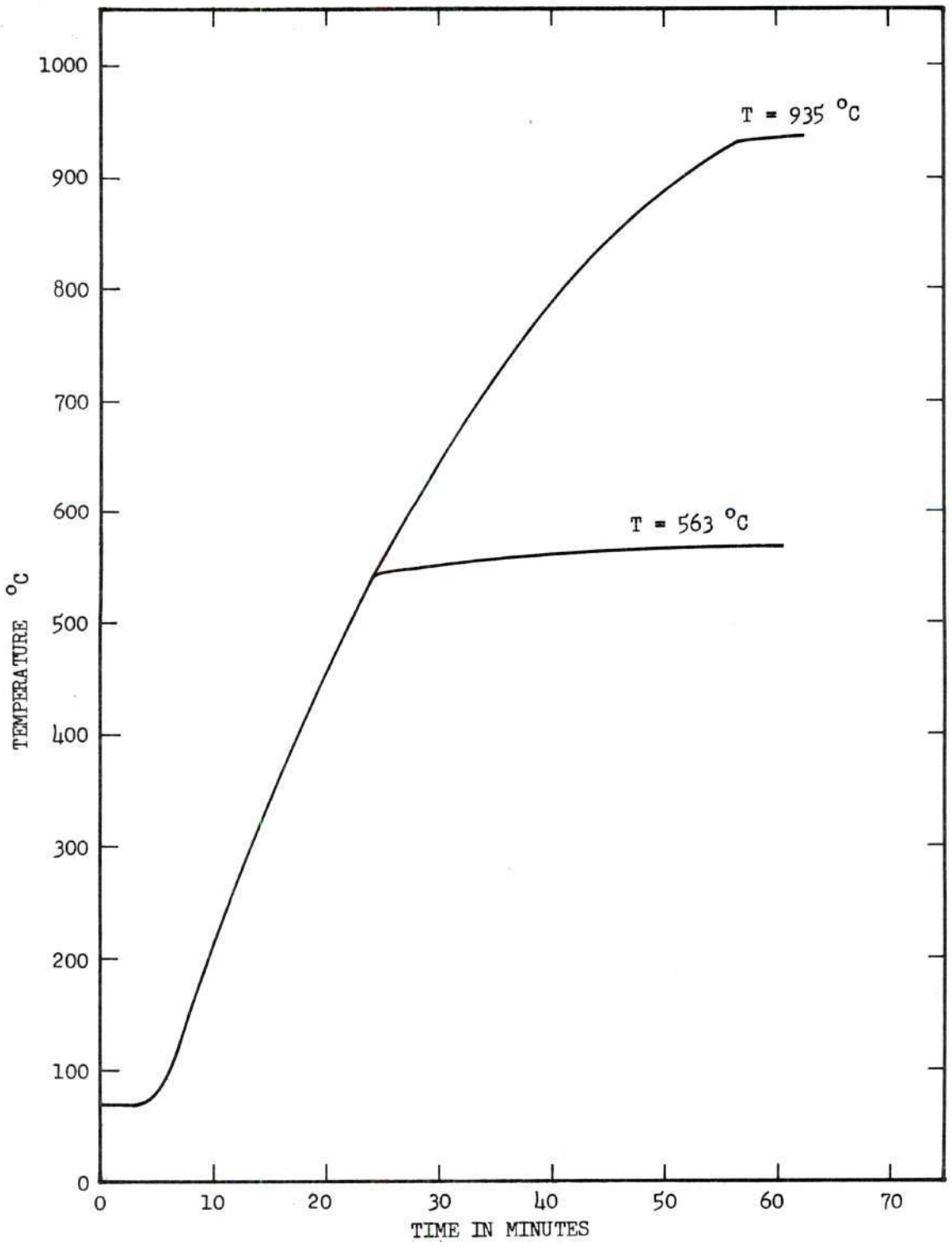

Figure 46. Heating Curves for the Thermobalance

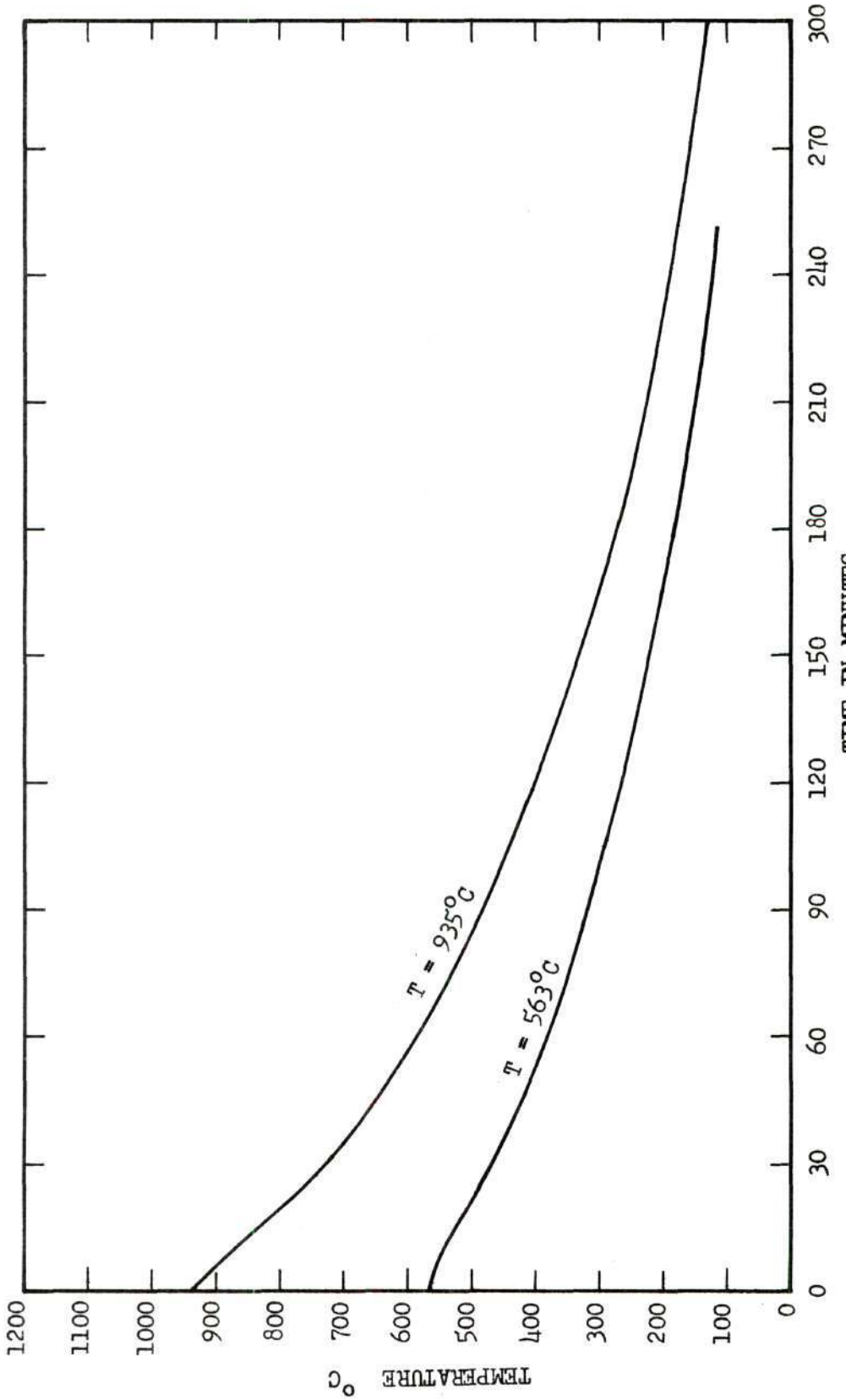

Figure 47. Cooling Curves for the Thermobalance

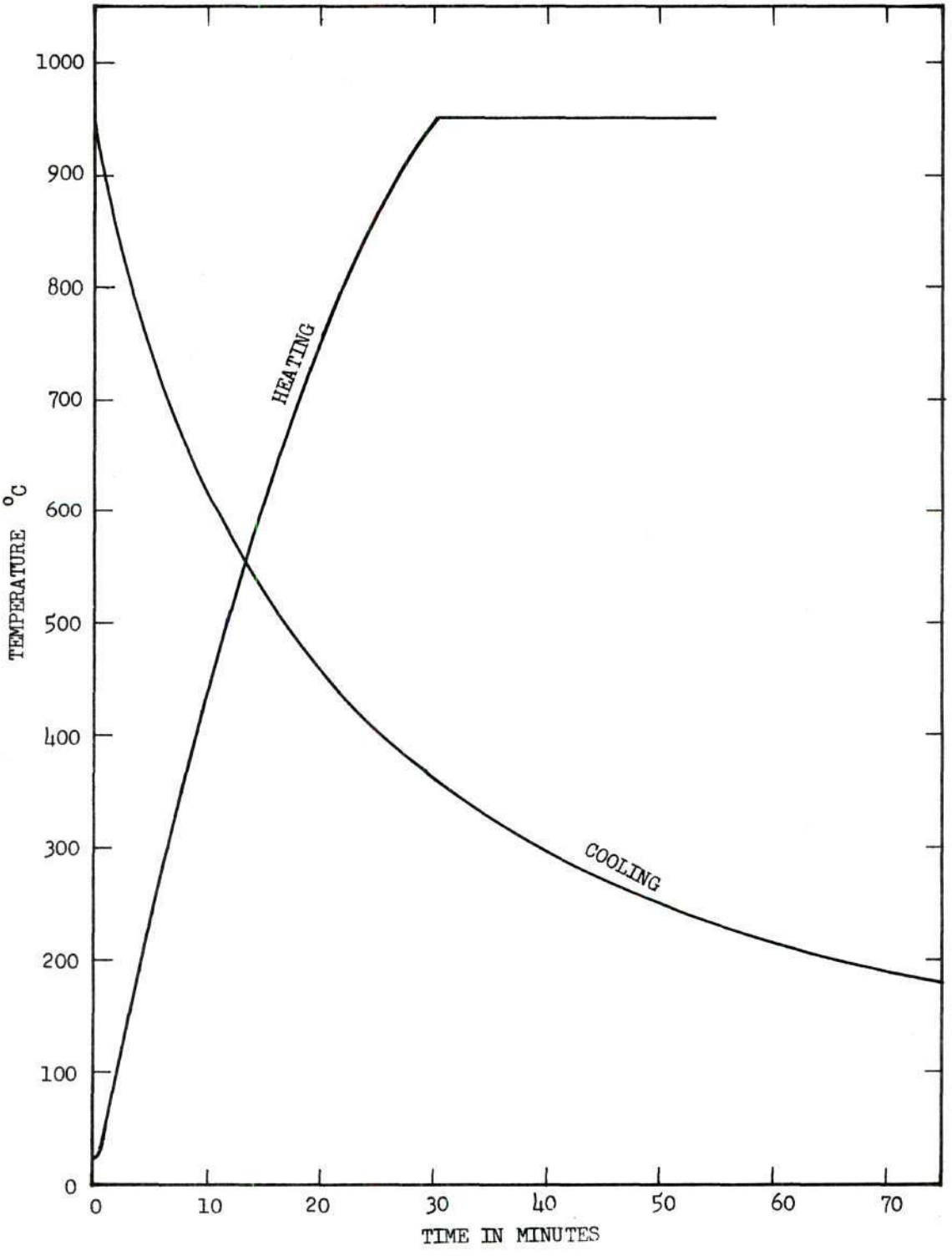

Figure 48. Heating and Cooling Curves for the Lindbergh Tube Furnace

APPENDIX C

DIFFUSION CALCULATIONS

Diffusion in alpha-iron has been established experimentally, and it has been shown by Homan (104) that low temperature results cannot be extrapolated to temperatures of 500°C and above. Homan (104) has obtained a good fit of diffusion data above 500°C using an empirical model which includes the possibility of a carbon-vacancy interaction. Values listed in Table 12 are calculated from this model. Since the solubility of carbon in ferrite is minuscule, the diffusivity of carbon can be considered as a function of ferrite temperature alone.

Austenitic diffusion is more complex than that of ferrite; due to the solubility of carbon in the gamma matrix, there is a definite relation between carbon content and diffusivity. Smith (105) has calculated the diffusivity of carbon at 802°C, 851°C and 1000°C using steady-state measurements. His data shows a decided concentration dependency with a D/D_i of about 3 for the extreme values of 1000°C. (D_i is diffusivity at infinite dilution.) Smith showed that a portion of the increase in diffusion was due to the concentration dependence of the activity coefficient of carbon in austenite. Asimow (103), in a semiquantitative analysis, further explained the concentration dependency, using Equation 3.

$$D = A\left[1 + \frac{d\ln\gamma}{d\ln c}\right] \exp\left[-\frac{\Delta G}{R T}\right] \qquad (3)$$

where

A = constant

γ = activity coefficient of carbon in austenite = $\frac{1}{1 - 6C}$

R = gas constant

T = absolute temperature

C = carbon concentration in atomic per cent

G = free energy change

attributing the only effect of C on ΔG to a negative pressure or a dilatation phenomena, he develops Equation 4.

Table 12. Summary of Diffusivity of Carbon in Iron

	Ferrite	Austenite	
T°C	D cm^2/gm	D_i cm^2/gm	D_{max} cm^2/gm
500	2.8×10^{-8}		
650	4.3×10^{-7}		
700	8.0×10^{-7}		
750	1.6×10^{-6}	7.9×10^{-9}	1.6×10^{-8}
800	3.0×10^{-6}	1.73×10^{-8}	4.0×10^{-8}
850	5.2×10^{-6}	3.65×10^{-8}	9.1×10^{-8}
900	6.5×10^{-6}	8.9×10^{-8}	2.5×10^{-7}
1000		2.4×10^{-7}	7.8×10^{-7}

D_i = Diffusivity at an imaginary infinite dilution.

D_{max} = Diffusivity at cementite solubility line.

$$D = A\left(1 + \frac{d\ln\gamma}{d\ln c}\right) \exp\left[-\frac{\Delta G_i}{R\,T} + \left(\frac{16\pi}{3}\right)\left(\frac{\varepsilon r_o^{\,3}}{a_o^{\,3}}\right)\frac{E\ \Delta V}{R\,T}\right] \qquad (4)$$

where,

i = at infinite dilution

a_o = lattice parameter of austenite

$(1+\varepsilon)r_o$ = size of carbon atom squeezed into a hole of radius r_o

Asimow showed that by approximating the values in Equation 4, the values for 1000°C agreed well with Smith's data at that temperature. Asimow's equation was

$$D = \frac{D_i}{1 - 6C}\, e^{10.5C} \qquad (5)$$

To obtain an expression approximating the diffusivity of carbon as a function of temperature and carbon concentration Asimow's equation was expanded to Equation 6.

$$D = \frac{0.273}{1 - 6C} \exp\left\{-\frac{17{,}800}{T} + \frac{13{,}400C}{T}\right\} \qquad (6)$$

where

D = diffusivity in cm^2/sec

C = carbon concentration in atomic fraction

T = absolute temperature °K

Calculated values for temperatures of interest are shown in Figure 49; also, Smith's experimental points are shown and the equation is

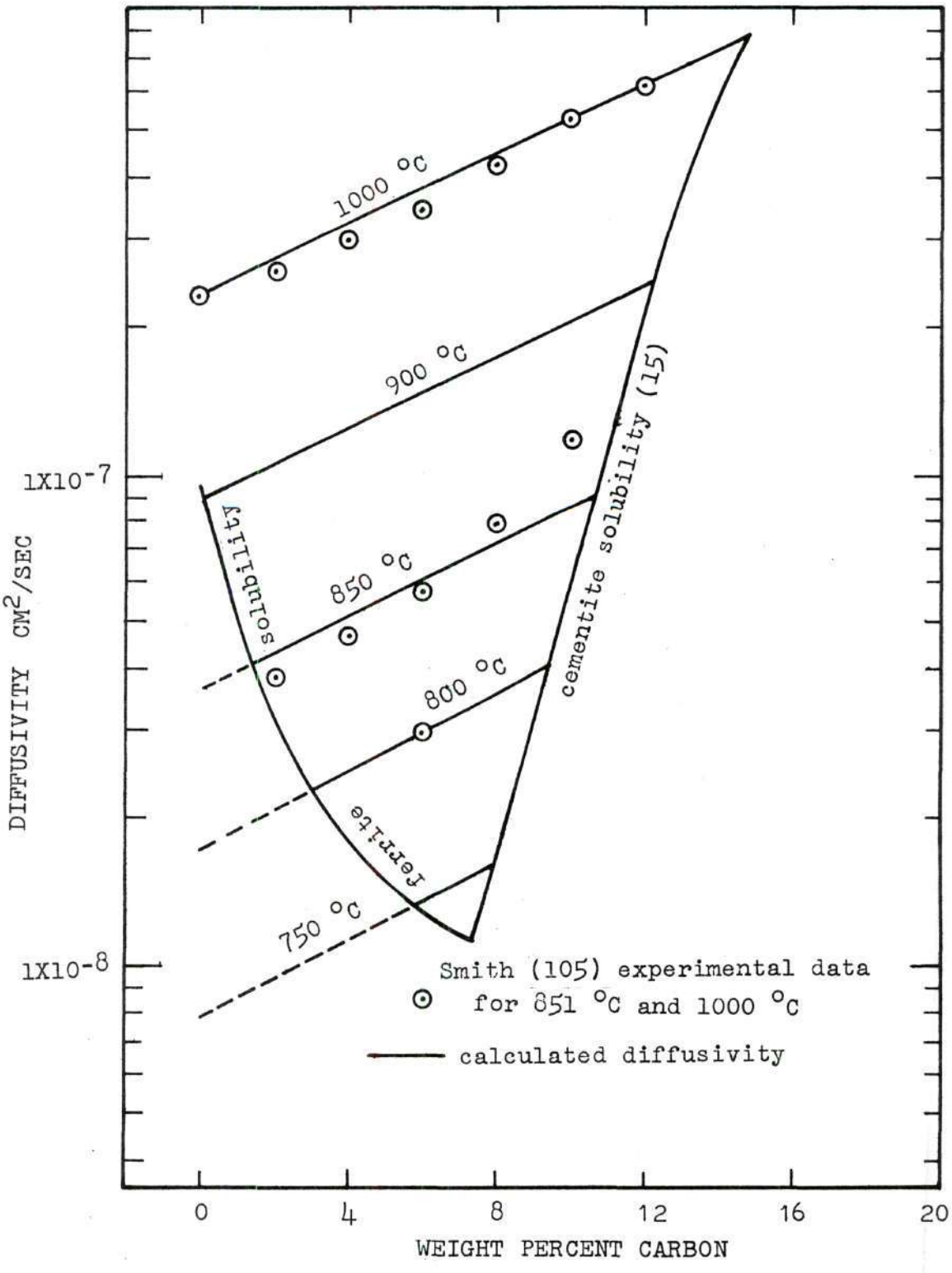

Figure 49. Diffusivity of Carbon in Austenite as a Function of Carbon Content

extrapolated to an imaginary infinite dilution. Although Equation 6 can only be a crude approximation, the values obtained do agree well with experimental results, especially at low concentrations.

The general diffusion equation (99) is

$$\frac{\partial C}{\partial t} = \nabla \cdot D\nabla C \tag{7}$$

where

c = concentration in atomic per cent

t = time

D = diffusivity

Since the experimental samples are wires, cylindrical coordinates are employed.

$$\frac{\partial C}{\partial t} = \frac{D}{r}\frac{\partial C}{\partial r} + \frac{\partial D}{\partial r}\frac{\partial C}{\partial r} + D\frac{\partial^2 C}{\partial r^2} \tag{8}$$

Theoretically, Equation 6 can be combined with Equation 8 to give a solution; such a solution is beyond the scope of this paper.
By assuming D constant the equation takes the form

$$\frac{\partial C}{\partial t} = D\left[\frac{1}{r}\frac{\partial}{\partial r}\left(r\frac{\partial C}{\partial r}\right)\right] \tag{9}$$

and solution is now possible (106). For a cylinder of radius a, a surface concentration for $0 \leq t < \infty$ of C_1 and a medium initially free of

solute the solution is

$$C = C_1\left[1 + \frac{2}{a}\sum_{1}^{\infty}\frac{1}{\alpha_n}\,\frac{J_o(\alpha_n r)}{J_o'(\alpha_n a)}\exp(-D\alpha_n{}^2 t)\right] \qquad (10)$$

where

J_o = zero order Bessel functions of the first kind

$\alpha_1 = \frac{2.405}{a}$

$\alpha_2 = \frac{5.520}{a}$

etc.

a = radius of wire

C_1 = constant surface concentration

from the above equation, concentration ratios are calculated.

APPENDIX D

RAW DATA OF REACTIVITY

Kinetic data from the thermobalance were read directly from the chart at increments of one hour (except for the first hour). These values were the gross weight change in divisions. When the equipment is operated without a sample, but under otherwise identical reaction conditions, a weight gain of 2.0 ± 0.7 divisions will be recorded. To obtain the actual weight gain, this value must be subtracted from the gross weight change. During the reaction the sensitivity of the balance is obtained by placing a 50 mg. weight on a pan, and measuring the deflection. Using this factor, the weight change recorded on the chart is converted from divisions to grams. For a sample calculation, take the result after 15 hours of Run 1. The gross weight change obtained from the chart was 2.2 divisions, the zero balance adjustment for 15 hours was 1.8 divisions.

$$\frac{2.2 \text{ div}}{\text{sample}} - \frac{1.8 \text{ div}}{\text{sample}} = \left(\frac{0.4 \text{ div}}{\text{sample}}\right)\left(\frac{0.050 \text{ gm}}{21.3 \text{ div}}\right)\left(\frac{1 \text{ sample}}{10 \text{ cm}^2}\right) = 0.94 \times 10^{-4} \frac{\text{gm}}{\text{cm}^2} \quad (11)$$

All wire samples were cut to the length of 62.7 cm, which corresponds to a surface area of 10 square centimeters.

The zero balance adjustment was found to vary with time, temperature, sensitivity and specimen holder. Periodic runs were made to

determine the most appropriate value. A large number of these runs were tabulated. As can be seen from the data, about half of the adjustment is made in the first hour. By observing the initial kinetics and using past experience, a judgment was made as to the best zero adjustment for each experiment. The total change amounts to about 4.5×10^{-4} gm/cm^2, which is a relatively small value for most experiments.

The values from the chart could be read to an accuracy of ±0.1 divisions.

Following is the tabulated data for each of the experimental runs using the thermobalance.

Table 12. Reaction Data

RUN 1				RUN 2		
T = 477°C Sensitivity 21.3 div/50mg				T = 511°C Sensitivity 21.3 div/50mg		
Time	Gross Weight Change Divisions	Zero Balance Adjustment	Weight Gain $gms/cm^2 \times 10^{-4}$	Gross Weight Change Divisions	Zero Balance Adjustment	Weight Gain $gms/cm^2 \times 10^{-4}$
0.2	0.6	0.4	0.47	0.3	0.4	-0.23
0.4	0.8	0.7	0.23	0.5	0.7	-0.47
0.6	0.9	0.8	0.23	0.7	0.7	0.0
0.8	1.0	0.9	0.23	0.8	0.8	0.0
1.0	1.1	1.0	0.23	1.0	1.0	0.0
1.5	1.1	1.2	-0.23	1.1	1.1	0.0
2	1.1	1.3	-0.47	1.2	1.2	0.0
3	1.2	1.5	-0.70	1.3	1.3	0.0
4	1.3	1.5	-0.47	1.5	1.5	0.0
5	1.4	1.5	-0.23	1.8	1.5	0.70
6	1.4	1.6	-0.47	2.5	1.6	2.11
7	1.5	1.6	-0.23	3.0	1.6	3.29
8	1.5	1.6	-0.23	3.4	1.6	4.23
9	1.5	1.6	-0.23	3.9	1.6	5.40
10	1.5	1.6	-0.23	4.4	1.6	6.58
11	1.6	1.7	-0.23	4.7	1.7	7.05
12	1.7	1.7	0.0	5.1	1.7	8.00
13	1.8	1.8	0.0	5.5	1.8	8.70
14	2.0	1.8	0.47	6.00	1.8	9.87
15	2.2	1.8	0.94	6.2	1.8	10.33
16	2.5	1.8	1.65	6.6	1.8	11.27
17	2.9	1.9	2.35	7.0	1.9	12.0
18	3.3	1.9	3.29	7.4	1.9	12.9
19	3.8	1.9	4.45	7.7	1.9	13.6
20	4.2	1.9	5.40	8.1	1.9	14.7

Table 14. Reaction Data

RUN 3 T = 521°C Sensitivity 21.3 div/50mg				RUN 4 T = 536°C Sensitivity 21.3 div/50mg		
Time	Gross Weight Change Divisions	Zero Balance Adjustment	Weight Gain $gms/cm^2 \times 10^{-4}$	Gross Weight Change Divisions	Zero Balance Adjustment	Weight Gain $gms/cm^2 \times 10^{-4}$
0.2	0.3	0.4	-0.23	0.5	0.4	+0.23
0.4	0.6	0.7	-0.23	0.7	0.7	0.0
0.6	0.7	0.8	-0.23	0.8	0.8	0.0
0.8	0.8	0.7	-0.23	0.9	0.9	0.0
1.0	0.8	1.0	-0.47	0.9	1.0	-0.23
1.5	0.9	1.2	-0.70	1.0	1.2	-0.47
2	1.1	1.3	-0.47	1.1	1.3	-0.47
3	1.2	1.5	-0.70	1.5	1.5	0.0
4	1.4	1.5	-0.23	1.9	1.5	0.94
5	1.8	1.5	0.70	2.5	1.5	2.30
6	2.2	1.6	1.41	3.1	1.6	3.50
7	2.5	1.6	2.11	3.7	1.6	4.93
8	2.9	1.6	3.05	4.2	1.6	6.10
9	3.3	1.6	4.00	4.8	1.6	7.50
10	3.6	1.6	4.70	53	1.6	8.67
11	3.8	1.7	4.95	5.9	1.7	9.85
12	4.1	1.7	5.65	6.3	1.7	10.8
13	4.4	1.8	6.10	6.9	1.8	12.0
14	4.7	1.8	6.83	7.4	1.8	13.1
15	4.9	1.8	7.30	7.9	1.8	14.3
16	5.2	1.8	8.00	8.7	1.8	16.2
17	5.5	1.9	8.46	9.4	1.9	17.6
18	5.8	1.9	9.17	10.3	1.9	19.7
19	6.1	1.9	9.87	11.1	1.9	21.6
20	6.4	1.9	10.6	11.9	1.9	23.5

Table 15. Reaction Data

RUN 5				RUN 6		
T = 566°C Sensitivity 21.5 div/50mg				T = 593°C Sensitivity 21.5 div/50mg		
Time	Gross Weight Change Divisions	Zero Balance Adjustment	Weight Gain $gms/cm^2 \times 10^{-4}$	Gross Weight Change Divisions	Zero Balance Adjustment	$gms/cm^2 \times 10^{-4}$
0.2	0.5	0.5	0.0	0.4	0.4	0.0
0.4	0.7	0.7	0.0	0.7	0.7	0.0
0.6	0.8	0.8	0.0	0.8	0.8	0.0
0.8	0.9	0.9	0.0	0.9	0.9	0.0
1.0	0.9	0.9	0.0	1.0	1.0	0.0
1.5	1.1	1.1	0.0	1.1	1.1	0.0
2	1.2	1.2	0.0	1.2	1.2	0.0
3	1.5	1.3	+0.47	1.4	1.3	+0.23
4	2.0	1.4	1.40	2.0	1.4	1.40
5	2.5	1.5	2.32	2.4	1.5	2.10
6	3.2	1.5	3.95	2.9	1.5	2.80
7	3.9	1.6	5.35	3.4	1.6	4.18
8	4.7	1.6	7.20	4.1	1.6	5.82
9	5.4	1.6	8.83	4.6	1.6	7.00
10	6.2	1.6	10.7	5.2	1.6	8.37
11	7.2	1.6	13.0	5.8	1.6	9.77
12	8.0	1.7	14.6	6.4	1.7	10.9
13	8.7	1.7	16.3	7.2	1.7	12.8
14	9.5	1.7	18.1	7.7	1.7	14.0
15	10.3	1.7	20.0	8.4	1.7	15.6
16	11.2	1.7	22.1	9.2	1.7	17.5
17	12.2	1.7	24.4	10.0	1.7	19.3
18	13.3	1.7	27.0	10.7	1.7	21.0
19	14.4	1.7	29.5	11.5	1.7	22.8
19.4	15.4	1.7	31.8	12.2	1.7	24.4

Table 16. Reaction Data

RUN 7

T = 625°C
Sensitivity 21.5 div/50mg

Time	Gross Weight Change Divisions	Zero Balance Adjustment	Weight Gain $gms/cm^2 \times 10^{-4}$
0.2	0.5	0.5	0.0
0.4	0.8	0.7	0.23
0.6	1.0	0.8	0.47
0.8	1.1	0.9	0.47
1.0	1.2	1.1	0.23
1.5	1.3	1.1	0.47
2	1.4	1.2	0.47
3	1.6	1.3	0.70
4	1.9	1.4	1.06
5	2.3	1.5	1.86
6	2.6	1.5	2.56
7	3.2	1.6	3.72
8	3.6	1.6	4.65
9	4.2	1.6	6.05
10	4.8	1.6	7.20
11	5.3	1.6	8.60
12	5.9	1.7	9.80
13	6.4	1.7	10.90
14	7.0	1.7	12.3
15	7.6	1.7	13.7
16	8.2	1.7	15.1
17 (End Run 7)			
18			
19			
20			

RUN 8

T = 650°C
Sensitivity 21.8 div/50mg

Gross Weight Change Divisions	Zero Balance Adjustment	$gms/cm^2 \times 10^{-4}$
0.6	0.6	0.0
0.8	0.8	0.0
1.0	1.0	0.0
1.0	1.0	0.0
1.1	1.1	0.0
1.2	1.2	0.0
1.4	1.3	0.23
1.07	1.4	0.69
1.9	1.4	1.15
2.2	1.5	1.60
2.4	1.5	2.07
2.7	1.5	2.76
3.0	1.5	3.45
3.4	1.5	4.37
3.9	1.6	5.28
4.3	1.6	6.20
4.17	1.6	7.25
5.1	1.6	9.20
5.4	1.6	8.72
5.7	1.6	9.90
6.3	1.6	10.8
6.7	1.6	11.7
7.1	1.6	12.6
7.5	1.6	13.5
7.9	1.6	14.5

Table 17. Reaction Data

RUN 9				RUN 10		
T = 675°C Sensitivity 22.5 div/50mg				T = 706°C Sensitivity 23.0 div/50mg		
Time	Gross Weight Change Divisions	Zero Balance Adjustment	Weight Gain $gms/cm^2 \times 10^{-4}$	Gross Weight Change Divisions	Zero Balance Adjustment	Weight Gain $gms/cm^2 \times 10^{-4}$
0.2	0.6	0.6	0.0	0.6	0.6	0.0
0.4	0.8	0.8	0.0	0.8	0.8	0.0
0.6	0.9	0.9	0.0	0.9	0.9	0.0
0.8	1.0	1.0	0.0	1.1	1.1	0.0
1.0	1.1	1.0	0.22	1.2	1.2	0.0
1.5	1.2	1.1	0.22	1.3	1.2	0.21
2	1.3	1.1	0.45	1.5	1.3	0.43
3	1.5	1.2	0.67	1.8	1.4	0.85
4	1.6	1.2	0.89	2.0	1.5	1.07
5	1.8	1.3	1.11	2.1	1.5	1.29
6	2.0	1.3	1.56	2.2	1.5	1.50
7	2.1	1.6	1.78	2.2	1.5	1.50
8	2.3	1.7	2.22	2.3	1.5	1.70
9	2.4	1.7	2.45	2.3	1.5	1.70
10	2.5	1.7	2.67	2.3	1.5	1.70
11	2.6	1.7	2.90	2.3	1.5	1.70
12	2.7	1.9	3.11	2.4	1.5	1.94
13	2.8	1.7	3.34	2.4	1.5	1.94
14	2.9	1.7	3.56	2.4	1.5	1.94
15	3.0	1.7	3.79	2.5	1.5	2.15
16	3.1	1.7	4.00	2.6	1.5	2.15
17	3.2	1.7	4.23	2.7	1.6	2.15
18	3.3	1.7	4.45	2.7	1.6	2.35
19	3.4	1.7	4.68	2.7	1.6	2.35
20	3.5	1.3	4.90	2.7	1.6	2.35

Table 18. Reaction Data

Time	RUN 11 T = 751°C Sensitivity 23.2 div/50mg Gross Weight Change Divisions	Zero Balance Adjustment	Weight Gain $gms/cm^2 \times 10^{-4}$	RUN 12 T = 726°C Sensitivity 23.0 div/50mg Gross Weight Change Divisions	Zero Balance Adjustment	$gms/cm^2 \times 10^{-4}$
0.2	0.7	0.7	0.0	0.7	0.2	
0.4	1.0	0.1	0.22	0.9	0.9	0.0
0.6		1.0	0.43	1.0	1.0	0.0
0.8	1.4	1.1	0.65	1.2	1.1	0.22
1.0	1.6	1.2	0.86	1.3	1.2	0.22
1.5	2.0	1.3	1.51	1.5	1.2	0.65
2	2.2	1.3	1.95	1.6	1.3	0.87
3	2.7	1.4	2.80	1.9	1.3	1.30
4	3.0	1.4	3.46	2.1	1.3	1.74
5	3.2	1.4	3.90	2.3	1.4	1.96
6	3.5	1.4	4.55	2.4	1.4	2.17
7	3.7	1.4	5.00	2.6	1.4	2.61
8	3.8	1.4	5.20	2.6	1.4	2.61
9	4.0	1.5	5.40	2.7	1.4	2.82
10	4.2	1.5	5.85	2.8	1.4	3.05
11	4.3	1.5	6.05	2.9	1.4	3.26
12	4.5	1.6	6.27	3.1	1.5	3.48
13	4.6	1.6	6.50	3.2	1.5	3.70
14	4.7	1.6	6.70	3.3	1.5	3.91
15	4.8	1.6	6.92	3.3	1.5	3.91
16	5.0	1.6	7.35	3.4	1.5	4.13
17	5.0	1.6	7.35	3.5	1.5	4.35
18	5.1	1.6	7.57	3.6	1.5	4.56
19	5.2	1.6	7.78	3.7	1.5	4.80
20	5.3	1.6	8.00	3.9	1.6	5.0

Table 19. Reaction Data

Time	RUN 13 T = 801°C Sensitivity 23 div/50mg Gross Weight Change Divisions	Zero Balance Adjustment	Weight Gain $gms/cm^2 \times 10^{-4}$	RUN 14 T = 779°C Sensitivity 23.5 div/50mg Gross Weight Change Divisions	Zero Balance Adjustment	$gms/cm^2 \times 10^{-4}$
0.2	0.8	0.8	0.0	0.9	0.8	0.21
0.4	1.2	1.0	0.43	1.2	1.0	0.42
0.6	1.8	1.1	1.52	1.6	1.1	1.15
0.8	2.1	1.2	1.96	2.1	1.2	1.90
1.0	2.8	1.2	3.48	2.5	1.2	2.75
1.5	3.8	1.3	5.43	3.2	1.3	4.05
2	4.3	1.4	6.30	3.7	1.3	5.10
3	5.1	1.4	8.04	4.3	1.4	6.15
4	5.5	1.4	8.90	4.7	1.4	7.00
5	5.8	1.4	9.55	5.0	1.4	7.65
6	6.4	1.4	10.9	5.3	1.4	8.3
7	6.8	1.4	11.7	5.6	1.5	8.7
8	7.2	1.4	12.6	5.5	1.5	9.00
9	7.8	1.4	13.9	5.9	1.5	9.35
10	8.2	1.5	14.5	6.15	1.5	9.9
11	8.7	1.5	15.6	6.3	1.5	10.2
12	9.2	1.5	16.7	6.5	1.6	10.4
13	9.8	1.5	18.0	6.7	1.6	10.8
14	10.3	1.5	19.1	6.9	1.6	11.2
15	10.8	1.5	20.2	7.1	1.6	11.7
16	11.3	1.5	21.3	2.3	1.6	12.1
17	11.7	1.6	21.9	7.6	1.7	12.5+
18	12.2	1.6	23.0	7.8	1.7	12.9
19	12.8	1.6	24.3	8.0	1.7	13.4
20	13.3	1.6	25.5	8.2	1.7	13.7

Table 19. Reaction Data

Time	RUN 15 T = 857°C Sensitivity 24 div/50mg Gross Weight Change Divisions	Zero Balance Adjustment	Weight Gain $gms/cm^2 \times 10^{-4}$	RUN 16 T = 872°C Sensitivity 23.5 div/50mg Gross Weight Change Divisions	Zero Balance Adjustment	Weight Gain $gms/cm^2 \times 10^{-4}$
0.2	1.1	0.9	0.42	0.8	0.7	0.21
0.4	1.7	1.2	1.06	1.4	1.0	0.85
0.6	2.4	1.5	1.90	1.8	1.2	1.28
0.8	3.0	1.7	2.75	2.3	1.3	2.13
1.0	3.5	1.7	3.80	2.8	1.4	3.0
1.5	4.8	1.8	6.35	3.8	1.5	4.9
2	6.0	1.8	8.90	4.7	1.5	6.8
3	7.0	1.9	10.8	6.1	1.6	9.6
4	7.4	2.0	11.4	6.6	1.6	10.6
5	7.9	2.0	12.5	6.9	1.6	11.3
6	8.3	2.1	13.1	7.3	1.6	12.1
7	8.7	2.2	13.8	7.5	1.6	12.5
8	9.2	2.2	14.8	7.7	1.6	13.0
9	9.7	2.2	7.5	8.0	1.6	13.6
10	10.25	2.2	17.0	8.5	1.6	14.7
11	11.0	2.2	18.6	9.0	1.7	15.5
12	11.6	2.3	19.7	9.6	1.7	16.8
13	12.3	2.3	21.2	10.6	1.7	18.9
14	13.2	2.3	23.1	11.6	1.7	21.1
15	14.1	2.3	25.0	12.7	1.7	23.4
16	15.1	2.3	27.1	13.7	1.7	25.6
17	16.2	2.4	29.2	14.6	1.7	27.5
18	17.3	2.4	31.6	15.3	1.7	29.0
19	18.4	2.4	33.9	16.1	1.7	30.7
20	20.5	2.4	36.1	16.9	1.7	32.4

Table 20. Reaction Data

Time	RUN 17 T = 872°C Sensitivity 23.0 div/50mg Gross Weight Change Divisions	Zero Balance Adjustment	Weight Gain $gms/cm^2 \times 10^{-4}$	RUN 18 T = 908°C Sensitivity 23 div/50mg Gross Weight Change Divisions	Zero Balance Adjustment	Weight Gain $gms/cm^2 \times 10^{-4}$
0.2	1.0	0.6	0.87	1.2	0.7	1.09
0.4	1.8	0.9	1.95	2.0	1.1	1.95
0.6	2.5	1.0	3.26	2.8	1.4	3.04
0.8	3.3	1.1	4.8	3.4	1.5	4.13
1.0	3.9	1.2	5.86	4.1	1.6	5.43
1.5	5.2	1.2	8.7	5.4	1.6	8.25
2	6.3	1.4	10.9	6.5	1.6	10.65
3	7.3	1.3	13.0	7.9	1.6	13.7
4	8.1	1.3	14.8	8.9	1.6	15.9
5	8.7	1.4	15.8	9.7	1.7	17.4
6	9.5	1.4	17.6	10.4	1.7	18.9
7	10.3	1.4	19.3	11.4	1.7	21.1
8	11.2	1.4	21.3	12.2	1.7	22.8
9	12.2	1.5	23.3	13.0	1.7	24.5
10	13.2	1.5	25.4	13.8	1.8	26.1
11	14.1	1.5	27.4	14.5	1.8	27.6
12	15.0	1.5	29.3	15.2	1.8	29.1
13	15.9	1.5	31.3	16.1	1.8	31.0
14	16.9	1.6	33.2	16.7	1.8	32.4
15	17.8	1.6	35.2	17.4	1.8	33.9
16	18.6	1.6	37.0	17.8	1.8	34.8
17	19.4	1.6	38.7	18.5	1.8	36.2
18	20.2	1.6	40.4	19.0	1.8	37.4
19	21.2	1.7	42.4	19.4	1.8	38.2
20	21.9	1.7	43.8	19.8	1.8	39.1

Table 21. Reaction Data

RUN 19 T = 981°C Sensitivity 23.0 div/50mg				RUN 20 T = 695°C Sensitivity 23.0 div/50mg		
Time	Gross Weight Change Divisions	Zero Balance Adjustment	Weight Gain $gms/cm^2 \times 10^{-4}$	Gross Weight Change Divisions	Zero Balance Adjustment	Weight Gain $gms/cm^2 \times 10^{-4}$
0.2	1.3	0.7	1.30	0.7	0.7	0.0
0.4	2.5	1.1	3.04	0.9	0.9	0.0
0.6	3.4	1.2	4.78	1.1	1.1	0.0
0.8	4.0	1.3	5.87	1.2	1.2	0.0
1.0	4.7	1.3	7.4	1.3	1.2	0.21
1.5	6.0	1.4	10.0	1.4	1.2	0.42
2	7.0	1.4	12.2	1.6	1.3	0.63
3	8.4	1.5	15.0	1.7	1.3	0.84
4	9.6	1.5	17.6	1.8	1.3	1.05
5	10.8	1.5	20.0	2.0	1.4	1.27
6	12.1	1.5	22.8	2.1	1.4	1.48
7	13.2	1.6	25.2	2.2	1.4	1.69
8	14.4	1.6	27.8	2.3	1.4	1.90
9	15.5	1.6	30.2	2.7	1.4	1.90
10	16.6	1.6	32.6	2.4	1.5	1.90
11	17.7	1.7	35.0	2.5	1.5	2.11
12	18.9	1.7	37.4	2.5	1.5	2.11
13	20.0	1.7	39.8	2.6	1.6	2.11
14	21.2	1.7	42.3	2.6	1.6	2.11
15	22.3	1.7	44.7	2.6	1.6	2.11
16	23.4	1.7	47.2	2.6	1.6	2.11
17	24.5	1.8	49.3	2.6	1.6	2.11
18	25.5	1.8	51.5	2.7	1.7	2.11
19	26.5	1.8	53.7	2.7	1.7	2.11
20	27.5	1.8	55.8	2.7	1.7	2.11

Table 23. Reaction Data

Time	RUN 21 T = 558°C Sensitivity 23.0 div/50mg Gross Weight Change Divisions	Zero Balance Adjustment	Weight Gain $gms/cm^2 \times 10^{-4}$	RUN 22 T = 932°C Sensitivity 23.0 div/50mg Gross Weight Change Divisions	Zero Balance Adjustment	Weight Gain $gms/cm^2 \times 10^{-4}$
0.2	0.8	0.8	0.0	1.2	0.7	1.50
0.4	0.9	0.9	0.0	2.2	1.1	2.32
0.6	0.9	0.9	0.0	2.9	1.6	2.74
0.8	0.9	0.9	0.0	3.6	1.7	4.00
1.0	1.0	1.0	0.0	4.3	1.8	5.27
1.5	1.3	1.3	0.0	5.5	1.8	7.80
2	2.0	1.4	1.3	6.6	1.9	9.90
3	4.8	1.5	7.17	8.0	1.9	12.85
4	8.3	1.5	14.8	8.9	1.9	14.7
5	10.9	1.5	20.4	9.8	2.0	16.4
6	13.4	1.6	25.6	10.5	2.0	17.9
7	15.5	1.6	30.2	11.2	2.0	19.4
8	17.5	1.6	34.4	11.9	2.0	20.8
9	19.4	1.7	37.8	12.6	2.0	22.3
10	20.8	1.7	41.5	13.3	2.0	23.8
11	22.4	1.7	44.4	13.9	2.0	25.0
12	23.8	1.7	48.0	14.7	2.1	26.5
13	25.2	1.7	51.1	15.3	2.1	27.8
14	26.6	1.7	54.1	15.9	2.1	29.0
15	28.0	1.7	57.2	16.7	2.1	30.8
16	29.8	1.8	60.8	17.3	2.1	32.0
17	31.5	1.8	64.5	17.9	2.2	33.1
18	33.2	1.8	68.3	18.6	2.2	34.6
19	35.7	1.8	71.5	19.0	2.2	35.4
20	37.3	1.8	75.0	19.5	2.2	36.9

Table 24. Reaction Data

Time	RUN 23 T = 525°C Sensitivity 23.0 div/50mg Gross Weight Change Divisions	Zero Balance Adjustment	Weight Gain $gms/cm^2 \times 10^{-4}$	RUN 24 T = 521°C Sensitivity 23.0 div/50mg Gross Weight Change Divisions	Zero Balance Adjustment	Weight Gain $gms/cm^2 \times 10^{-4}$
0.2	1.4	0.8	-1.26	0.7	0.7	0.0
0.4	1.3	1.0	-0.63	0.9	0.9	0.0
0.6	1.2	1.1	-0.21	1.0	1.0	0.0
0.8	1.2	1.2	0.0	1.0	1.0	0.0
1.0	1.3	1.2	+0.21	1.1	1.1	0.0
1.5	2.2	1.3	+1.90	1.2	1.2	0.0
2	3.9	1.4	5.27	1.4	1.4	0.0
3	8.5	1.4	15.0	1.6	1.4	0.25
4	12.3	1.4	25.1	2.0	1.4	1.26
5	15.5	1.4	29.7	3.0	1.4	3.37
6	18.4	1.4	35.8	4.0	1.5	5.27
7	20.7	1.4	40.7	5.1	1.5	7.58
8	22.8	1.4	45.0	6.1	1.5	9.48
9	24.5	1.4	48.7	7.0	1.5	11.6
10	26.1	1.5	51.8	7.9	1.5	13.5
11	27.5	1.5	54.8	8.8	1.6	15.3
12	28.7	1.5	57.3	9.7	1.6	17.0
13	29.8	1.5	59.6	10.7	1.6	19.2
14	30.8	1.5	61.7	11.6	1.6	21.0
15	31.7	1.5	63.6	12.6	1.6	23.1
16	32.6	1.6	65.3	13.6	1.6	25.2
17	33.3	1.6	66.8	14.6	1.6	27.3

Table 25. Reaction Data

Time	RUN 25 T = 933°C Sensitivity 23.5 div/50mg Gross Weight Change Divisions	Zero Balance Adjustment	Weight Gain $gms/cm^2 \times 10^{-4}$	RUN 26 T = 969°C Sensitivity 23.5 div/50mg Gross Weight Change Divisions	Zero Balance Adjustment	Weight Gain $gms/cm^2 \times 10^{-4}$
0.2	1.4	0.9	1.07	1.3	0.9	0.85
0.4	2.5	1.2	2.77	2.3	1.2	2.34
0.6	3.5	1.5	4.04	3.2	1.5	3.63
0.8	4.2	1.7	5.32	3.6	1.7	4.04
1.0	4.9	1.8	6.60	4.3	1.7	5.53
1.5	0.2	1.9	9.15	5.6	1.8	7.97
2	7.2	1.9	11.30	6.4	1.8	10.00
3	8.5	2.0	13.82	7.9	1.9	12.74
4	9.6	2.0	16.15	9.0	2.0	14.85
5	10.7	2.1	18.28	10.2	2.0	17.4
6	11.8	2.1	20.6	11.3	2.1	19.6
7	12.9	2.1	23.6	12.3	2.1	21.7
8	13.9	2.1	25.0	13.4	2.1	24.0
9	15.0	2.2	27.25	14.4	2.1	26.2
10	16.0	2.2	29.3	15.5	2.2	28.3
11	17.1	2.3	31.5	16.5	2.2	30.5
12	18.1	2.3	33.5	17.6	2.3	32.4
13	19.1	2.3	35.7	18.6	2.3	34.6
14	20.1	2.3	37.9	19.6	2.3	36.8
15	21.0	2.3	40.2	20.6	2.3	38.8
16	41.8	2.3	41.3	21.6	2.3	40.9
17	22.6	2.3	43.2	22.6	2.3	43.1
18	23.4	2.3	44.8	23.6	2.3	45.2
19	24.2	2.3	46.5	24.6	2.3	47.3
20	25.0	2.3	49.2	25.0	2.3	49.3

Table 26. Reaction Data

RUN 27				RUN 28		
T = 801°C Sensitivity 23 div/50mg				T = 785°C Sensitivity 21.5 div/50mg		
Time	Gross Weight Change Divisions	Zero Balance Adjustment	Weight Gain $gms/cm^2 \times 10^{-4}$	Gross Weight Change Divisions	Zero Balance Adjustment	Weight Gain $gms/cm^2 \times 10^{-4}$
0.2	1.0	0.9	0.0	0.8	0.6	0.46
0.4	1.3	1.2	0.0	1.2	0.8	0.93
0.6	1.6	1.5	0.0	1.4	0.8	1.39
0.8	1.7	1.7	0.0	1.7	0.9	1.86
1.0	2.0	1.7	0.65	1.9	0.9	2.32
1.5	2.7	1.8	1.96	2.4	1.0	3.25
2	3.2	1.8	3.04	2.9	1.1	4.17
3	4.5	1.9	5.63	3.7	1.2	5.80
4	5.0	2.0	6.50	4.1	1.2	6.73
5	5.3	2.0	7.17	4.6	1.3	7.66
6	5.6	2.1	7.60	5.0	1.3	8.59
7	5.8	2.1	8.03	5.3	1.3	9.28
8	5.9	2.1	8.25	5.5	1.3	9.75
9	6.0	2.1	8.45	5.6	1.3	9.98
10	6.1	2.1	8.68	5.7	1.3	10.20
11	6.2	2.1	8.90	5.9	1.3	10.55
12	6.4	2.2	9.10	6.0	1.3	10.90
13	6.6	2.2	9.55	6.2	1.3	11.30
14	6.8	2.2	9.98	6.3	1.3	11.60
15	7.0	2.3	10.20	6.4	1.3	11.83
16	7.2	2.3	10.65	6.5	1.3	12.06
17	7.4	2.3	11.06	6.6	1.3	12.30
18	7.6	2.3	11.48	6.7	1.3	12.53
19	7.8	2.3	11.90	6.8	1.3	12.76
20	8.0	2.3	12.30	6.9	1.3	13.0

Table 27. Reaction Data

RUN 29				RUN 30		
T = 785°C Sensitivity 21.5 div/50mg				T = 785°C Sensitivity 21.5 div/50mg		
Time	Gross Weight Change Divisions	Zero Balance Adjustment	Weight Gain $gms/cm^2 \times 10^{-4}$	Gross Weight Change Divisions	Zero Balance Adjustment	Weight Gain $gms/cm^2 \times 10^{-4}$
0.2	0.8	0.6	0.46	0.2	0.2	0.0
0.4	1.0	0.7	0.70	0.4	0.3	0.23
0.6	1.2	0.7	1.16	0.7	0.4	0.70
0.8	1.4	0.7	1.62	1.0	0.4	1.29
1.0	1.6	0.8	1.85	1.3	0.4	2.09
1.5	2.0	0.9	2.55	1.8	0.4	3.25
2	2.5	1.0	3.50	2.5	0.4	4.88
3	3.4	1.2	5.10	3.5	0.5	6.97
4	4.1	1.3	6.50	4.0	0.5	8.13
5	4.5	1.3	7.43	4.4	0.5	9.05
6	4.8	1.3	8.12	4.8	0.6	9.75
7	5.0	1.3	8.59	5.0	0.6	10.20
8	5.2	1.4	8.82	5.2	0.6	10.70
9	5.3	1.4	9.05	5.3	0.6	10.9
10	5.4	1.4	9.29	5.5	0.6	11.37
11	5.5	1.4	9.52	5.7	0.6	11.83
12	5.7	1.4	9.98	5.9	0.6	12.30
13	5.8	1.4	10.22	6.1	0.6	12.75
14	6.0	1.4	10.70	6.3	0.6	13.20
15	6.1	1.4	10.92	6.5	0.6	13.70
16	6.3	1.4	11.40	6.7	0.6	14.15
17	6.4	1.4	11.62	6.9	0.6	14.60
18	6.5	1.4	11.85	7.1	0.6	15.10
19	6.7	1.4	12.32	7.3	0.6	15.55
20	6.8	1.4	12.55	7.5	0.6	16.05

Table 28. Reaction Data

Time	RUN 31 T = 573°C Sensitivity 21.5 div/50mg Gross Weight Change Divisions	Zero Balance Adjustment	Weight Gain $gms/cm^2 \times 10^{-4}$	RUN 32 T = 550°C Sensitivity 22 div/50mg Gross Weight Change Division	Zero Balance Adjustment	Weight Gain $gms/cm^2 \times 10^{-4}$
0.2	0.8	0.0	0.0	0.5	0.5	0.0
0.4	1.0	1.0	0.0	0.7	0.7	0.0
0.6	1.1	1.1	0.0	0.9	0.9	0.0
0.8	1.1	1.1	0.0	1.0	1.0	0.0
1.0	1.2	1.2	0.0	1.1	1.1	0.0
1.5	1.5	1.2	0.70	1.1	1.1	0.0
2	1.7	1.2	1.16	1.1	1.1	0.0
3	2.0	1.2	1.86	1.2	1.1	0.23
4	2.2	1.2	2.32	1.3	1.1	0.45
5	2.4	1.2	2.79	1.6	1.2	0.91
6	3.2	1.2	4.65	2.4	1.2	2.73
7	4.0	1.2	6.52	3.3	1.2	4.78
8	4.8	1.2	8.37	4.2	1.2	6.82
9	5.6	1.2	10.24	5.1	1.2	8.86
10	6.4	1.2	12.20	5.9	1.2	10.68
11	7.3	1.3	13.95	6.8	1.3	12.50
12	8.3	1.3	16.27	7.7	1.3	14.52
13	9.3	1.3	18.60	8.7	1.3	16.8
14	10.4	1.3	21.10	9.8	1.3	19.3
15	11.5	1.3	23.7	10.9	1.3	21.8
16	12.7	1.3	26.5	12.4	1.3	25.2
17	14.0	1.4	29.3	13.8	1.3	28.4
18	15.2	1.4	32.1	15.7	1.3	32.7
19	16.4	1.4	34.9	17.6	1.3	37.0
20	17.7	1.5	37.7	19.5	1.3	41.3

Table 29. Reaction Data

Time	RUN 33 T = 546°C Sensitivity 22 div/50mg Gross Weight Change Divisions	Zero Balance Adjustment	Weight Gain $gms/cm^2 \times 10^{-4}$	RUN 34 T = 546°C Sensitivity 22 div/50mg Gross Weight Change Divisions	Zero Balance Adjustment	Weight Gain $gms/cm^2 \times 10^{-4}$
0.2			0.0	0.6	0.6	0.0
0.4			0.0	0.8	0.8	0.0
0.6			0.0	0.8	0.8	0.0
0.8			0.0	0.9	0.9	0.0
1.0	1.0	1.0	0.0	0.9	0.9	0.0
1.5	1.0	1.0	0.0	1.0	1.0	0.0
2	1.1	1.1	0.0	1.0	1.0	0.0
3	1.4	1.1	0.68	1.2	1.1	0.23
4	2.0	1.1	2.04	1.9	1.1	1.82
5	3.0	1.1	4.32	2.8	1.1	3.86
6	4.0	1.2	6.36	3.8	1.2	5.91
7	5.0	1.2	8.63	4.7	1.2	7.95
8	6.0	1.2	10.90	5.7	1.3	10.00
9	7.0	1.2	13.17	6.5	1.3	11.80
10	8.0	1.2	15.45	7.5	1.3	14.1
11	9.0	1.3	17.50	8.5	1.3	16.35
12	10.2	1.3	20.20	9.6	1.3	18.85
13	12.0	1.3	24.3	10.7	1.3	21.3
14	13.8	1.3	28.4	11.9	1.3	24.1
15	15.7	1.3	32.7	13.4	1.3	27.5
16	17.7	1.3	37.2	14.8	1.3	30.7
17	19.6	1.3	41.6	16.0	1.3	33.4
18	21.0	1.3	44.7	17.1	1.3	35.9
19	22.4	1.3	48.0	18.6	1.3	39.3
20	23.7	1.3	51.1	19.7	1.3	41.8

Table 30. Reaction Data

Time	RUN 35 T = 540°C Sensitivity 22 div/50mg Gross Weight Change Division	Zero Balance Adjustment	Weight Gain $gms/cm^2 \times 10^{-4}$	RUN 36 T = 594°C Sensitivity 22 div/50mg Gross Weight Change Division	Zero Balance Adjustment	Weight Gain $gms/cm^2 \times 10^{-4}$
0.2	0.7	0.7	0.0	0.7	0.7	0.0
0.4	0.8	0.8	0.0	0.8	0.8	0.0
0.6	0.8	0.8	0.0	0.8	0.8	0.0
0.8	0.9	0.9	0.0	0.9	0.9	0.0
1.0	1.0	1.0	0.0	1.0	1.0	0.0
1.5	1.0	1.0	0.0	1.1	1.1	0.0
2	1.0	1.0	0.0	1.2	1.1	0.23
3	1.1	1.1	0.0	2.0	1.1	2.04
4	1.1	1.1	0.0	3.2	1.2	4.55
5	1.3	1.1	0.45	4.7	1.2	7.95
6	1.9	1.1	1.82	6.1	1.2	11.12
7	2.7	1.2	3.40	7.6	1.2	14.53
8	3.4	1.2	5.0	9.2	1.2	18.16
9	4.1	1.2	6.59	10.9	1.2	22.00
10	5.0	1.2	8.63	12.2	1.3	24.8
11	5.8	1.3	10.22	14.0	1.3	28.85
12	6.4	1.3	11.59	15.9	1.3	33.20
13	7.3	1.3	13.63	17.6	1.3	37.00
14	8.3	1.3	15.90	19.5	1.3	41.30
15	9.2	1.3	17.95	21.4	1.3	45.70
16	10.1	1.3	20.00	23.3	1.3	50.00
17	11.3	1.3	22.70	25.2	1.3	54.30
18	12.6	1.3	25.70	27.2	1.3	58.80
19	14.0	1.3	28.90	29.1	1.3	63.20
20	15.2	1.3	31.60	31.1	1.3	67.7

Table 31. Reaction Data

Time	RUN 37 T = 515°C Sensitivity 22 div/50mg Gross Weight Change Division	Zero Balance Adjustment	Weight Gain $gms/cm^2 \times 10^{-4}$	RUN 38 T = 969°C Sensitivity 21.7 div/50mg Gross Weight Change Division	Zero Balance Adjustment	Weight Gain $gms/cm^2 \times 10^{-4}$
0.2	0.7	0.7	0.0	1.7	0.7	2.30
0.4	0.8	0.8	0.0	2.6	0.8	4.15
0.6	0.9	0.9	0.0	3.5	0.8	6.22
0.8	0.9	0.9	0.0	4.1	0.9	7.37
1.0	1.1	1.0	0.0	4.6	0.9	8.07
1.5	1.1	1.0	0.0	5.7	0.9	11.05
2	1.2	1.1	0.23	6.6	0.9	13.13
3	1.3	1.2	0.23	8.0	0.9	16.35
4	1.6	1.2	0.91	9.3	1.0	19.10
5	1.9	1.2	1.59	10.6	1.0	22.1
6	2.2	1.2	2.27	11.9	1.0	25.1
7	2.8	1.2	3.63	13.2	1.0	28.1
8	3.4	1.2	5.00	14.4	1.0	30.9
9	4.0	1.2	6.36	15.6	1.0	33.7
10	4.7	1.3	7.72	16.7	1.0	36.2
11	5.3	1.3	9.09	17.7	1.0	38.5
12	5.9	1.3	10.45	18.7	1.0	40.8
13	6.5	1.3	11.80	19.7	1.0	43.1
14	7.1	1.3	13.20	20.7	1.0	45.4
15	7.8	1.3	14.75	21.7	1.0	47.7
16	8.5	1.3	16.35	22.7	1.0	50.0
17	9.1	1.3	17.70	23.7	1.0	52.3
18	9.9	1.3	19.53	24.6	1.0	54.4
19	10.7	1.3	21.5	25.6	1.0	56.7
20	11.6	1.3	23.4	26.6	1.0	59.0

Table 32. Reaction Data

RUN 39 T = 820°C Sensitivity 21.7 div/50mg				RUN 41 T = 340°C Sensitivity 21.5 div/50mg		
Time	Gross Weight Change Division	Zero Balance Adjustment	Weight Gain $gms/cm^2 \times 10^{-4}$	Gross Weight Change Division	Zero Balance Adjustment	Weight Gain $gms/cm^2 \times 10^{-4}$
0.2	0.7	0.7	0.0	0.4	0.4	0.0
0.4	1.2	0.8	0.69	0.6	0.6	0.0
0.6	1.3	0.8	0.92	0.7	0.7	0.0
0.8	1.8	0.9	2.07	0.8	0.8	0.0
1.0	2.1	1.0	2.53	0.9	0.9	0.0
1.5	3.1	1.1	4.60	1.0	1.0	0.0
2	4.0	1.2	6.45	1.1	1.1	0.0
3	4.9	1.3	8.30	1.2	1.2	0.0
4	5.5	1.3	9.68	1.3	1.3	0.0
5	5.7	1.3	10.15	1.3	1.3	0.0
6	6.0	1.3	10.83	1.3	1.3	0.0
7	6.4	1.4	11.52	1.4	1.4	0.0
8	6.6	1.4	11.98	1.4	1.4	0.0
9	7.1	1.4	13.13	1.4	1.4	0.0
10	7.6	1.4	14.28	1.4	1.4	0.0
11	8.3	1.4	15.90	1.4	1.4	0.0
12	8.8	1.4	17.05	1.4	1.4	0.0
13	9.7	1.4	19.10	1.4	1.4	0.0
14	10.5	1.4	21.0	1.4	1.4	0.0
15	11.3	1.4	22.8	1.4	1.4	0.0
16	12.1	1.4	24.7	1.4	1.4	0.0
17	12.8	1.4	26.3	1.4	1.4	0.0
18	13.5	1.4	27.9	1.4	1.4	0.0
19	14.3	1.4	29.7	1.4	1.4	0.0
20	15.1	1.4	31.6	1.4	1.4	0.0

Table 33. Reaction Data

RUN 42				RUN 43		
T = 276°C Sensitivity 21.5 div/50mg				T = 586°C Sensitivity 21.5 div/50mg		
Time	Gross Weight Change Division	Zero Balance Adjustment	Weight Gain $gms/cm^2 \times 10^{-4}$	Gross Weight Change Division	Zero Balance Adjustment	Weight Gain $gms/cm^2 \times 10^{-4}$
0.2	0.4	0.4	0.0	0.3	0.3	0.0
0.4	0.6	0.6	0.0	0.5	0.5	0.0
0.6	0.8	0.8	0.0	0.7	0.7	0.0
0.8	0.8	0.8	0.0	0.8	0.8	0.0
1.0	0.8	0.8	0.0	0.9	0.9	0.0
1.5	0.8	0.8	0.0	1.1	1.1	0.0
2	0.8	0.8	0.0	1.5	1.2	0.70
3	1.0	1.0	0.0	2.2	1.3	2.09
4	1.0	1.0	0.0	3.2	1.3	4.42
5	1.0	1.0	0.0	4.5	1.3	7.45
6	1.1	1.1	0.0	5.9	1.4	10.46
7	1.1	1.1	0.0	7.3	1.4	13.72
8	1.1	1.1	0.0	8.7	1.4	16.97
9	1.1	1.1	0.0	10.0	1.4	20.00
10	1.2	1.2	0.0	11.4	1.4	23.30
11	1.2	1.2	0.0	12.8	1.4	26.50
12	1.2	1.2	0.0	14.2	1.5	29.5
13	1.2	1.2	0.0	15.8	1.5	33.3
14	1.2	1.2	0.0	17.3	1.5	36.7
15	1.2	1.2	0.0	19.1	1.6	40.7
16	1.2	1.2	0.0	20.8	1.6	44.7
17	1.2	1.2	0.0	22.5	1.6	48.7
18	1.2	1.2	0.0	24.2	1.6	52.6
19	1.2	1.2	0.0	25.9	1.6	56.5
20	1.2	1.2	0.0	27.5	1.6	60.3

Table 34. Reaction Data

Time	RUN 44 T = 624°C Sensitivity 2.13 div/50mg Gross Weight Change Divisions	Zero Balance Adjustment	Weight Gain $gms/cm^2 \times 10^{-4}$	RUN 45 T = 380°C Sensitivity 21.3 div/50mg Gross Weight Change Divisions	Zero Balance Adjustment	Weight Gain $gms/cm^2 \times 10^{-4}$
0.2	0.8	0.8	0.0	0.7	0.7	0.0
0.4	0.9	0.9	0.0	0.8	0.8	0.0
0.6	1.0	1.0	0.0	0.9	0.9	0.0
0.8	1.1	1.1	0.0	1.0	1.0	0.0
1.0	1.1	1.1	0.0	1.1	1.1	0.0
1.5	1.4	1.2	0.47	1.3	1.3	0.0
2	1.6	1.2	0.94	1.4	1.4	0.0
3	1.8	1.2	1.41	1.5	1.5	0.0
4	2.0	1.2	1.88	1.5	1.5	0.0
5	2.3	1.3	2.35	1.5	1.5	0.0
6	2.7	1.3	3.29	1.5	1.5	0.0
7	3.1	1.4	4.00	1.5	1.5	0.0
8	3.6	1.4	5.17	1.5	1.5	0.0
9	4.1	1.4	6.34	1.6	1.6	0.0
10	4.8	1.4	7.98	1.6	1.6	0.0
11	5.6	1.5	9.63	1.6	1.6	0.0
12	6.1	1.5	10.80	1.6	1.6	0.0
13	6.7	1.5	12.21	1.6	1.6	0.0
14	7.2	1.5	13.38	1.6	1.6	0.0
15	7.9	1.5	15.03	1.6	1.6	0.0
16	8.6	1.5	16.67	1.6	1.6	0.0
17	9.3	1.5	18.30	1.6	1.6	0.0
18	9.8	1.5	19.50	1.6	1.6	0.0
19	10.3	1.5	20.70	1.6	1.6	0.0
20	10.8	1.5	21.85	1.6	1.6	0.0

Table 35. Reaction Data

RUN 46
T = 545°C
Sensitivity 22 div/50mg

Time	Gross Weight Change Divisions	Zero Balance Adjustment	Weight Gain $gms/cm^2 \times 10^{-4}$
0.2			0.0
0.4			0.0
0.6			0.0
0.8			0.0
1.0	1.0	1.0	0.0
1.5	1.0	1.0	0.0
2	1.1	1.1	0.0
3	1.3	1.1	0.45
4	1.8	1.1	1.59
5	2.5	1.1	3.18
6	3.5	1.1	5.45
7	4.5	1.2	7.50
8	5.5	1.2	9.76
9	6.5	1.2	12.0
10	7.5	1.2	14.3
11	8.5	1.2	16.6
12	9.5	1.2	18.8
13	10.5	1.2	21.1
14	11.5	1.2	23.4
15	12.0	1.3	26.6
16	15.0	1.3	31.1
17	17.0	1.3	35.6
18	18.5	1.3	39.0
19	20.0	1.3	42.5
20	21.2	1.3	44.0

APPENDIX E

DATA FROM PROLONGED EXPOSURE

Experiments were performed in the horizontal tube furnace using coiled wire and a reaction time of about 70 hours. Fifty-degree temperature intervals were used. Initial-terminal weight changes were used as a measure of the reaction. The data is tabulated in Table 36, and also presented graphically in Figure 18.

Due to the length of the reaction, massive carbon deposits were obtained at the lower temperatures. Because of the ease with which the surface carbon was dislodged, the samples were shaken to remove as much of the deposits as possible. Above 900°C the wire began to fall apart during the reaction, so the experiments were terminated at 900°C.

Table 36. Summary of Prolonged Exposure Experiments in Horizontal Tube Furnace

Run Number	Temperature	Total Hours	Weight Change of Wire (grams)	Free Carbon (grams)	Total Weight Change (grams)
100	500	69.5	0.01115	0.27740	0.28855
101	550	69.0	-0.01290	0.55200	0.53910
102	600	66.75	0.00020	0.51070	0.51090
103	650	70.0	+0.0109	0.0000	+0.0109
104	700	69.7	+0.01440		0.01440
105	750	67.0	0.03765		0.03765
106	800	27.0	0.01845		0.01845
107	800	66.5	0.05280		0.05280
108	850	72	0.05600		0.05600
109	900	70	0.09065		0.09065

APPENDIX F

HIGH-TEMPERATURE X-RAY RESULTS

The results of the at-temperature reaction x-ray studies are presented in tabular form. As the reaction proceeded the samples had a tendency to deform. Figure 50 shows the major recovered part of each sample. It is interesting to note the changes in size. Since the temperature varied as part of each run, the experiment is labeled by its most characteristic temperature. The details of the experiments are found in the following tables.

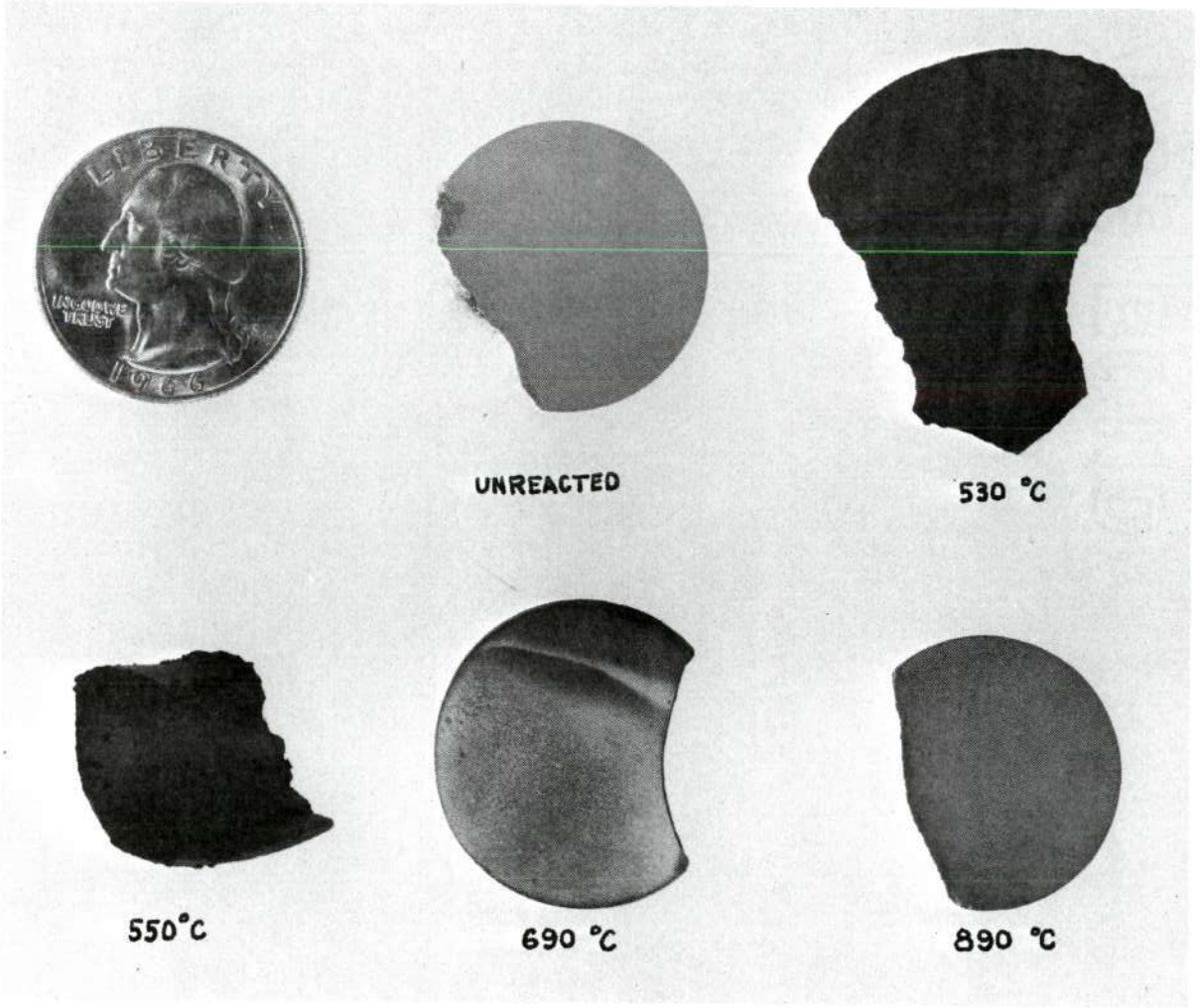

Figure 50. Reacted At-Temperature X-ray Samples

Table 36. High-Temperature X-ray Results
Run No. 1

Element	ASTM Card d space °A	I/I_1	Helium T=20°C		Helium T=500°C		CO t=10 min T=550°C		CO t=30 min T=550°C	
			d °A	I	d °A	I	d °A	I	d °A	I
Fe_3O_4	2.530	100					2.56	2.6		
FeO	2.486	80					2.51	1.5	2.50	2.0
Fe_3C	2.38	65							2.40	1.0
Fe_3C	2.26	25							2.26	0.6
Fe_3C	2.20	25							2.8	0.6
FeO	2.153	100					2.16	2.0		
Fe_3C	2.10	60							2.10	0.7
Fe_3O_4	2.097	50					2.10	0.7		
α-Fe	2.027	100	2.03	17.0	2.03	18.0	2.04	9.6	2.03	9.0
Fe_3C	2.01	100							P	
Fe_3C	1.97	55							1.98	0.5
Fe_3C	1.85	40							1.86	0.4
Fe_3O_4	1.714	40					1.72	0.6		
Fe_3O_4	1.615	60					1.62	0.6		
FeO	1.523	60					1.53	1.9	1.53	1.9
Fe_3O_4	1.484	70					1.48	0.6		
α-Fe	1.433	19	1.43	2.4	1.43	2.2	1.44	1.4	1.44	1.6
Fe_3C	1.324	M							1.33	0.5
FeO	1.299	25					1.30	0.5	1.31	0.8
Fe_3O_4	1.279	30					1.28	0.4		
FeO	1.243	15					1.24	0.5	1.24	0.6
Fe_3C	1.20	M							1.20	0.4
α-Fe	1.17	30	1.17	4.0	1.17	3.6	1.18	2.0	1.18	2.0

Table 37. High-Temperature X-ray Results
Run No. 2

Element	ASTM Card d space °A	I/I_1	Helium T=20°C d °A	I	Helium T=660°C d °A	I	CO t=10 min T=690°C d °A	I	CO t=35 min T=690°C d °A	I
FeO	2.49						2.51	2.7	2.52	1.8
Fe_3C	2.38	65					2.37	0.4	2.37	0.4
Fe_3C	2.20	25					2.23	0.2	2.20	0.3
FeO	2.15	100					2.17	4.8	2.18	3.0
Fe_3C	2.10	60					2.10	0.6	2.11	0.8
α-Fe	2.02	100	2.02	13.5	2.04	12.4	2.05	1.4	2.05	2.8
Fe_3C	2.02	100								
Fe_3C	2.02	100							2.02	0.4
Fe_3C	1.97	55					1.99	0.6	1.99	0.6
FeO	1.52	60					1.54	2.0	1.54	1.2
α-Fe	1.43	19	1.43	1.9	1.44	1.4	1.44	0.4	1.45	0.6
Fe_3C	1.32	M					1.33	0.6	1.33	0.8
FeO	1.30						1.32	0.5		
α-Fe	1.17	30	1.17	3.1	1.18	2.2	1.18	0.6	1.18	0.7

Table 38. High Temperature X-ray Results
Run No. 3

Element	d space °A	I/I_1	Helium T=800 d °A	I	CO t=10 min T=890°C d°A	I	CO t=40 min T=890°C d°A	I	CO t=75 min T=890°C d°A	I	CO t=175 min T=675°C d°A	I	CO t=210 min T=550°C d°A	I
C	3.35	100			3.35	0.5	3.35	3.0	3.35	6.0	3.35	10.5	2.37	8.0
Fe_3C	2.38	65											2.37	0.4
Fe_3C	2.0	60											2.11	0.6
γ-Fe	2.06				2.12	12.0	2.12	9.5	2.12	8.4	2.10	7.0		
α-Fe	2.02	100	2.05	16.0							2.04	5.0	2.04	13.3
Fe_3C	1.97	55											1.97	0.6
Fe_3C	1.85	40											1.88	0.6
γ-Fe	1.78				1.84	5.0	1.84	3.5	1.84	3.3	1.81	1.3		
α-Fe	1.43	19	1.45	2.0							1.44	1.6	1.44	1.7
γ-Fe	1.26				1.30	2.0	1.30	1.4	1.30	1.2				
α-Fe	1.17	30	1.19	2.3							1.18	2.0	1.18	2.4

Table 39. High Temperature X-ray Results
Run No. 4

Element	Standard d space °A	I/I_1	Helium T=500°C d°A	I	CO t=4 min T=530°C d°A	I	CO t=21 min T=540°C d°A	I
Fe_3O_4	2.530	100	2.55	0.4	2.55	1.6	2.55	0.4
FeO	2.486	80	2.50	0.6			2.50	0.4
Fe_3C	2.38	65					2.39	0.3
Fe_3C	2.26	25						
Fe_3C	2.20	25						
FeO	2.153	100	P		2.14	0.3	2.14	0.4
Fe_3C	2.10	60					2.09	0.5
Fe_3O_4	2.097	50			P		2.09	0.5
α-Fe	2.027	100	2.03	14.0	2.03	12.7	2.03	10.0
Fe_3C	2.01	100					P	
Fe_3C	1.97	55					1.99	0.4
Fe_3C	1.85	40					1.86	0.3
Fe_3O_4	1.714	40						
Fe_3O_4	1.615	60			1.61	0.3	1.61	0.1
FeO	1.523	60					1.52	0.2
Fe_3O_4	1.484	70			1.48	0.6	P	
α-Fe	1.433	19	1.43	2.0	1.43	1.4	1.43	1.0
Fe_3C	1.22	M					1.21	1.2
Fe_3C	1.19	M					1.19	0.2
α-Fe	1.17	30	1.18	3.2	1.18	3.3	1.18	3.0

BIBLIOGRAPHY

BIBLIOGRAPHY

1. Leslie Aitchison, *A History of Metals, Volume Two,* Interscience Publishers, Inc., New York (1960).

2. I. Lowthian Bell, "The Chemistry of the Blastfurnace," *Journal of the Chemical Society, 22,* 203 (1869).

3. John Pattinson, "On Carbon and Other Deposits from Gases of Blast Furnaces in Cleveland," *Journal of the Iron and Steel Institute, 10,* 85 (1876).

4. M. O. Boudouard, "Research on Chemical Equilibria," *Annales de Chimie et de Physique, 24,* 5 (1901).

5. Georges Charpy, "The Action of Carbon Monoxide on Iron and Its Oxides," *Comptes Renduvs, 137,* 120 (1903).

6. Georges Charpy, "The Action of Carbon Monoxide on Chromium, Nickel and Manganese, Their Oxides and Their Alloys," *Comptes Rendus, 148,* 560 (1909).

7. Georges Charpy, "The Role of Carbon and Carbon Monoxide in Metallurgical Reactions," *Revue de Metallurgie, 7,* 962 (1910).

8. T. F. E. Rhead and R. V. Wheeler, "The Effect of Temperature and Pressure on the Equilibrium $2CO \rightleftarrows CO_2 + C$," *Journal of the Chemical Society, 99,* 1140 (1911).

9. R. Schenck and Zimmerman, "The Decomposition of Carbon Monoxide and Blastfurnace Equilibrium," *Berichte, 36,* 1231 (1903).

10. S. Hilbert and T. Dieckmann, "Iron Carbides and their Catalytic Action on the Decomposition of Carbon Monoxide," *Berichte, 48,* 1281 (1915).

11. V. Falcke, "Reaction Between Ferrous Oxide and Carbon and Between Carbon Monoxide and Iron," *Zeitschrift für Elektrochemie, 21,* 37-50 (1915).

12. A. Stoffel, "The Reaction Between Carbon Monoxide and Iron," *Zeitschrift für Anorganische Chemie, 84,* 56 (1914).

13. H. C. H. Carpenter and C. C. Smith, "Some Experiments on the Reaction Between Pure Carbon Monoxide and Pure Electrolytic Iron Below the A1 Inversion," *Journal of the Iron and Steel Institute, 98,* 139 (1918).

14. R. Hochman and J. Burson, "The Fundamentals of Metal Dusting," *Division of Refining, 46,* 331 (1966).

15. L. Darken and R. Gurry, *Physical Chemistry of Metals,* McGraw-Hill Book Company, Inc. (1953).

16. A. Matsubara, "Chemical Equilibrium between Iron, Carbon and Oxygen," *American Institute of Mining and Metallurgical Engineers, 67,* 3 (1922).

17. A. Johansson and R. Von Seth," The Equilibria of the Carburisation and Decarburisation of Iron," *Journal of the Iron and Steel Institute, 64,* 295 (1926).

18. V. Falcke and W. Fischer, "The Equilibrium between Carbon Monoxide, Carbon, and Carbon Dioxide," *Zeitschrift für Elektrochemie, 32,* 194 (1926).

19. H. Tropsch and A. Von Philippovich,"Comparative Experiments on the Decomposition of Carbon Monoxide by Contact Substances," *Gesammelte Abhandlungen zur Kenntnis der Kohle, 7,* 44 (1925).

20. R. Schench, "Equilibrium Relations between Iron, Oxygen and Carbon," *Stahl und Eisen, 46,* 665 (1926).

21. R. Schenck, "Equilibrium Relations in the Reduction, Oxidation and Carburization of Iron I," *Zeitschrift für Anorganische und Allgemeine Chemie, 164,* 145 (1927).

22. R. Schenck, "Equilibrium Relations in the Reduction, Oxidation and Carburization of Iron IV," *Zeitschrift für Anorganische und Allgemeine Chemie, 167,* 254 (1927).

23. V. Hofmann, "The Deposition of Carbon from Carbon Monoxide and Benzene in the Presence of Iron," *Chemische Berichte, 61B,* 1180 (1928).

24. Ulrich Hofmann and E. Groll, "The Formation of Iron Oxides and Carbides in the Solid Phase," *Zeitschrift fur Anorganische und Allgemeine Chemie, 191,* 414 (1930).

25. F. Wüst, "Carbon Monoxide Dissociation in the Blast Furnace," *Zeitschrift für Anorganische und Allgemeine Chemie, 188,* 143 (1930).

26. H. Tutiya, "Iron as a Catalyst in the Catalytic Decomposition of Carbon Monoxide," *Scientific Papers of the Institute of Physical and Chemical Research (Tokyo) 10,* 69 (1929).

27. H. Tutiya, "Is the So-called X-Carbide Really Formed in the Iron Catalyst?" *Bulletin of the Institute of Physical and Chemical Research (Tokyo) 8,* 609 (1929).

28. H. Tutiya, "Catalytic Decomposition of Carbon Monoxide. III. The behavior of iron carbides," *Bulletin of the Institute of Physical and Chemical Research (Tokyo) 10,* 556 (1931).

29. A. Bramley and H. Lord, "The Equilibrium between Mixtures of Carbon Monoxide and Carbon Dioxide at Various Pressures in Contact with Steels of Different Carbon Concentrations at 750-1150°C," *Journal of the Chemical Society,* 1641 (1932).

30. W. Baukloh and G. Hieber, "Influence of Various Metals and Metallic Oxides upon Carbon Monoxide Decomposition," *Zeitschrift für Anorganische und Allgemeine Chemie, 226,* 321 (1936).

31. C. Wells, "Graphitization in High Purity Iron-Carbon Alloys," *Transactions: American Society for Metals, 26,* 289 (1938).

32. R. Mehl and C. Wells, "Constitution of High-purity Iron-carbon Alloys," *Transactions AIME, 125,* 429 (1937).

33. T. F. Berry, R. N. Ames and R. B. Snow, "Influence of Impurities and the Role of Iron Carbides in the Deposition of Carbon from Carbon Monoxide," *Journal of the American Ceramic Society, 39,* 308 (1956).

34. R. Gurry, "The Solubility of Carbon as Graphite in Gamma Iron," *Transactions AIME, 150,* 147 (1942).

35. R. A. Anderson, *Iron Catalysis of the Carbon-Carbon Dioxide Reaction,* The Pennsylvania State University, 1963.

36. P. L. Walker, Jr., J. F. Rakszawski and G. R. Imperial, "Carbon Formation over Iron Catalysts: I. Properties of Iron Formed, and II. Rates of Carbon Formation," *Journal of Physical Chemistry, 63,* 133, 140 (1959).

37. J. F. Henry, "On the Metal Catalyzed Deposition of Carbon from Carbon Monoxide," *Bulletin Des Societes Chemiques Belges, 72,* 740 (1963).

38. P. P. Smith, "Equilibrium of Iron-Carbon Alloys with Mixtures of CO-CO_2 and CH_4-H_2," *Journal of the American Chemical Society, 68,* 1163 (1946).

39. M. Hansen, *Constitution of Binary Alloys,* 2nd edition, McGraw-Hill Book Company, Inc., New York (1939).

40. H. A. Schwartz, "The Metastability of Cementite," *Transaction of the American Society for Metals, 23,* 126 (1935).

41. W. Baukloh, P. Chatterjee and P. Das, "Decomposition of Carbon Monoxide in the Presence of Iron, Cobalt and Nickel as Catalysts," *Transactions: Indian Institute of Metals, 4,* 271 (1950).

42. F. Körber, W. Wiemer and W. A. Fischer, "The Thermal Disintegration of Carbon Monoxide on Iron and its Alloys and in Mixtures with Carbon," *Archiv für das Eisenhuttenwesen, 17,* 43 (1943).

43. P. Das and P. Chatterjee, "Iron as a Catalyst in the Decomposition of Carbon Monoxide," *Transactions: Indian Institute of Metals, 6,* 279 (1952).

44. M. Tenenbaum and T. L. Joseph, "Reduction of Iron Ores under Pressure by Carbon Monoxide," *Transactions: American Institute of Mining and Metallurgical Engineers, 140,* 106 (1940).

45. F. Olmer, "Decomposition of Carbon Monoxide by Ferromagnetic Metals," *Journal of Physical Chemistry, 46,* 405 (1942).

46. P. Das and P. Chatterjee, "The Nature of the Catalyst in the Decomposition of Carbon Monoxide in Presence of Iron," *Transactions: Indian Institute of Metals, 7,* 189 (1953).

47. B. Fleureau, "The Formation of Graphite by the Catalytic Decomposition of Carbon Monoxide," *Comptes Rendus, 237,* 330 (1953).

48. W. R. Davis, R. J. Slawson and G. R. Rigby, "An Unusual Form of Carbon," *Nature, 171,* 756 (1953).

49. A. P. Lyuban, "Nature of the Bell Reaction and its Significance for the Heat Balance of Smelting," *Stal, 7,* 199 (1947).

50. H. Akamatsu and K. Sats, "Catalytic Decomposition of Carbon Monoxide," *Bulletin: Chemical Society of Japan, 22,* 127 (1949).

51. J. J. Trillot and S. Oketani, "Electronic Diffraction Study of Cementation of Iron by Carbon Monoxide," *Metaux and Corrosion, 25,* 263 (1950).

52. L. V. Radushkevich and V. M. Luk'yamovich, "Structure of the Carbon Produced in the Thermal Decomposition of Carbon Monoxide on an Iron Catalyst," *Zurnal Fizicheskoi Khimii, 26,* 88 (1952).

53. B. Chatterjee and P. Das, "Nature of the Catalyst in the Decomposition of Carbon Monoxide in Presence of Iron," *Nature, 173,* 1046 (1954).

54. P. Guiraldenq and P. Lacombe, "Measurement of Intergranular Self-diffusion Coefficients in Austenite," *Acta Metallurgica, 13(1),* 51 (1965).

55. J. Hui and A. Boulle, "Catalytic Decomposition of Carbon Monoxide in the Presence of Iron," *Comptes Rendus, 254,* 1806 (1962).

56. J. Taylor, "The Carbon Deposition Reaction over Iron Catalysts," *Journal of the Iron and Steel Institute, 184,* 1 (1956).

57. C. Decroly, "Experimental Study of the Hot Diffusion of Carbon Monoxide in Certain Stainless Steels," *Compte Rendu du Congres de Chimie Industrielle, 17 me Congres, Paris, Sept. 1937,* 347 (1937).

58. H. Forestier and Nury, "The Speeds of Reaction in the Vicinity of Magnetic Transformation Points,""Application to the Cementation of Iron," *Bulletin: Societe Chimique de France, 16(2),* 193 (1949).

59. R. Baukloh, O. Knacke and W. Löscher, "The Pressure Exerted by the Growth of Carbon," *Archiv für das Eisenhuttenwesen, 27,* 95 (1956).

60. L. J. E. Hofer and E. M. Cohn, "Synthesis of Cementite," *Journal of Chemical Physics, 18,* 766 (1950).

61. L. J. E. Hofer, E. M. Cohn and W. C. Peebles, "The Modifications of the Carbide Fe_2C; their Properties and Identification," *The American Chemical Society Journal, 71,* 189 (1949).

62. M. Manes, A. Damick, M. Mentser, E. Cohn and L. Hofer, "Hexagonal Iron Carbide as an Intermediate in the Carbiding of Iron Fischer-Tropsch Catalysts," *Journal: The American Chemical Society, 74,* 6207 (1952).

63. H. Carlton and J. Oxley, "Kinetics of the Heterogeneous Decomposition of Iron Pentacarbonyl," *American Institute of Chemical Engineers Journal, 11,* 79 (1965).

64. L. Hofer, E. Sterling, and J. McCartney, "Structure of the Carbon Deposited from Carbon Monoxide on Iron, Cobalt and Nickel," *Journal of Physical Chemistry, 59,* 1153 (1955).

65. L. Darken and R. Gury, "Free Energy of Formation of Cementite and the Solubility of Cementite in Austenite," *Transactions AIME, 191,* 1018 (1951).

66. L. W. Ross, F. H. Haynie and R. F. Hochman, "Thermodynamic Functions of Nickel Carbonyl and Iron Pentacarbonyl," *Journal of Chemical Engineering Data, 9,* 339 (1964).

67. F. Pettit, R. Yinger and J. Wagner, "The Mechanism of Oxidation of Iron in Carbon Monoxide-Carbon Dioxide Mixtures," *Acta Metallurgica, 8,* 617 (1960).

68. M. J. Duggin and L. Hofer, "Nature of x-Iron Carbide," *Nature, 212,* 248 (1966).

69. K. H. Jack and S. Wild, "Nature of x-Carbide and its Possible Occurrence in Steels," *Nature, 212,* 248 (1966).

70. H. Podgurski, J. Kummer, T. DeWitt, and P. Emmett, "Preparation, Stability and Absorptive Properties of the Carbides of Iron," *Journal of the American Chemical Society, 72,* 5382 (1950).

71. H. Abbott, "Encyclopedia on Chemical Technology," *Interscience Encyclopedia, Inc.,* New York, *Vol. 23,* 23 (1949).

72. L. J. E. Hofer, "Nature of the Carbides of Iron," *U. S. Bureau of Mines Bulletin 631* (1966).

73. A. Cox, "The High Temperature Reactions of Carbon Monoxide with Iron, Nickel, and Austenitic Stainless Steel," M.S. Thesis, Georgia Institute of Technology, 1962.

74. R. C. Ruhl and M. Cohen, "A New Metastable H. C. P. Phase in the Iron-Carbon System," *Acta Metallurgica, 15,* 159 (1967).

75. J. Chipman, "Thermodynamics of Binary Fe-C, Austenite and Cementite," *Transactions of the Metallurgical Society of AIME, 239,* 2 (1967).

76. W. Baukloh and G. Henke, "Effect of Metals and Metal Oxides on the Decomposition of Carbon Monoxide and its Technical Significance," *Metallwirtschaft, 19,* 463 (1940).

77. H. Schenck, M. Nacken and E. Potthast, "Zone of Existence of Iron Carbides Determined by Electron Microscopy and Electron Diffraction," *Archiv für das Eisenhüttenwesen, 37,* 341 (1966).

78. W. Baukloh and B. Edwin, "The Effect of Temperature and Pressure on the Disintegration of Carbon Monoxide and the Action of the Driving Effect of Carbon," *Archiv für das Eisenhüttenwesen, 16,* 197 (1942).

79. P. A. Letrancois and W. B. Hoyt, "Chemical Thermodynamics of High Temperature Reactions in Metal Dusting Corrosion," *Corrosion, 19,* 360t (1963).

80. W. B. Hoyt and R. H. Caughey, "High Temperature Metal Deterioration in Atmospheres Containing Carbon Monoxide and Hydrogen," *Corrosion, 15,* 308t (1959).

81. Hopkinson and Copson, "Internal Carburization and Oxidation of Nickel Chromium Alloys in Carbon Monoxide Type Atmospheres," *Corrosion, 16,* 608t (1960).

82. O. L. Burns, "Corrosion on a New Distillation Unit Processing Low Sulfur Crude," *Corrosion, 6,* 169 (1950).

83. W. G. Hubbell, "Carbon Absorption of 18-8 Stainless Steel," *The Iron Age, 157,* June 20, 56 (1946).

84. R. D. Merrick, "High Temperature Furnace Corrosion of Type 309 Alloy Steel," *Corrosion, 16,* 578t (1960).

85. F. A. Prange, "Corrosion in a Hydrocarbon Conversion System," *Corrosion, 15,* 619t (1959).

86. F. T. Eberle and R. D. Wylie, "Attack on Metals by Synthesis Gas from Methane-Oxygen Combustion," *Corrosion, 15,* 622t (1959).

87. Max Hansen, *Constitution of Binary Alloys* 2nd Edition, McGraw-Hill Book Co., Inc., New York (1958).

88. Metal Progress Data Sheet No. 32 (1946).

89. Samuel Epstein, *The Alloys of Iron and Carbon Vol. I,* McGraw-Hill Book Co., Inc., New York (1936).

90. M. Manes, A. Domick, M. Mentser, E. Cohn and C. Hoffer, "Hexagonal Iron Carbide as an Intermediate in the Carbiding of Iron Fischer-Tropsch Catalysts," *Journal of the American Chemical Society, 74,* 6207 (1952).

91. G. Hägg, "Powder Photographs of a New Iron Carbide," *Zeitschrift Kristallographie, 89,* 92 (1934).

92. W. Ruston, M. Warzee, J. Hennaut and J. Waty, "Basic Studies of the Growth of Carbon Deposition from Carbon Monoxide on a Metal Catalyst," SERAI Contract No. CON/WIN/52350-OE.3852 (Dragon Project), First Annual Report, June 21, 1965.

93. R. Hochman, "Metal Deterioration in High Temperature Carbonaceous Environments," Annual Report No. 1, Project A-753, Georgia Institute of Technology, 1965.

94. E. Camp, C. Phillips and L. Gross, "Corrosion of 18-8 Alloy Furnace Tubes in High-Temperature Vapor Phase Cracking Service," *Corrosion, 1,* 149 (1945).

95. D. Laidler and J. Taylor, "A Study of the Carburization Process with Special Reference to Gas Carburizing," *Journal of the Iron and Steel Institute, 165,* 23 (1950).

96. C. Wicks and F. Block, "Thermodynamic Properties of 65 Elements--Their Oxides, Halides, Carbides, and Nitrides," *Bureau of Mines Bulletin, 605* (1963).

96. C. Wicks and F. Block, "Thermodynamic Properties of 65 Elements--Their Oxides, Halides, Carbides, and Nitrides," *Bureau of Mines Bulletin, 605* (1963).

97. J. Ratliff, personal communication.

98. J. Ratliff, unpublished work (1964).

99. R. Bird, W. Stewart and E. Lightfoot, *Transport Phenomena,* John Wiley and Sons, Inc., New York (1960).

100. Kehl, *Principles of Metallographic Laboratory Practice,* McGraw-Hill Book Company, New York (1949).

101. *Cumulative Alphabetical and Grouped Numerical Index of X-ray Diffraction Data,* American Society for Testing Materials, Philadelphia, Pennsylvania (1955).

102. P. Walker, Jr., J. Rakszawski and A. Armington, "Distinguishing Between Graphitic and Amorphous Carbon," *American Society for Testing Materials Bulletin, 1955,* 178 (1955).

103. R. M. Asimow, Analysis of the Variation of the Diffusion Constant of Carbon in Austenite with Concentration," *Transaction of the Metallurgical Society of AIME, 230,* 611 (1964).

104. C. G. Homan, "Diffusion of Carbon in Alpha Iron," *Acta Metallurgica, 12,* 1071 (1964).

105. R. P. Smith, "The Diffusivity of Carbon in Iron by the Steady-State Method," *Acta Metallurgica, 1,* 578 (1953).

106. R. M. Barrer, *Diffusion in and Through Solids,* The MacMillan Company, New York (1941).

107. J. Fleming, J. Johnson, Boland, and Bomar, "Materials for High Temperature Nuclear Engineering Applications," Quarterly Report No. 4 Project No. B-153, Engineering Experiment Station of the Georgia Institute of Technology, Atlanta, Georgia, January 1, 1963 to April 1, 1963.

VITA

Richard Vernon Westerman was born in San Diego, California, on June 4, 1940. He attended the public schools in Arlington, Virginia; Boston, Massachusetts; District of Columbia; Honolulu, Hawaii, and Bethesda, Maryland. He was graduated from Bethesda-Chevy Chase High School in 1958. He entered Northwestern University the same year and was graduated in June, 1963, receiving the degree of Bachelor of Chemical Engineering. Under the cooperative plan at Northwestern he was employed by E. I. du Pont de Nemours and Company, Wilmington, Delaware, and Abbott Laboratories, North Chicago, Illinois.

In September, 1963, he enrolled in the Graduate Division of the Georgia Institute of Technology and completed requirements for the Master of Science in Chemical Engineering in June, 1964. He was employed by the Engineering Experiment Station and received graduate fellowships from the National Science Foundation.

In 1967, he was married to the former Nancy Susan Hill of Atlanta, Georgia.